

NASA
Contractor Report 179635

AVSCOM
Technical Report 87-C-14

Local Heat/Mass Transfer and Pressure Drop in a Two-Pass Rib-Roughened Channel for Turbine Airfoil Cooling

(NASA-CR-179635) LOCAL HEAT/MASS TRANSFER AND PRESSURE DROP IN A TWO-PASS RIB-ROUGHENED CHANNEL FOR TURBINE AIRFOIL COOLING Final Report (Texas A&M Univ.) 170
p Avail: NTIS HC A08/MF A01 CSCL 20D G3/34 0109764 N88-12039 Unclass

J.C. Han and P.R. Chandra
Texas A & M University
College Station, Texas

September 1987

Prepared for
Lewis Research Center
Under Contract NAS3-24227

NASA
National Aeronautics and
Space Administration



TABLE OF CONTENTS

	Page
1.0 SUMMARY	1
2.0 INTRODUCTION	3
2.1 Background	3
2.2 Objective	5
3.0 EXPERIMENTAL APPARATUS AND DATA REDUCTION	7
3.1 Experimental Apparatus	7
3.2 Data Reduction	10
4.0 EXPERIMENTAL RESULTS AND DISCUSSION	13
4.1 Experimental Results for the Smooth Channel	13
4.2 Experimental Results for the Ribbed Channel	16
4.2.1 Local Mass Transfer Data	16
4.2.2 Average Mass Transfer Data and Correlations	23
4.2.3 Comparison with Heat Transfer Data	26
5.0 PRESSURE DROP MEASUREMENT	29
5.1 Test Section and Data Analysis	29
5.2 Results and Discussion	31
6.0 CONCLUSIONS AND RECOMMENDATIONS	35
7.0 REFERENCES	38
APPENDICES	85
Appendix A: Mass Loss due to Natural Convection	85
Appendix B: Tabulated Local Mass Transfer Data	90
Appendix C: Tabulated Local Pressure Drop Data	159

NOMENCLATURE

D	channel width; also hydraulic diameter
e	rib height
\bar{f}_{at}	fully developed average friction factor after the turn
\bar{f}_{bt}	fully developed average friction factor before the turn
$\bar{f}(FD)$	fully developed four-sided smooth channel friction factor
g_c	conversion factor
G	mass flux, ρV
h_m	local mass transfer coefficient, equation (1)
K_c	loss coefficient due to contraction
K_t	loss coefficient due to sharp turn
\dot{m}''	local mass transfer rate per unit area, equation (2)
M	cumulative mass transfer
Nu	Nusselt number
P	rib pitch
ΔP	pressure drop across the test section
P_w	naphthalene vapor pressure at the wall, equation (4)
Pr	Prandtl number of air
\dot{Q}	volumetric flow rate of air
Re	Reynolds number based on channel hydraulic diameter
Sc	Schmidt number for naphthalene
Sh	local Sherwood number, equation (6)
Sh_0	Sherwood number of fully developed turbulent flow in square duct
\bar{Sh}	average Sherwood number on each of the channel surfaces
$\overline{\overline{Sh}}$	overall average Sherwood number on all surfaces
t	thickness of the inner (divider) wall

Δt	duration of the test run
T_w	naphthalene wall temperature, equations (3) and (4)
V	average velocity of air
X	axial distance from channel entrance
\tilde{D}	diffusion coefficient, equation (6)
α	rib angle-of-attack
ρ	average density of air
ρ_b	bulk naphthalene vapor density, equation (5)
ρ_s	density of solid naphthalene
ρ_w	local naphthalene vapor density at wall, equation (3)
ν	kinematic viscosity of pure air

1.0 SUMMARY

This is an extended research report for the program of Measurement of Heat Transfer and Pressure Drop in Rectangular Channels with Turbulence Promoters. This project was conducted by the Turbomachinery Laboratories of the Texas A&M University and was funded in part through Curtis Walker at the U.S. Army Research and Technology Laboratories. The project was monitored by Robert Boyle at the NASA-Lewis Research Center under NASA Contract No. NAS 3-24227.

Based on the research results from the NASA Contract No. NAS 3-24227, a final report entitled "Measurement of Heat Transfer and Pressure Drop in Rectangular Channels with Turbulence Promoters" was published (NASA CR 4015 September 1986 or AVSCOM TR 86-C-25 by J.C. Han, J.S. Park, and M.Y. Ibrahim). In that report, the combined effects of the channel aspect ratio and the rib angle-of-attack on the friction factor and on the local and the average heat transfer coefficients in straight, rectangular channels with a pair of opposite ribbed walls were investigated for three Reynolds numbers ($Re = 10,000, 30,000$ and $60,000$), two rib spacings ($P/e = 10$ and 20), two rib heights ($e/D = 0.047$ and 0.078), four rib angles ($\alpha = 90^\circ, 60^\circ, 45^\circ, \text{ and } 30^\circ$), and three channel aspect ratios ($W/H = 1, 2, \text{ and } 3$, ribs on side W). The test channels were heated by passing current through thin stainless steel foils and instrumented with 180 thermocouples. The local distributions of the heat transfer coefficient on both the smooth side and the ribbed side walls from the channel entrance to the downstream region were measured.

The present investigation was aimed at measuring the detailed mass transfer distributions in a two-pass smooth, square, channel and in a

similar two-pass square channel with a pair of opposite rib-roughened walls, via the naphthalene sublimation technique. The top, bottom, outer, and inner walls of the test channel were all naphthalene-coated plates. For ribbed channel tests, metallic ribs (without naphthalene coating) were placed on the top and bottom walls of the naphthalene-coated test channel such that the corresponding ribs on the two walls were directly opposite each other. The highly detailed mass transfer distributions on the top wall (rib-roughened), the outer wall (smooth), and the inner wall (smooth) were determined between the channel entrance and far downstream of the second straight channel, for three Reynolds numbers ($Re = 15,000, 30,000, \text{ and } 60,000$), two rib spacings ($P/e = 10 \text{ and } 20$), two rib heights ($e/D = 0.063 \text{ and } 0.094$), and three rib angles ($\alpha = 90^\circ, 60^\circ, \text{ and } 45^\circ$). The mass transfer coefficients before the turn, in the turn, and after the sharp 180° turn on each wall of the test channel were then averaged, compared, and correlated. The corresponding pressure drops and the friction factors were also measured and correlated.

2.0 INTRODUCTION

2.1 Background

In advanced gas turbine airfoils, as depicted in Figure 1, rib turbulators are cast onto two opposite walls of internal cooling passages to enhance the heat transfer to the cooling air. A typical cooling passage can be modeled as a straight or a multipass rectangular channel with two opposite rib-roughened walls. Han (1984) and Han et al. (1984, 1985) investigated systematically the effects of the rib pitch, the rib height, and the rib angle-of-attack on the average heat transfer and the pressure drop in a fully developed air flow in a uniformly heated, straight, square channel with two opposite ribbed walls. The results showed that ribs with oblique angles-of-attack (α) of 30° and 45° provided higher heat transfer enhancement than ribs with an angle-of-attack of 90° for the same pumping power consumption.

Recently, Han et al. (1986) reported the combined effects of the channel aspect ratio and the rib angle-of-attack on the friction factor and on the local and the average heat transfer coefficients in straight, rectangular channels with a pair of opposite ribbed walls for Reynolds numbers varying from 10,000 to 60,000. The channel aspect ratio (W/H) was varied from 1 to 2 and to 4. The rib height-to-hydraulic diameter ratio (e/D) was varied from 0.047 to 0.078, the rib pitch-to-height ratio (P/e) was varied from 10 to 20, and the rib angle-of-attack (α) was varied from 90° to 60° to 45° and to 30° , respectively. The test channels were heated by passing current through thin stainless steel foils and instrumented with 180 thermocouples. The local distributions of the heat transfer coefficient on both the smooth side and the ribbed side walls from the channel sharp entrance to the downstream region were

measured. The results confirmed that, in the square channel, the heat transfer for the slant ribs ($\alpha = 30^\circ$ to 45°) was about 30% higher than that the transverse ribs ($\alpha = 90^\circ$) for the same pumping power consumption. However, in the rectangular channels ($W/H = 2$ and 4 , ribs on side W), the heat transfer at $\alpha = 30^\circ$ to 45° was only about 5% higher than that $\alpha = 90^\circ$. The results also showed that, in the square channel, the highest heat transfer was obtained at $\alpha = 60^\circ$ accompanying with the highest pressure drop, however, in the rectangular channel with $W/H = 4$, both the highest heat transfer and pressure drop were obtained at $\alpha = 90^\circ$.

In a multipass rectangular channel, in addition to the rib turbulators, the flow separation and recirculation in the turn around regions and the flow redevelopment downstream of the turns are expected to have significant effects on the distribution of the local heat transfer coefficient and on the overall channel heat transfer. Boyle (1984) studied the heat transfer in a two-pass square channel with four smooth walls and in a similar two-pass square channel with two smooth walls and two opposite ribbed walls ($\alpha = 90^\circ$). The top and bottom walls of the test channels were heated uniformly by passing current through thin foils and were instrumented with thermocouples, while the other two walls were unheated. The results showed that the heat transfer coefficients at the turn in the smooth channel and in the rib-roughened channel were about 2 to 3 and 3 to 4 times the fully developed values, respectively. In both cases, the heat transfer decreased in the main flow direction after the turn. Since the test channels for the study were sparsely instrumented with thermocouples, the detailed distributions of the heat transfer coefficient around the sharp 180°

turns could not be determined.

Experimental data on the detailed distributions of the heat transfer coefficient around sharp 180° turns in multipass channels are important for two reasons. Firstly, they help design engineers understand the effect of sharp 180° turns on the surface heat transfer in multipass channels. Knowledge of the flow field and heat transfer characteristics in multipass channels facilitates the design of effectively cooled turbine blades which are not susceptible to structural failure due to uneven thermal stresses. Secondly, detailed local heat transfer results provide a data base for researchers and engineers to develop numerical models to predict the flow field and heat transfer characteristics in multipass channels of various geometries.

2.2 Objective

The present investigation was aimed at measuring the detailed mass transfer distributions around sharp 180° turns in a smooth channel and in a rib-roughened channel, via the naphthalene sublimation technique. The test section was a two-pass square channel, which resembled turbine blade cooling passages. The top, bottom, outer, and inner walls of the test channel were all naphthalene-coated plates. For ribbed channel tests, metallic ribs (without naphthalene-coated) were placed on the top and bottom walls of the naphthalene-coated test channel such that the corresponding ribs on the two walls were directly opposite each other. The rib height-to-hydraulic-diameter ratios (e/D) were 0.063 and 0.094. The rib pitch-to-height ratios (P/e) were 10 and 20. The rib angles-of-attack (α) were 90° , 60° , and 45° . In both the smooth channel and the ribbed channel experiments, the highly detailed mass transfer distributions on the top wall (rib-roughened), the outer wall (smooth),

and the inner wall (smooth) were determined between the channel entrance and far downstream of the second straight channel, for three Reynolds numbers of 15,000, 30,000, and 60,000. The mass transfer coefficients before the turn, in the turn, and after the turn on each wall of the test channel were then averaged, compared, and correlated. Fourteen test runs were performed. The test conditions of the runs are given in Table 1. The corresponding pressure drops and the friction factors were also determined.

3.0 EXPERIMENTAL APPARATUS AND DATA REDUCTION

3.1 Experimental Apparatus and Instrumentation

The main components of the test apparatus are the test section, a settling chamber, a calibrated orifice flow meter, a control valve, and a centrifugal blower. The entire apparatus, together with the measuring instruments, was located in an air-conditioned laboratory, which was maintained at a constant temperature of 21°C (70°F) throughout the tests.

Test Section

A schematic diagram of the test section is shown in Figure 2. The test section was a multipass channel with a 2.54-cm (1-in.) square cross-section. The top, the bottom, and the outer walls of the channel were constructed of 0.95-cm (0.375-in.) thick aluminum plates. The inner (divider) wall was constructed of two 0.325-cm (0.125-in.) thick aluminum plates, bonded together back-to-back with double-sided tape. The clearance at the tip of the divider wall was 2.54 cm (1 in.). To simulate actual turbine cooling passages, the ratio of the before-turn (and also after-turn) channel length to the channel width, X/D , and the ratio of the divider wall thickness to the channel width, t/D , were kept at 13 and 0.25, respectively.

All of the aluminum plates which made up the walls of the test channel were hollowed out and were filled with naphthalene by casting against a highly polished stainless steel plate. As a result, all of the interior surfaces of the test channel were smooth naphthalene surfaces. For the roughened channel experiments, brass ribs (with no naphthalene) with a 0.159-cm (0.063-in.) or 0.238-cm (0.094-in.) square cross-section were glued periodically on to the top and bottom

naphthalene surfaces of the two straight sections of the test channel. The rib pitch-to-height ratio was 10 or 20. There was no rib in the turn region. The rib height-to-hydraulic-diameter ratios corresponding to the two types of ribs were 0.063 and 0.094. The glue thickness was estimated to be less than 0.0127 mm (0.005 in.).

A relatively large metallic baffle was attached to the inlet of the test section to provide a sudden contraction flow entrance condition. During a test run, air from the naphthalene-free laboratory was drawn through the test section and ducted to the outside of the building.

Instrumentation

The most important part of any naphthalene sublimation experiment is the instrumentation used to measure the highly detailed distributions of the local mass transfer on the naphthalene surfaces. In this investigation, a Starrett electronic depth gage with an accuracy of 0.00001 in./0.0001 mm was used to determine the contours of the various naphthalene surfaces before and after a test run. The depth gage consisted of an electronic amplifier and a lever-type gaging head. The naphthalene plate, whose contour was to be measured, was mounted firmly on a coordinate table. The coordinate table facilitated the traversing of the naphthalene plate in two perpendicular directions tangential to the plate surface. The gaging head was affixed to a stand mounted on the stationary base of the coordinate table, and was hung over the naphthalene plate to be measured.

To measure the elevation at a point on the naphthalene surface, the platform of the coordinate table was moved so that the gaging head rested against the naphthalene surface at the measurement point. The deflection of the tip of the gaging head was converted into an

electrical signal (DC voltage) by the amplifier. The signal was recorded with a Texas Instruments Professional Computer which was connected to the amplifier through an A/D converter. The elevation measurement stations for a typical ribbed channel experiment are shown in Figure 3a. The photos of the test section, the traversing table, and the associated instrumentation are shown in Figure 3b.

Five, 36-gage, copper-constantan thermocouples were used along with a digital temperature indicator to measure the temperature of the flowing air and the temperatures at four stations on the naphthalene surfaces during a test run.

Procedure

After all of the naphthalene plates were prepared under a fume hood, they were tightly sealed individually in plastic bags to prevent sublimation. They were then left in the laboratory for six to eight hours to attain thermal equilibrium. Before a test run, the surface contours of all the naphthalene plates were measured and recorded. In a ribbed channel test run, ribs were glued on to the appropriate naphthalene surfaces. The test section was then assembled and attached to the rest of the test rig.

To initiate the test run, the blower was switched on to allow air to flow through the test channel at a predetermined rate. During the test run, the air temperature, the temperatures at the four stations on the naphthalene surfaces, the pressure drop across the orifice, the static pressure upstream of the orifice, and the atmospheric pressure were recorded periodically. A typical run lasted about 30 minutes. At the completion of the test run, the contours of the naphthalene surfaces were measured again. From the corresponding before-run and after-run

surface contours, the depth change at each measurement station on the naphthalene surfaces was calculated.

Separate tests were conducted to determine the mass losses from the various naphthalene surfaces due to natural convection while the surface contours were being measured and while the ribs were being glued on to the appropriate naphthalene surfaces. It was found that the total mass loss by natural convection was no more than four percent of the total mass transfer during any test run. The mass losses due to natural convection were referred to the Appendix A. In calculating the local Sherwood numbers, these losses of mass from the various naphthalene surfaces were taken into account accordingly.

3.2 Data Reduction

The local mass transfer coefficient at any measurement point was determined from the rate of mass transfer per unit surface area and the local naphthalene vapor density at the measurement point, and the local bulk naphthalene vapor density.

$$h_m = \dot{m}'' / (\rho_w - \rho_b). \quad (1)$$

The rate of mass transfer per unit surface area at the measurement point was evaluated from the density of solid naphthalene, the measured change of elevation at the measurement point, and the duration of the test run.

$$\dot{m}'' = \rho_s \cdot \Delta z / \Delta t. \quad (2)$$

The local naphthalene vapor density was calculated from the ideal gas law in conjunction with the measured naphthalene surface temperature and with the vapor pressure-temperature relationship for naphthalene developed by Sogin (1958).

$$\rho_w = P_w / (R_v T_w), \quad (3)$$

$$\log_{10} P_w = A - B/T_w, \quad (4)$$

where R_v , A , and B were given by Sogin (1958).

The local bulk naphthalene vapor density was evaluated by the equation

$$\rho_b = M/\dot{Q}. \quad (5)$$

The cumulative mass, M , was the total mass which entered the airstream from the four channel walls between the entrance and the measurement station over the duration of the test.

Based on the definition of the local Sherwood number,

$$Sh = h_m \cdot D/\tilde{D} = h_m \cdot D/(v/Sc), \quad (6)$$

where the Schmidt number for naphthalene was 2.5, according to Sogin (1958). The local Sherwood number was normalized by the Sherwood number for fully developed turbulent flow in a smooth square channel.

$$\frac{Sh}{Sh_0} = \frac{h_m D/\tilde{D}}{0.023 Re^{0.8} Pr^{0.4} (Sc/Pr)^{0.4}}, \quad (7)$$

where the correlation of Dittus and Boelter and the heat/mass transfer analogy, $Nu/Sh = (Pr/Sc)^{0.4}$, were used.

Uncertainties in Data Reduction

For a 0.56°C (1°F) variation in the naphthalene surface temperature, it was found that there was a 6 percent change in the local naphthalene vapor density, according to equations (3) and (4). In the present study, the naphthalene surface temperatures were measured at two

stations in each of the two straight sections of the test channel. The variation of the four temperatures for any test run was never more than 0.28°C (0.5°F). Therefore, the uncertainties in the local vapor density calculations were relatively small although the surface temperatures at all the elevation measurement stations were not measured.

It should be noted that the measured naphthalene surface temperatures were about 0.56°C (1°F) higher than the inlet air temperature in any test run. If the naphthalene surface temperatures had not been measured and if the naphthalene surface temperatures had been assumed to be the same as the inlet air temperature, the calculated local vapor densities would have been 6 percent too low. As a result, the local Sherwood numbers would have been 6 percent higher than what they were supposed to be.

Since the surface contours were measured at discrete points along one, two, or three lines on the naphthalene surfaces, errors were introduced into the calculations of the bulk vapor densities when they were determined from the cumulative mass transferred into the airstream. Fortunately, the bulk vapor densities were generally much smaller than the local naphthalene vapor densities. The maximum values of the former did not exceed 10 percent of the latter.

The maximum uncertainty in the calculations of $(\rho_w - \rho_b)$ was estimated to be 6 percent. Other uncertainties in the calculations of the density of solid naphthalene (ρ_s), of the contour measurement (ΔZ), and of the duration of the test run (Δt) were estimated to be 2, 4, and 3 percent, respectively. By using the uncertainty estimation method of Kline and McClintock (1953), it was found that the maximum uncertainty in the calculated local Sherwood numbers was less than 8 percent.

4.0 EXPERIMENTAL RESULTS AND DISCUSSION

The local mass transfer results are presented in this section as the axial distributions of a normalized Sherwood number ratio, Sh/Sh_0 , as given in equation (7). For each set of data, the Sherwood number ratios along the inner line, the center line, and the outer line (Figure 3a) on the top wall are plotted separately from those along the two axial lines (inner line and center line) on the inner and outer walls. Along the axial lines, the Sh/Sh_0 data are not evenly distributed. For the smooth channel test runs, there are more data points around the turn than along the straight sections of the channel. For the ribbed channel runs, there are many data points between adjacent ribs on the top wall to illustrate the axially periodic nature of the Sh/Sh_0 distributions. A list of mass transfer test runs with all the variable parameters is presented in Appendix B.

4.1 Experimental Results for the Smooth Channel

The local Sherwood number ratio results for the smooth channel are shown in Figures 4, 5, and 6 for the three Reynolds numbers studied. In Figure 4, the Sh/Sh_0 data along the entire test channel are shown, while in Figures 5 and 6, only the data in the before-turn region, in the turn region, and in the after-turn region are plotted so that the effect of the turn on the Sh/Sh_0 can be examined closely. In this paper, the before-turn and after-turn regions refer to the sections of the test channel between $X/D = 9$ and 12 , and $X/D = 14$ and 17 (3D upstream and 3D downstream of the turn), respectively.

Attention is first focused on the Sh/Sh_0 distribution on the top wall in Figure 4. In the entrance section, the Sherwood number ratio decreases monotonically with increasing axial distance until it attains

the value of one at $X/D \approx 10$. The Sh/Sh_0 distribution compares well with that for a straight smooth channel of large aspect ratio by Sparrow and Cur (1982).

Entering the turn region, the Sh/Sh_0 increases with a rapid increase along the outer line. The increase is believed to be the result of the secondary flow induced by the turn. The dip in the Sh/Sh_0 distribution along the outer line at $X/D \approx 12.5$ indicates that there is a low mass transfer zone at the outside corner of the turn region. The outer-line Sh/Sh_0 then increases gradually and reaches a maximum at the end of the turn ($X/D \approx 14.5$). The large Sh/Sh_0 values near the outer wall at the end of the turn are caused by the flow being forced outward by the sharp turn.

The low Sherwood number ratios along the inner line at $X/D \approx 13.5$ are due to the flow separation at the tip of the inner wall. The downturn of the Sh/Sh_0 distribution along the center line at $X/D \approx 14$ can also be attributed to the flow separation. The large values of the Sh/Sh_0 at $X/D \approx 15$ along the inner line are due to the flow reattachment and the flow being pushed back toward the inner wall after the turn. In general, the top-wall Sh/Sh_0 values in the after-turn region are much higher than those in the before-turn region.

Leaving the after-turn region, the top-wall Sh/Sh_0 drops gradually. The flow becomes almost redeveloped near the end of the second straight section of the test channel.

Attention is now turned to the Sh/Sh_0 distributions on the inner wall and on the outer wall. In the before-turn region, the values of Sh/Sh_0 on both the inner and outer walls are about one. In the turn region, the outer-wall Sh/Sh_0 increases gradually around the turn. In

the after-turn region, the Sh/Sh_0 along the outer wall is high at $X/D \approx 14$. The flow is being forced toward the outer wall at the end of the turn. Further downstream, the outer-wall Sh/Sh_0 reaches a minimum at $X/D \approx 15$ and then a peak at $X/D \approx 16$, showing that the flow is being pushed away from the outer wall and then back toward the outer wall again.

The effect of the flow separation (at the tip of the inner wall) and reattachment on the flow field can be seen very clearly in the inner-wall Sh/Sh_0 distribution in the after-turn region. The inner-wall Sh/Sh_0 distribution is initially very low at $X/D \approx 14.5$ and has a high peak at $X/D \approx 15.5$.

The inner-wall and outer-wall Sh/Sh_0 values in the after-turn region are generally higher than those in the before-turn region. Downstream of the after-turn region, the Sh/Sh_0 drops gradually as the effect of the turn on the flow diminishes. In the downstream straight section of the test channel, the criss-crossing pattern of the Sh/Sh_0 distribution shows that the flow is being pushed toward the inner wall and the outer wall alternately.

The Sh/Sh_0 distribution for $Re = 15,000$ presented in Figure 5 exhibits the same general trends as that for $Re = 30,000$. Again, in the turn region, low Sh/Sh_0 zones on the top wall are evident at the outside corner at $X/D \approx 12.5$ (due to flow recirculation) and near the tip of the inner wall at $X/D \approx 13.0$ (due to flow separation).

In the after-turn region, the Sh/Sh_0 distributions are very high near the flow reattachment zone on the inside of the top wall and on the inner wall at $X/D \approx 15.5$. The inner-line Sh/Sh_0 on the outer wall drops to a minimum at $X/D \approx 15.5$ and reaches a peak at $X/D \approx 16$, showing that

the flow may be forced away from the outer wall and the inner wall alternately in the after-turn region, as in the case of $Re = 30,000$.

The Sh/Sh_0 distribution for $Re = 60,000$ (Figure 6) is only slightly different from those for $Re = 30,000$ and $15,000$. Just before entering the turn region ($X/D \approx 11.5$), the inner-wall Sh/Sh_0 increases while the outer-wall Sh/Sh_0 decreases to below one. The flow being forced inward due to the turn is more evident in this case than in the two previous cases.

The recirculation zone at the outside corner of the turn at $X/D \approx 12.5$ as well as the flow reattachment zone on the inner wall and on the inside of the top wall at $X/D \approx 15.5$ can be identified very easily. In the turn region, the inner-line Sh/Sh_0 on the top wall remains quite constant. Otherwise, the Sh/Sh_0 distribution for $Re = 60,000$ is similar to those for the two low Reynolds numbers studied.

4.2 Experimental Results for the Rib-Roughened Channel

4.2.1 Local Mass Transfer Data

The experimental results for the rib-roughened channel with $e/D = 0.063$, $P/e = 10$, and $\alpha = 90^\circ$ are shown in Figures 7, 8, and 9. Firstly, the Sh/Sh_0 distribution for $Re = 60,000$ shown in Figure 7 will be examined. In the entrance section of the test channel, the axial Sh/Sh_0 distribution on the top wall decreases with increasing distance, and settles into a periodic pattern with a small spanwise variation, just before entering the sharp turn. In the periodic region, the maximum Sh/Sh_0 value between adjacent ribs is approximately equal to 3. The axial location where the value of Sh/Sh_0 is maximum (due to flow reattachment) is about 2 to 3 times the rib-height downstream of a rib. At $X/D \approx 11$, the top-wall Sh/Sh_0 increases with a faster increase along

the outer-line than along the inner-line as the flow begins to turn inward.

In the turn region, the top-wall Sh/Sh_0 is relatively low since there is no rib in the region. In the after-turn region, the top-wall Sh/Sh_0 distribution is generally higher than that in the before-turn region. There is an increase in the Sh/Sh_0 in the spanwise direction toward the outer wall. Further downstream of the turn, the peak between adjacent ribs in the Sh/Sh_0 distribution decreases gradually and the spanwise variation becomes smaller. The Sh/Sh_0 becomes periodic again near the end of the second straight section of the channel.

In the before-turn region, the Sh/Sh_0 distribution on the inner wall is about the same as that on the outer wall with the inner-line Sh/Sh_0 values on each wall slightly higher than the corresponding center-line Sh/Sh_0 values (due to the proximity of the ribs on the top wall to the inner line on each wall). The outer-wall Sherwood number ratios in the turn region are generally higher than those in the before-turn region.

After the turn, the side-wall Sherwood number ratios remain as high as those in the turn region, with the values on the inner-wall slightly higher than those on the outer wall. The initial low values of the inner-wall Sh/Sh_0 at $X/D \approx 14.5$ are due to the flow separation at the tip of the inner wall. The flow reattaches at $X/D \approx 15$, resulting in the peak in the inner-wall Sh/Sh_0 distribution. In the downstream straight section of the channel, the inner-wall and the outer-wall distributions cross several times more. It appears that the flow is being pushed toward the inner wall and the outer wall alternately as a result of the turn.

In Figures 8 and 9, the Sh/Sh_0 distributions are shown for $Re = 30,000$ and $15,000$, respectively. Only the Sh/Sh_0 data in the before-turn, the turn, and the after-turn regions are presented. As in the previous case, the top-wall Sh/Sh_0 distribution is periodic in the before-turn region with an increasing spanwise Sh/Sh_0 variation just before entering the turn region. A close examination of the figures reveals that, for $Re = 15,000$, the increase of the spanwise Sh/Sh_0 variation begins earlier than that in the higher Reynolds number case. Comparing Figures 7, 8, and 9, there is a definite increase in the spanwise Sh/Sh_0 variation in the after-turn region as the Reynolds number decreases. For all three Reynolds numbers, the after-turn top-wall Sherwood number ratios near the outer wall are higher than those near the inner wall.

Effect of Rib Spacing

The experimental results for a ribbed channel with $e/D = 0.063$, $P/e = 20$, and $\alpha = 90^\circ$ are shown in Figure 10 for $Re = 30,000$. The top-wall Sh/Sh_0 distribution has many of the characteristics of that for a ribbed channel case with a smaller rib spacing of $P/e = 10$. The effect of increasing the rib spacing (P/e) on the Sh/Sh_0 distribution around a sharp 180° turn is the overall lower Sh/Sh_0 values. In the before turn region, the top-wall Sh/Sh_0 distribution is axially periodic with a relatively small spanwise variation. The after-turn, top-wall Sh/Sh_0 distribution is generally higher than that in the before-turn region with the larger values of the Sh/Sh_0 along the outer line. As the peak between adjacent ribs in the after-turn Sh/Sh_0 distribution drops gradually with increasing axial distance, the spanwise variation decreases. The peak in the outer-line, top-wall Sh/Sh_0 distribution for

$P/e = 20$ drops in the streamwise direction slightly faster than that for $P/e = 10$.

Effect of Rib Height

The effect of the height of the ribs on the heat transfer around a sharp turn is studied by examining Figures 8 and 11, in which the Sh/Sh_0 distributions for $e/D = 0.063$ and 0.094 , respectively, are shown. The top-wall Sh/Sh_0 distribution for $e/D = 0.094$ is higher than that for $e/D = 0.063$ around the sharp turn. In both cases, the peaks in the top-wall Sh/Sh_0 distributions in the after-turn region drop with increasing axial distance at about the same rate.

The spanwise variation of the after-turn top-wall Sh/Sh_0 for ribs with a large e/D is smaller than that for ribs with a small e/D .

On the inner and outer walls, the Sh/Sh_0 distributions for $e/D = 0.094$ are again higher than those for $e/D = 0.063$ around the turn. In the after-turn region, the inner-wall and outer-wall Sherwood number ratios for $e/D = 0.094$ stay about constant with the inner-wall Sh/Sh_0 values higher than the outer-wall values. There is no crossing of the inner-wall and the outer wall Sh/Sh_0 distributions in the $e/D = 0.094$ case. It appears that the larger ribs keep the flow from being deflected laterally downstream of the turn.

Effect of Rib Angle on Local Sherwood Number Ratio

The distributions of the ribbed-wall Sherwood number ratio along three axial lines for $\alpha = 90^\circ$ and for $Re = 30,000$ are shown in Figure 12. The periodic nature of the distributions in the entrance duct is evident. The Sherwood number ratios attain their maximum values at the points of flow reattachment, which occur slightly upstream of the mid points between adjacent ribs. The variations of the Sherwood number

ratio in the spanwise direction are very small compared with the axial variations.

In the turn region, where there is no rib on either the top wall or the bottom wall, the Sherwood number ratios along the outer line are higher than those along the inner line. The trend carries onto the after-turn region, where the ribbed-wall Sherwood number ratios near the outer wall are higher than those near the inner wall. The low ribbed-wall Sherwood number ratios near the inner wall are the results of the flow separation at the tip of the inner wall. The strong lateral pressure gradient due to the sharp turn forces the main flow to impinge onto the outer wall. The flow then gets pushed back toward the inner wall, resulting in the high ribbed-wall Sh/Sh_0 near the outer wall. In general, the values of the Sherwood number ratios after the turn are greater than those before the turn.

Further downstream of the turn, as the effect of the turn on the flow field vanishes gradually, both the peak Sherwood number ratio and the spanwise Sh/Sh_0 variation decrease with increasing axial distance, until the axial Sh/Sh_0 distributions become periodic again.

The axial distributions of the ribbed-wall, inner-wall, and outer-wall Sherwood number ratios for angles-of-attack of 60° and 45° are shown in Figures 13 and 14, respectively. The Reynolds number is 30,000 in both cases. Selected segments of the axial distributions before and after the turn from Figures 13 and 14 are replotted on an enlarged scale in Figures 15a and 15b. These figures facilitate the close examination of the effects of the rib angle and the sharp turn on the local ribbed-wall Sh/Sh_0 in the before-turn and after-turn regions. In Figures 15a and 15b, the axial locations of the measurement stations relative to the

ribs are also illustrated.

For $\alpha = 60^\circ$, the magnitude of the variations of the before-turn top-wall Sh/Sh_0 in the spanwise direction is comparable to those of the axial periodic Sh/Sh_0 distributions. The values of the before-turn Sh/Sh_0 along the outer line are always greater than the corresponding values along the inner line. These lateral variations of the ribbed-wall Sh/Sh_0 in the before-turn region are due to the secondary flow along the rib axes toward the inner wall.

In the turn, the values of Sh/Sh_0 are lower than those before the turn with Sh/Sh_0 along the outer line generally higher than those along the center line and the inner line.

After the turn, the peak Sherwood number ratios along the outer line decrease significantly from the before-turn values, meanwhile, the decreases (from the before-turn values) of the peak Sh/Sh_0 along the center line and along the inner line are successively lower than those along the outer line. The spanwise variations of Sh/Sh_0 are relatively small after the turn. This may be caused by the complicated interaction between the main flow, which is forced toward the inner wall due to the turn (as described earlier), and the secondary flow along the rib axes toward the outer wall.

For $\alpha = 45^\circ$, the top-wall Sh/Sh_0 distributions before the turn are similar to those for $\alpha = 60^\circ$. Again, the Sherwood number ratios along the outer line are higher than those along the center line, which, in turn, are higher than those along the inner line. The Sherwood number ratio is relatively uniform in the turn. The after-turn values of Sh/Sh_0 are about the same as those in the before-turn region.

Attention will now be turned to the top of Figures 13 and 14, where

the axial inner-wall and the outer-wall Sherwood number distributions are given. For $\alpha = 60^\circ$, the spanwise variations of the before-turn Sh/Sh_0 on the inner (divider) wall are much larger than those on the outer wall. The before-turn Sherwood number ratios along the inner line on the inner wall are much greater than those along the center line on the inner wall, while on the outer wall, the center-line Sh/Sh_0 were only slightly higher than the inner-line Sh/Sh_0 . The secondary flow created by the oblique ribs impinges onto the inner wall, resulting in the high Sh/Sh_0 on the inner wall near the ribbed walls. For $\alpha = 45^\circ$, the before-turn Sh/Sh_0 exhibit the same trends except that the spanwise Sh/Sh_0 variations on the inner wall are not as large as those for $\alpha = 60^\circ$.

After the turn, the inner-wall Sh/Sh_0 for both $\alpha = 60^\circ$ and $\alpha = 45^\circ$ are large compared to the corresponding outer-wall Sh/Sh_0 . The high Sh/Sh_0 on the inner wall is believed to be caused by flow reattachment along with the main flow, which is being forced toward the inner wall due to the turn. On the outer wall, the after-turn Sh/Sh_0 along the inner line are higher than those along the center line for $\alpha = 60^\circ$. However, the reverse is true in the case of $\alpha = 45^\circ$.

Effect of Reynolds Number

The effect of the Reynolds number on the local Sherwood number will now be examined. Experimental data for $\alpha = 60^\circ$ and 45° and for $Re = 15,000$ and $60,000$ are presented in Figures 16 through 19.

Attention is focused first on Figures 16 and 17, along with Figure 13. The top-wall Sherwood number ratios in all three cases are very similar. The spanwise top-wall Sh/Sh_0 variations decrease with increasing Reynolds number. Before the turn, there are much larger

spanwise Sh/Sh_0 variations on the inner wall than on the outer wall for all Reynolds numbers. However, the differences are less evident in the case of $Re = 15,000$. After the turn, the inner-wall Sherwood number ratios are always higher than the corresponding outer-wall values and the differences are smaller at higher Reynolds numbers.

Comparing Figures 18 and 19 with Figure 14, it can be seen that the spanwise variations of the before-turn, top-wall Sh/Sh_0 are again very large at low Reynolds numbers. The differences between the before-turn Sh/Sh_0 variations on the inner wall and those on the outer wall are most pronounced at $Re = 15,000$.

In general, the flow Reynolds number has only a modest effect on the local Sherwood number ratio.

4.2.2 Average Mass Transfer Data and Correlations

Results for Smooth Channel and for Transverse Ribs ($\alpha = 90^\circ$)

The local Sherwood number ratios were averaged over various segments of the interior channel surfaces in the before-turn region, in the turn region, and in the after-turn region. The averaging of the local Sherwood number ratios was area-weighted. A typical set of \overline{Sh}/Sh_0 results for $Re = 30,000$ and $\alpha = 90^\circ$ is given in Figure 20. In the figure, the top-wall, the outer-wall, and the inner-wall average Sherwood number ratios for the smooth and roughened channel cases studied are shown in three separate charts.

Figure 20 shows that the present \overline{Sh}/Sh_0 data for the smooth channel are always lower than those for the rib-roughened channel. For instance, the top-wall \overline{Sh}/Sh_0 values for the smooth channel in the before-turn region, in the turn region, and in the after-turn region are 1.1, 1.7, and 2.05, respectively. The corresponding \overline{Sh}/Sh_0 values for a

typical roughened channel with $P/e = 10$, $e/D = 0.063$, and $\alpha = 90^\circ$ are 2.6, 2.55, and 3.5. Increasing the rib height results in a higher \overline{Sh}/Sh_0 around the turn due to the higher turbulence level in the flow for the larger rib case. However, increasing the rib pitch lowers the \overline{Sh}/Sh_0 around the turn because of the longer boundary layer between adjacent ribs downstream of the reattachment zone.

The after-turn \overline{Sh}/Sh_0 values are always higher than the corresponding before-turn values as a result of the sharp turn. For the smooth channel, the top-wall \overline{Sh}/Sh_0 in the turn region is more than fifty percent higher than that in the before-turn region. However, for the roughened channel cases, the top-wall \overline{Sh}/Sh_0 values in the turn region are slightly lower than the respective before-turn \overline{Sh}/Sh_0 values because there is no rib on the top-wall in the turn region.

In all of the cases studied, the values of the outer-wall \overline{Sh}/Sh_0 in the turn region are only slightly different from the corresponding after-turn values.

The \overline{Sh}/Sh_0 data for both the smooth and roughened channels were found to be correlated well by the following equation:

$$\overline{Sh}/Sh_0 = a Re^b [(e/D)/0.063]^m \cdot [(P/e)/10]^n, \quad (8)$$

with the numerical values of a , b , m , and n listed in Table 2. Equation (8) correlates all of the \overline{Sh}/Sh_0 data of the present investigation to within ± 6 percent. Readers should be cautioned that equation (8) applies only to a smooth channel or a ribbed channel with a rib angle-of-attack of 90° . Correlations for other angle-of-attack cases can be found in equation (9). In Figures 21a and 21b, the present top-wall \overline{Sh}/Sh_0 data in the before-turn and the after-turn regions for both the

smooth and roughened channels are plotted against the flow Reynolds number along with the correlation of equation (8).

Results for Angled Ribs ($\alpha = 90^\circ$, 60° , and 45°)

For all the cases studied, the local Sherwood number ratios for individual segments of the channel walls before the turn, in the turn, and after the turn were averaged. Typical average Sherwood number ratios, those for $Re = 30,000$, are shown in Figures 22a and 22b. In Figure 22a, the average Sherwood number ratios (Sh/Sh_0) are plotted as functions of the rib angle. Before the turn, the top-wall Sh/Sh_0 are much greater than the outer-wall Sh/Sh_0 and the inner-wall Sh/Sh_0 for all three angles-of-attack of 90° , 60° , and 45° . The top-wall Sh/Sh_0 , the outer-wall Sh/Sh_0 , and the inner-wall Sh/Sh_0 for $\alpha = 60^\circ$ are all higher than their counterparts for $\alpha = 90^\circ$ and $\alpha = 45^\circ$.

After the turn, the inner-wall Sh/Sh_0 are higher than the outer-wall Sh/Sh_0 for all three rib angles. Also, the top-wall Sh/Sh_0 for $\alpha = 60^\circ$ decreases significantly after the turn from its before-turn value while those for $\alpha = 90^\circ$ and 45° increase after the turn from their corresponding before-turn values. These trends are also evident in Figure 22b, where the Sh/Sh_0 results are replotted to show the effect of the sharp 180° turn on the average Sherwood number ratios for the three rib angles-of-attack studied.

The average Sherwood number ratios for the various segments of the channel walls were found to be correlated well with the Reynolds number and the rib angle by the following equation

$$\overline{Sh/Sh_0} = a Re^b (\alpha/90^\circ)^c, \quad (9)$$

where a , b , and c are constant coefficients. The numerical values of

these coefficients are listed in Table 3. Equation (9) with coefficients from Table 3 correlate the experimental data of the present study to within ± 6 percent. It should be noted that equation (9) applies to $e/D = 0.063$ and $P/e = 10$ only. Correlations for the cases of other e/D and P/e ratios can be found in equation (8).

Figure 23a shows $(\overline{Sh}/Sh_0)(90^\circ/\alpha)^C$ as a function of the flow Reynolds number. The experimental data points shown in the figure are the top-wall \overline{Sh}/Sh_0 obtained in the present study. The figure shows that the present experimental before-turn and after-turn results are well represented by the equations.

The Sherwood number ratios for all of the surfaces in and around the 180° turn were averaged. The overall average Sherwood number ratios $(\overline{\overline{Sh}}/Sh_0)$ for the three rib angles studied are plotted versus the flow Reynolds number in Figure 23b. The overall Sherwood number ratio is independent of the rib angle but decreases slightly with increasing Reynolds number. It was found that the following equation

$$\overline{\overline{Sh}}/Sh_0 = 7.0 Re^{-0.1} \quad (10)$$

correlates the data to within ± 4 percent.

4.2.3 Comparison with Heat Transfer Data

Results for Smooth Channel and for Transverse Ribs ($\alpha = 90^\circ$)

The results of the present study will now be compared with published heat transfer data for smooth and roughened channels with $\alpha = 90^\circ$. The present smooth channel data are presented in Figure 24a along with the heat transfer data for a smooth two-pass channel of an aspect ratio of 0.4 reported by Metzger and Sahm (1985). In Figure 24a, the present overall Sherwood number ratio in the before-turn, the turn, or

the after-turn region, \overline{Sh}/Sh_0 , is the area-weighted average of the Sh/Sh_0 values on the top and side walls in the respective region. The heat transfer data are based on the Nusselt number-Reynolds number correlations in regions 2, 3, and 4 given by Metzger and Sahm (1985). The Nusselt numbers are converted to the corresponding Sherwood numbers by $Sh = (Sc/Pr)^{0.4} Nu$.

Both the present mass transfer data and the published heat transfer data show that, for all three Reynolds numbers, the average Sherwood number ratios in the after-turn region and in the turn region are successively higher than those in the before-turn region. In addition, both the present data and those of Metzger and Sahm (1985) decrease slightly with increasing Reynolds number.

For the typical case of $Re = 30,000$, the present mass transfer data in the before-turn region and in the turn region are about 4 and 12 percent higher than the corresponding heat transfer data, while the present \overline{Sh}/Sh_0 in the after turn region is about 9 percent lower. Considering the differences in the channel aspect ratios and in the channel surfaces over which the data are averaged in the two studies, the agreement between the present data and those by Metzger and Sahm (1985) is very good.

In Figure 24b, the present ribbed channel data are compared with the heat transfer data by Han et al. (1985, 1986). The heat transfer data are for the fully developed flow of air in a uniformly heated, straight, square channel with two opposite ribbed walls, and with the same values of e/D , P/e , and Re as those of the present study. The fully developed Nusselt numbers on the ribbed walls are converted to their corresponding Sherwood numbers. They are then plotted along with

the before-turn, top-wall \overline{Sh}/Sh_0 data of the present study for the three Reynolds numbers of 15,000, 30,000, and 60,000. Figure 24b shows that the present mass transfer data are slightly higher (by up to 10 percent) than the heat transfer data. This may be due to the effect of the turn on the top-wall \overline{Sh}/Sh_0 at the end of the before-turn region.

Results for Angled Ribs ($\alpha = 90^\circ$, 60° , and 45°)

In Figure 25, the averages of the before-turn ribbed-wall Sherwood numbers for all the cases studied were compared with the fully developed average heat transfer data reported by Han et al. (1985, 1986). The average heat transfer data are those for the fully developed flow of air in a uniformly heated, straight, square channel with two opposite ribbed walls, and with the same values of e/D , P/e , α , and Re as those of the present study. The Nusselt numbers from the heat transfer studies were converted to their corresponding Sherwood numbers.

It can be seen from Figure 25 that the present mass transfer results compared very well with the published heat transfer data in most cases. The deviations between the heat transfer and mass transfer data are less than 10 percent, except for the case of $\alpha = 45^\circ$ and $Re = 60,000$, the deviation of which is 14 percent. The good agreement between the heat and mass transfer data reaffirms that the naphthalene sublimation technique is a reliable tool for the determination of highly localized distributions of the heat transfer coefficient in complicated channel flows, such as those encountered in the present study. The published heat transfer data in NASA CR-4015 (Han 1986) shows an incorrect rib orientation for the square duct. A published errata gives the correct orientation.

5.0 PRESSURE DROP MEASUREMENT

5.1 Test Section and Data Analysis

A schematic diagram of the test section for pressure drop/friction factor experiments is shown in Figure 26. The flow geometry of this apparatus models situations that exist in actual turbine engine airfoils. The internal geometry of the test section and the construction were very similar to that of the mass transfer test section described earlier. The only difference was of the material used for construction. In this case, Plexiglas was used instead of aluminum.

To measure the pressure drop, twenty (20) pressure taps (1/32-in) in all were drilled in the channel walls at locations shown in Figure 26. Fifteen (15) out of twenty (20) pressure taps were along the outer wall of the test channel with eight (8) taps before the turn and seven (7) taps after the turn region. The remaining five (5) taps were provided on the top wall with two (2) taps each before and after the turn and one (1) in the turn region. The pressure taps number 3, 7, 11, and 15 were thoughtfully used to take into account the difference in pressure drop data at the top wall and the side wall (if any). For the calculations of the pressure drop and friction factor, the average values were considered at these four cross-sectional locations.

For the rough channel tests, the brass ribs were placed and glued onto the top and the bottom walls in the pre-determined fashion as was done in the case of mass transfer test runs.

The pressure drop across the channel route was measured by an inclined or a U-tube manometer. During the experiments, it was seen that the magnitude of the pressure drop was almost the same on the smooth side and the ribbed side walls. Therefore, the pressure drop and

the friction factor calculated were on the basis of the average values. The average friction factor of the present investigation was based on the adiabatic conditions (non-heating test runs).

The Blasius equation,

$$\bar{f}(\text{FD}) = 0.079 \text{ Re}^{-0.25} \quad (11)$$

was used to provide reference values of the friction factor to compare the smooth channel fully-developed results in the two straight sections of the present test channel.

The following equation was used to calculate the friction factors in the fully-developed before and after turn regions of the channel, f_{bt} and f_{at} .

$$\bar{f} = \frac{\Delta P}{4(L/D) (G^2/2\rho g_c)} \quad (12)$$

where,

L = length of the test channel corresponding to the pressure drop, ΔP ,
 $L = 6.25$ inches for before-turn fully-developed region [Tap 3 to 7], and
 $L = 5.00$ inches for after-turn fully-developed region [Tap 14 to 16].

The loss factor due to sudden contraction at the entrance, K_c , and the loss factor for the turn region, K_t , was calculated by using the following relation;

$$K_c \text{ (or } K_t) = \frac{\Delta P}{\rho V^2/2g_c} \quad (13)$$

The pressure drop for the entrance loss factor, K_c , corresponded to 35/16 inches of channel entrance length (Tap 3) and for

the turn loss factor, K_t , corresponded to 7 inches of channel length (Tap 7 to 14).

For a better comparison, the pressure drop values were non-dimensionalised by the dynamic pressure ($1/2\rho V^2$) and the plots were drawn between the non-dimensional pressure drop and distance, X/D .

5.2 Results and Discussion

Pressure Distribution

The non-dimensional pressure drop $[(P - P_{atm})/(1/2\rho V^2)]$ results are plotted against non-dimensional axial distance $[X/D]$. Each channel geometry investigated was tested at six flow rates, covering Reynolds numbers from 10,000 to 60,000. A list of pressure drop test runs with all the variable parameters is presented in Appendix C. Figures 27-32 show the plots with different channel/rib geometries in the same order as the list given in Appendix c.

Pressure distributions in all the cases show almost the same trend, that is, the non-dimensional pressure drop increasing with decreasing Reynolds number. The pressure drops (Tap 1, $X/D = 0.31$) sharply at the sudden contraction entrance of the channel to almost the same value in all the cases. The effect of Reynolds number is also very minimal. The pressure then rises by the next tap location ($X/D = 2.19$, Tap 2) and then drops in a linear fashion till tap 7 ($X/D = 10.94$). The results show that from $X/D = 4.69$ (Tap 3) to $X/D = 10.94$ (Tap 7) can be treated as the fully-developed flow region before the turn. The pressure then rises slightly in the vicinity of the upstream corner of the turn ($X/D = 11.56$, Tap 8). A rapid drop in pressure has been seen in the turn region ($X/D = 11.56$, Tap 8 to $X/D = 14.44$, Tap 10), and just after the turn in the downstream section of the channel ($X/D = 15.06$, Tap 11).

The pressure then increases again slightly (except for cases with higher size rib, $e/D = 0.094$), as shown in Figure (32). A linear pressure drop towards the fully-developed region of the downstream section (between $X/D = 18.8$, Tap 14 and $X/D = 23.8$, Tap 16) is clearly visible.

Examination of the individual pressure distributions for each test reveals that their trends are highly independent of the Reynolds number and the normalized distributions are virtually identical over the entire range of Reynolds number for a given channel geometry.

Figures 33-35 represent the effect of the rib geometry on non-dimensional pressure drop distribution for $Re = 10,000$, $Re = 30,000$, and $Re = 60,000$, respectively. Again, the results are almost independent of the Reynolds number. But on looking at these plots individually, it is very clear that the pressure drop in the case of the smooth channel is lowest, maximum pressure drop is attained in the case of the channel with higher rib size ($e/D = 0.094$). In order, the results with higher pitch ($P/e = 20$), angle-of-attack (α) = 45° , and angle-of-attack (α) = 60° show an increase in pressure drop, but remain in between the smooth channel and with $e/D = 0.094$ cases.

Friction Factor and Loss Coefficients

On the basis of the normalized pressure distribution results and to cover the entire test channel under present investigation, the channel was divided into four regions, namely, the entrance region ($X/D = 0$ to 4.69 , Tap 3), the fully-developed before-turn region ($X/D = 4.69$, Tap 3 to 10.94 , Tap 7), the turn region ($X/D = 10.94$, Tap 7 to 18.8 , Tap 14), and the fully-developed after-turn region ($X/D = 18.8$, Tap 14 to 23.8 , Tap 16).

The plots for average fully-developed friction factors, \bar{f}_{bt} and \bar{f}_{at}

vs Reynolds number for the different rib and channel geometries are shown in Figures 36 and 37. The loss coefficients, K_c and K_t , for the entrance and the turn regions respectively, are plotted against Reynolds number in Figures 38 and 39.

In Figure 36 for \bar{f}_{bt} , the friction factor for the smooth channel case differs by 6% from the Blasius equation (11). For $\alpha = 90^\circ$ and $\alpha = 60^\circ$, the friction factor approaches an approximately constant value as the Reynolds number increases, while the friction factor is maximum with higher size rib and minimum with higher rib spacing. The friction factor with $\alpha = 60^\circ$ is about 45% higher than that with $\alpha = 90^\circ$. Also the friction factor with $\alpha = 45^\circ$ is less than that with $\alpha = 90^\circ$, but not by much.

The trend of Figure 37 for \bar{f}_{at} looks the same as that of \bar{f}_{bt} in Figure 36, except that the variation is not very smooth and also the values with $\alpha = 45^\circ$ are lower than that with $P/e = 20$ at some locations. For the smooth channel case, the friction factor is approximately 100% higher than the values calculated by equation (11). It is interesting to note that the average friction factor for the fully-developed after-turn region is higher than the corresponding fully-developed before-turn region, except in cases with $\alpha = 60^\circ$ and $\alpha = 45^\circ$, in which \bar{f}_{at} is lower than their respective values of \bar{f}_{bt} .

The loss coefficient in the entrance section of the channel, K_c , decreases with increasing Reynolds number, as shown in Figure 38. Figure 39 shows the loss coefficient, K_t , against Reynolds number for the turn region. It decreases with increasing Reynolds number. The effect of rib geometry on these two loss coefficients are identical as far as the trend and the overall range is concerned. It is noted that,

for $\alpha = 90^\circ$ and $P/e = 10$, K_C is lower than with same P/e but with $\alpha = 60^\circ$ and $\alpha = 45^\circ$. However, K_t for $\alpha = 90^\circ$ is higher than that for $\alpha = 60^\circ$ and 45° for the same $P/e = 10$. Both loss coefficients remain maximum with higher rib size in all cases.

For all the cases investigated, the values of all the four friction factors are tabulated in Table 4.

Correlations

The two fully-developed friction factors, \bar{f}_{bt} and \bar{f}_{at} , and the two loss coefficients, K_C and K_t were correlated by one single equation of the following form:

$$\bar{f} \text{ (or } K) = a (Re)^b ((P/e)/10)^c ((e/D)/0.063)^m (\alpha/90^\circ)^n \quad (14)$$

where the coefficients, a , b , c , m , and n , are given in Table 5. The deviations in equation (14) from the test data are $\pm 7\%$, $\pm 10\%$ (8% for 95% data points), $\pm 5.5\%$, and $\pm 6.6\%$, respectively, for \bar{f}_{bt} , \bar{f}_{at} , K_C and K_t .

6.0 CONCLUSIONS AND RECOMMENDATIONS

The detailed mass transfer distributions around the sharp 180° turns in a smooth channel and in a rib-roughened channel have been studied. The following conclusions can be drawn:

A. Smooth Channel and Transverse Ribs:

1. For the smooth channel, the heat/mass transfer around the turn is influenced by the flow separation at the tip of the divider (inner) wall and the secondary flow induced by the centrifugal force at the turn. The heat/mass transfer after the turn is higher than that before the turn. The heat/mass transfer in the turn is also high compared with that before the turn except at the first outside corner of the turn.
2. For the rib-roughened channel, the heat/mass transfer around the turn is influenced not only by the flow separation and the secondary flow at the turn, but also by the presence of repeated ribs on the top and bottom walls. The heat/mass transfer coefficients on the smooth side walls and on the rib-roughened top and bottom walls around the turn are larger than the corresponding coefficients for the smooth channel. The axially periodic distribution of the top-wall heat/mass transfer coefficient after the turn is higher than that before the turn with a more noticeable spanwise variation. The inner-wall and outer-wall heat/mass transfer coefficients after the turn are higher than the respective before-turn coefficients.
3. For the range of Reynolds number studied, the average Sherwood number ratios around the sharp turns in the smooth and rib-roughened channels decrease slightly with increasing Reynolds

number. For the ribbed channel, the spanwise variation of the top-wall Sherwood number ratio in the after-turn region increases with decreasing Reynolds number.

4. The heat/mass transfer around the turn in the ribbed channel decreases with increasing rib spacing and increases with increasing rib height.
5. The average Sherwood number ratios for individual wall segments around the turns in the smooth and ribbed channels can be correlated by equation (8) to within ± 6 percent.
6. The published heat transfer results for straight rib-roughened channels can be applied to the design of the straight section before the first sharp turn in a multipass ribbed cooling passage in a turbine blade.

B. Angled Ribs:

1. Before the turn, the axial distributions of the ribbed-wall Sherwood number are periodic for all three rib angles-of-attack studied. The local ribbed-wall Sherwood numbers for $\alpha = 60^\circ$ and 45° near the outer wall are higher than those near the inner wall due to the secondary flow along the rib axes. The spanwise Sherwood number variations decrease as the Reynolds number increases. The spanwise variations of the local ribbed-wall Sherwood number for $\alpha = 90^\circ$ are very small.
2. After the turn, the ribbed-wall Sherwood numbers near the outer wall are higher than those near the inner wall for all three rib angles studied. For $\alpha = 60^\circ$ and 45° , the spanwise variations of the ribbed-wall Sherwood numbers after the turn are smaller than those before the turn.

3. Before the turn, the average ribbed-wall Sherwood number for $\alpha = 60^\circ$ is higher than that for $\alpha = 45^\circ$, which, in turn, is higher than that for $\alpha = 90^\circ$. However, after the turn, the average ribbed-wall Sherwood number for $\alpha = 90^\circ$ is higher than those for $\alpha = 45^\circ$ and 60° .
4. For any rib angle-of-attack, the average inner-wall Sherwood number after the turn is always higher than both the average inner-wall Sherwood number before the turn and the average outer-wall Sherwood number after the turn.
5. The average Sherwood number ratios for individual channel surfaces can be correlated with equations in the form of $Sh/Sh_0 = a Re^b (\alpha/90^\circ)^c$.
6. The overall average Sherwood number ratio in the region around the sharp turn is independent of the rib angle, but decreases slightly as the Reynolds number increases.
7. The two fully-developed friction factors (\bar{f}_{bt} and \bar{f}_{at}), and the two loss coefficients (K_c and K_t) can be correlated by equation (14).

C. Recommendations:

1. Use naphthalene-coated ribs, instead of using metallic ribs, to study the local heat/mass transfer coefficients in a two-pass rib-roughened channel.
2. Study the effect of the channel aspect ratio on the local heat/mass transfer coefficients in two-pass ribbed channels.
3. Study the three-pass ribbed channels.

7.0 REFERENCES

Han, J.C., 1984, "Heat Transfer and Friction in Channels with Two Opposite Rib-Roughened Walls," ASME Journal of Heat Transfer, Vol. 106, pp. 774-781.

Han, J.C., Park, J.S., and Lei, C.K., 1984, "Heat Transfer and Pressure Drop in Blade Cooling Channels with Turbulence Promoters," NASA CR-3837.

Han, J.C., Park, J.S., and Lei, C.K., 1985, "Heat Transfer Enhancement in Channels with Turbulence Promoters," ASME Journal of Engineering for Gas Turbines and Power, Vol. 107, pp. 628-635.

Han, J.C., Park, J.S., and Ibrahim, M.Y., 1986, "Measurement of Heat Transfer and Pressure Drop in Rectangular Channels with Turbulence Promoters," NASA CR-4015 or USAAVSCOM-TR-86-C-25.

Boyle, R.J., 1984, "Heat Transfer in Serpentine Passages with Turbulence Promoters," ASME Paper No. 84-HT-24.

Sogin, H.H., 1958, "Sublimation from Disks to Air Streams Flowing Normal to Their Surfaces," Trans. of ASME, Vol. 80, pp. 61-69.

Kline, S.J., and McClintock, F.A., 1953, "Describing Uncertainties in Single-Sample Experiments," Mechanical Engineering, Vol. 75, pp. 3-8.

Sparrow, E.M., and Cur, N., 1982, "Turbulent Heat Transfer in a Symmetrically or Asymmetrically Heated Flat Rectangular Duct with Flow Separation at Inlet," J. of Heat Transfer, Vol. 104, pp. 82-89.

Metzger, D.E., and Sahm, M.K., 1985, "Heat Transfer Around Sharp 180 Degree Turns in Smooth Rectangular Channels," ASME Paper No. 85-GT-122.

TABLE 1. LIST OF HEAT/MASS TRANSFER TEST RUNS

CHANNEL	Re	P/e	e/D	α
SMOOTH	15,000	—	—	—
	30,000	—	—	—
	60,000	—	—	—
ROUGH	15,000	10	0.063	90°
	30,000	10	0.063	90°
	60,000	10	0.063	90°
ROUGH	15,000	10	0.063	60°
	30,000	10	0.063	60°
	60,000	10	0.063	60°
ROUGH	15,000	10	0.063	45°
	30,000	10	0.063	45°
	60,000	10	0.063	45°
ROUGH	30,000	20	0.063	90°
ROUGH	30,000	10	0.094	90°

Re : REYNOLDS NUMBER

P/e : PITCH-TO-RIB HEIGHT RATIO

e/D : RIB HEIGHT-TO-HYDRAULIC DIAMETER RATIO

α : RIB ANGLE-OF-ATTACK

**Table 2. Numerical Values of the Coefficients a, b, m, and n
in Equation (8)**

Region	Surface	a	b	m	n
before turn, smooth channel	top wall	2.02	-0.06	0	0
	outer wall	2.10	-0.06	0	0
	inner wall	2.08	-0.06	0	0
in turn, smooth channel	top wall	3.21	-0.06	0	0
	outer wall	3.23	-0.06	0	0
after turn, smooth channel	top wall	3.84	-0.06	0	0
	outer wall	3.45	-0.06	0	0
	inner wall	4.07	-0.06	0	0
before turn, ribbed channel	top wall	7.2	-0.1	0.22	-0.3
	outer wall	4.6	-0.1	0.69	-0.11
	inner wall	4.6	-0.1	0.53	-0.15
in turn, ribbed channel	top wall	6.7	-0.1	0.23	-0.31
	outer wall	7.0	-0.1	0.31	-0.52
after turn, ribbed channel	top wall	9.3	-0.1	0.13	-0.49
	outer wall	6.7	-0.1	0.4	-0.30
	inner wall	7.3	-0.1	0.68	-0.14

TABLE 3. Coefficients a, b, and c in equation (9)

Region	Surface	a	b	c if $\alpha \geq 60^\circ$	c if $\alpha < 60^\circ$
before turn	top wall	7.2	-0.1	-0.58	-0.059
	outer wall	4.6	-0.1	-0.74	-0.26
	inner wall	4.8	-0.1	-0.63	-0.3
in turn	top wall	6.7	-0.1	0.24	0.02
	outer wall	7.0	-0.1	0.11	0.18
after turn	top wall	9.3	-0.1	0.4	0.15
	outer wall	6.7	-0.1	0	0.066
	inner wall	7.3	-0.1	-0.099	-0.077

Table 4 FRICTION AND LOSS FACTORS

CHANNEL	Re	\bar{f}_{bt}	\bar{f}_{at}	K_c	K_t
SMOOTH	10,000	0.0075	0.0162	1.3200	1.6703
	20,000	0.0064	0.0128	1.2061	1.6631
	30,000	0.0057	0.0117	1.1387	1.5994
	40,000	0.0054	0.0101	1.0934	1.5980
	50,000	0.0051	0.0097	1.0905	1.5841
	60,000	0.0049	0.0097	1.0992	1.4452
ROUGH P/e=10 e/D=0.063 $\alpha = 90^\circ$	10,000	0.0319	0.0377	1.7996	2.5754
	20,000	0.0311	0.0352	1.7847	2.5487
	30,000	0.0301	0.0329	1.7042	2.4560
	40,000	0.0303	0.0320	1.6990	2.4223
	50,000	0.0300	0.0323	1.6810	2.3103
	60,000	0.0297	0.0344	1.5725	2.2674
ROUGH P/e=10 e/D=0.063 $\alpha = 60^\circ$	10,000	0.0431	0.0431	2.1821	1.9666
	20,000	0.0441	0.0433	2.1498	1.8591
	30,000	0.0436	0.0419	2.0726	1.8090
	40,000	0.0445	0.0404	1.9513	1.7797
	50,000	0.0440	0.0388	1.9181	1.6810
	60,000	0.0440	0.0389	1.8540	1.6380
ROUGH P/e=10 e/D=0.063 $\alpha = 45^\circ$	10,000	0.0302	0.0269	1.9935	2.1013
	20,000	0.0309	0.0270	1.9511	2.0078
	30,000	0.0298	0.0252	1.8719	1.9947
	40,000	0.0279	0.0269	1.8739	1.9378
	50,000	0.0268	0.0226	1.7672	1.8266
	60,000	0.0258	0.0232	1.6923	1.7971
ROUGH P/e=20 e/D=0.063 $\alpha = 90^\circ$	10,000	0.0259	0.0307	1.7241	2.2414
	20,000	0.0243	0.0270	1.7442	2.2174
	30,000	0.0242	0.0240	1.6114	2.1565
	40,000	0.0256	0.0269	1.5812	2.0522
	50,000	0.0249	0.0269	1.5970	1.9397
	60,000	0.0219	0.0285	1.4976	1.9394
ROUGH P/e=10 e/D=0.094 $\alpha = 90^\circ$	10,000	0.0513	0.0539	2.3437	3.0011
	20,000	0.0487	0.0500	2.2715	3.0557
	30,000	0.0479	0.0509	2.2164	2.9352
	40,000	0.0487	0.0505	2.1700	2.8697
	50,000	0.0483	0.0517	2.0690	2.7586
	60,000	0.0473	0.0509	1.9768	2.6507

Re : REYNOLDS NUMBER, P/e : PITCH-TO-RIB HEIGHT RATIO, e/D : RIB HEIGHT-TO-HYDRAULIC DIAMETER RATIO, α : RIB ANGLE-OF-ATTACK

\bar{f}_{bt} : AVERAGE FRICTION FACTOR BEFORE TURN

\bar{f}_{at} : AVERAGE FRICTION FACTOR AFTER TURN

K_c : LOSS FACTOR OF CONTRACTION AT THE ENTRANCE

K_t : LOSS FACTOR IN THE TURN

Table 5. Coefficients a, b, c, m, and n in equation (14)

REGION/FACTOR	a	b	c	m	n if $\alpha \geq 60^\circ$	n if $\alpha < 60^\circ$
\bar{f}_{bt}	0.0432	-0.034	-0.342	1.173	-0.865	0.105
\bar{f}_{at}	0.0476	-0.032	-0.37	0.99	-0.447	0.46
K_c	2.54	-0.04	-0.05	0.595	-0.435	-0.12
K_t	3.25	-0.029	-0.215	0.42	0.75	0.32

\bar{f}_{bt} : AVERAGE FRICTION FACTOR BEFORE TURN

\bar{f}_{at} : AVERAGE FRICTION FACTOR AFTER TURN

K_c : LOSS FACTOR OF CONTRACTION AT THE ENTRANCE

K_t : LOSS FACTOR IN THE TURN

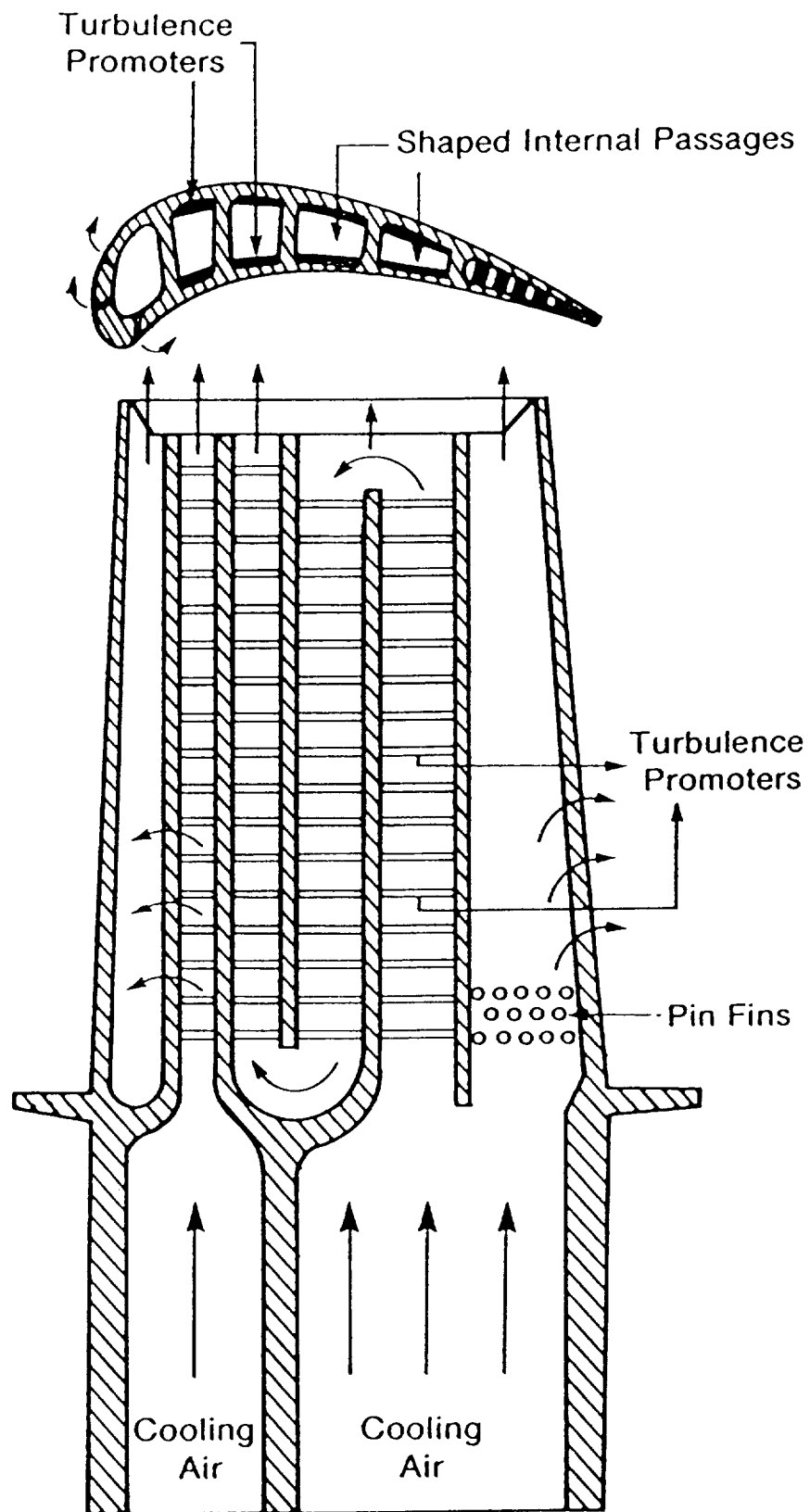
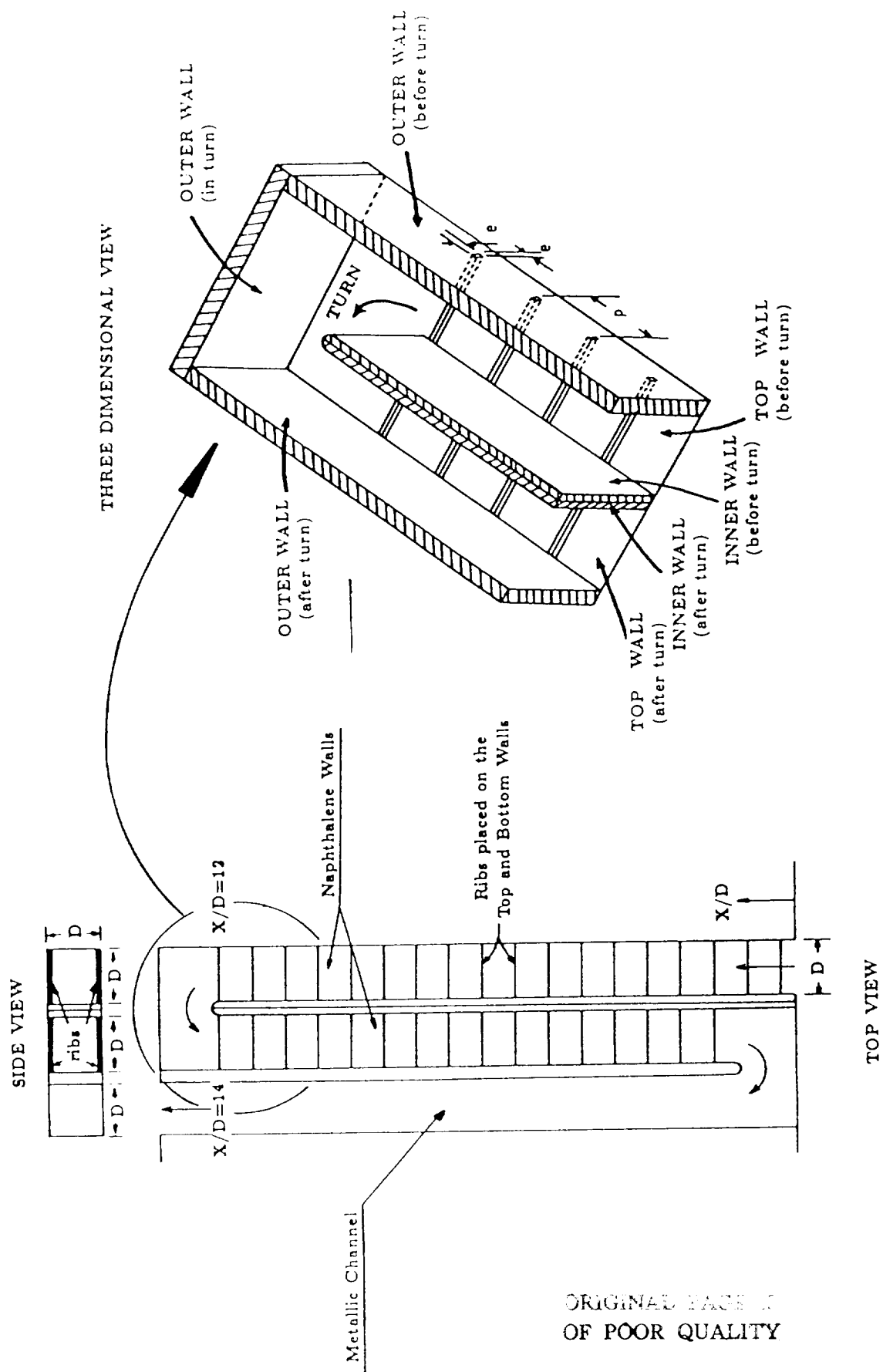


Fig. 1. Cooling concept of a modern multipass turbine blade with ribs at right angle.



ORIGINAL PAGE 2
OF POOR QUALITY

Fig. 2. Sketch of the test section for mass transfer experiments.

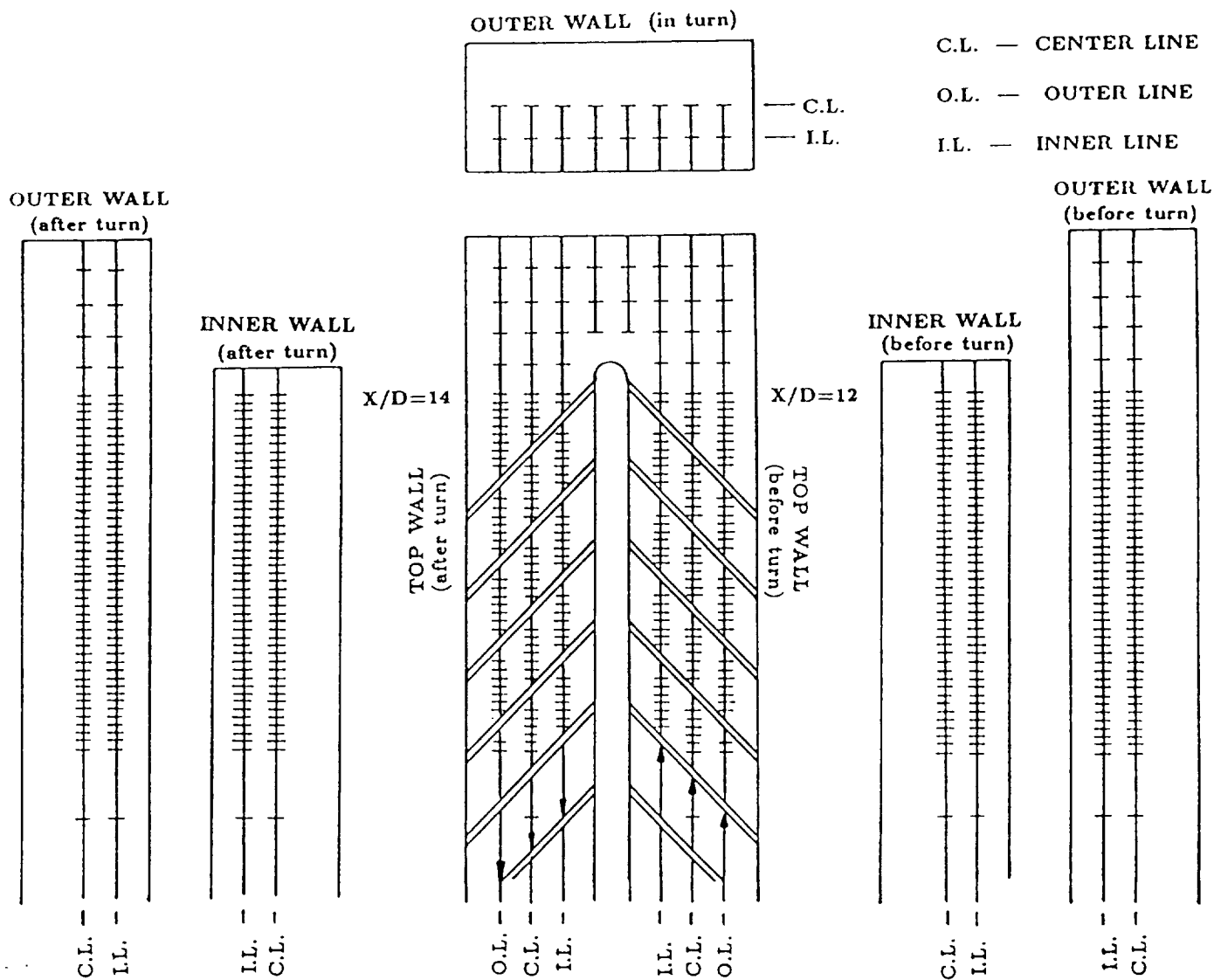


Fig. 3a. Measurement points before, in, and after the turn for a typical test run

ORIGINAL PAGE IS
OF POOR QUALITY

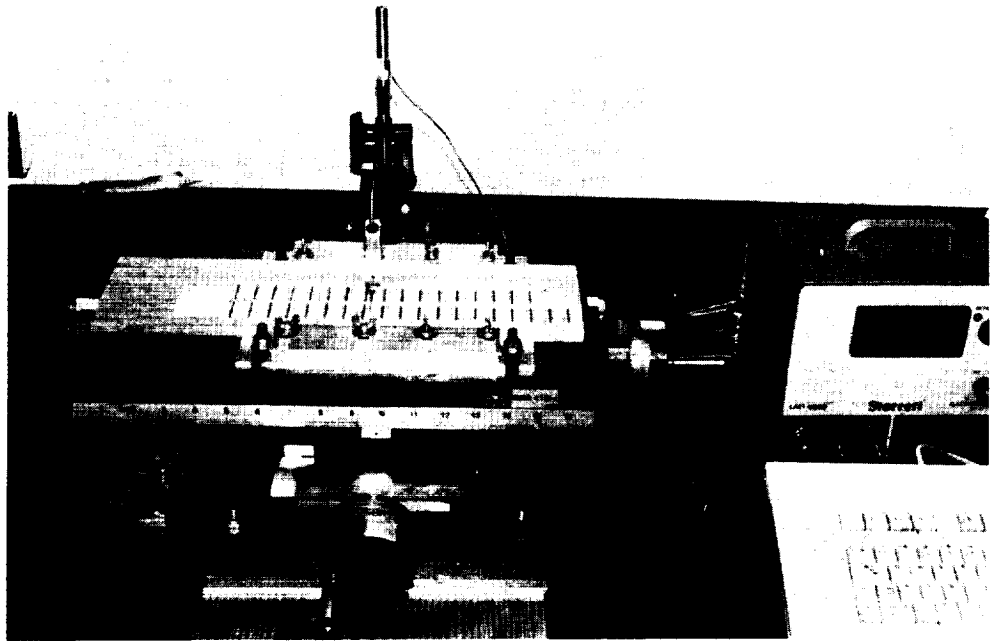
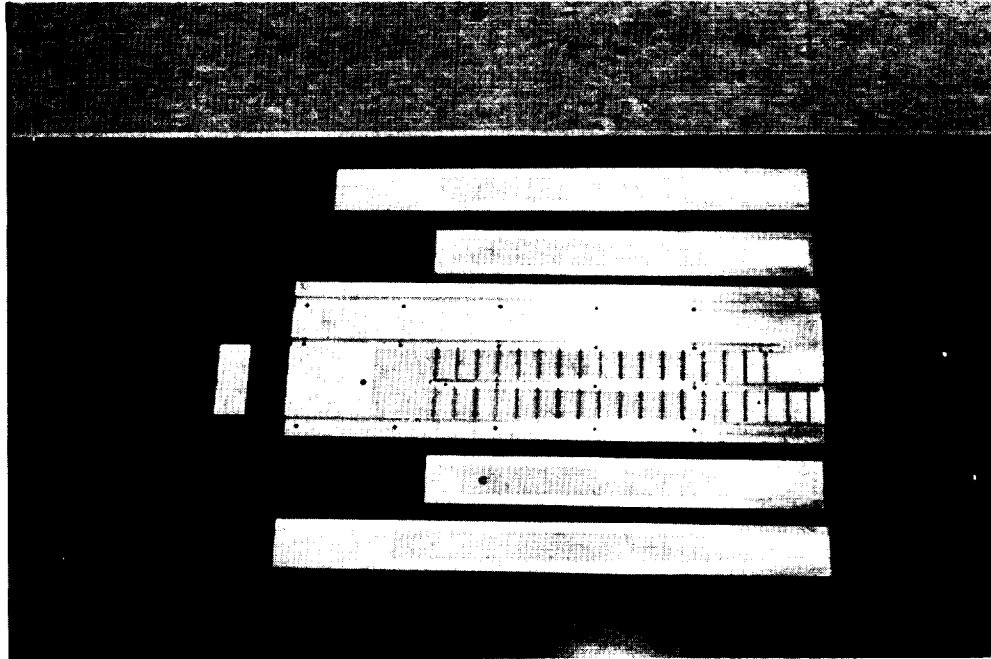


Fig. 3b. Upper Photo - Test Section with Naphthalene Plates
Lower Photo - Transversing Table and Instrumentation

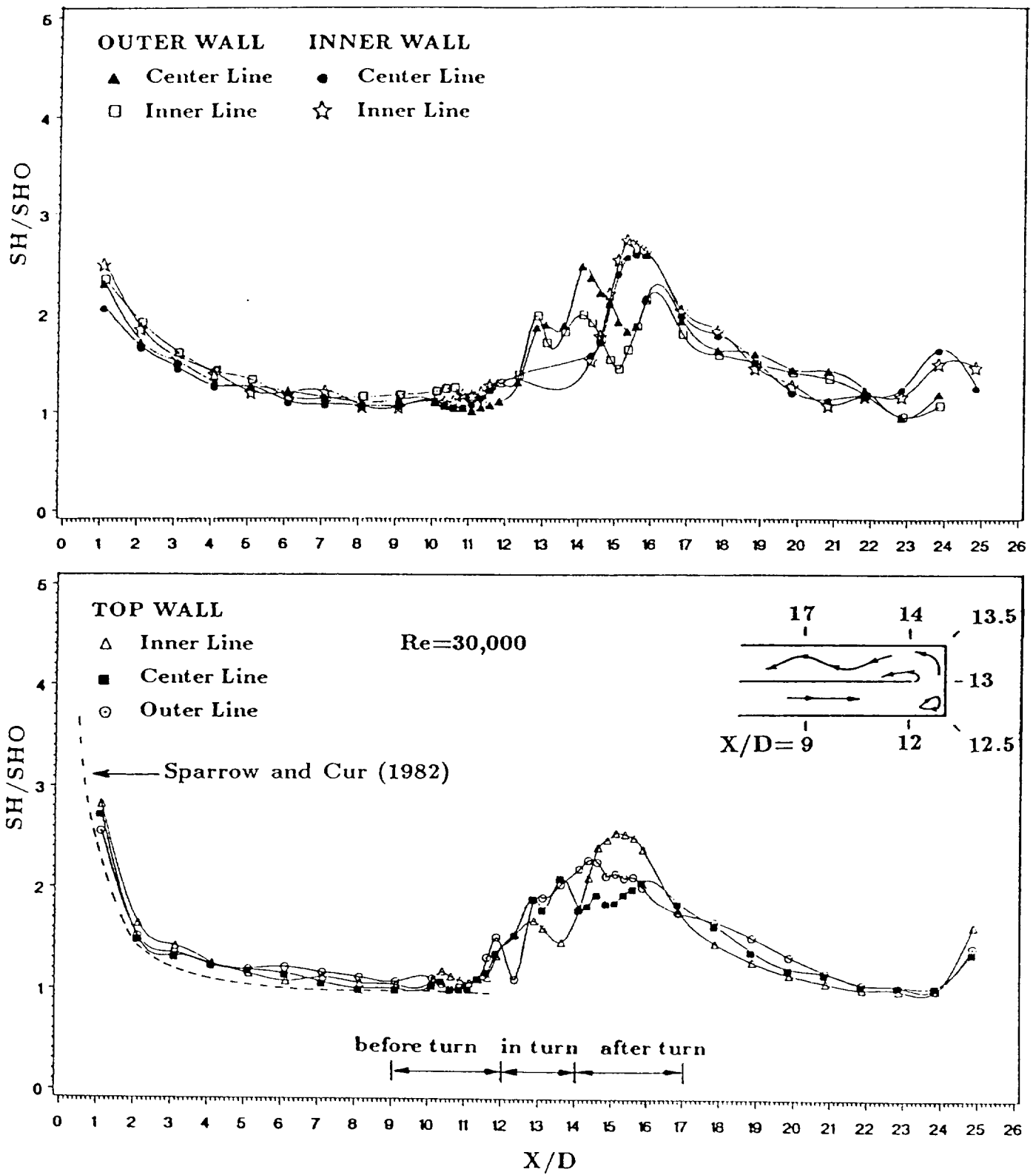


Fig. 4. The Local Sherwood No. Ratio for Smooth Channel with $Re=30,000$

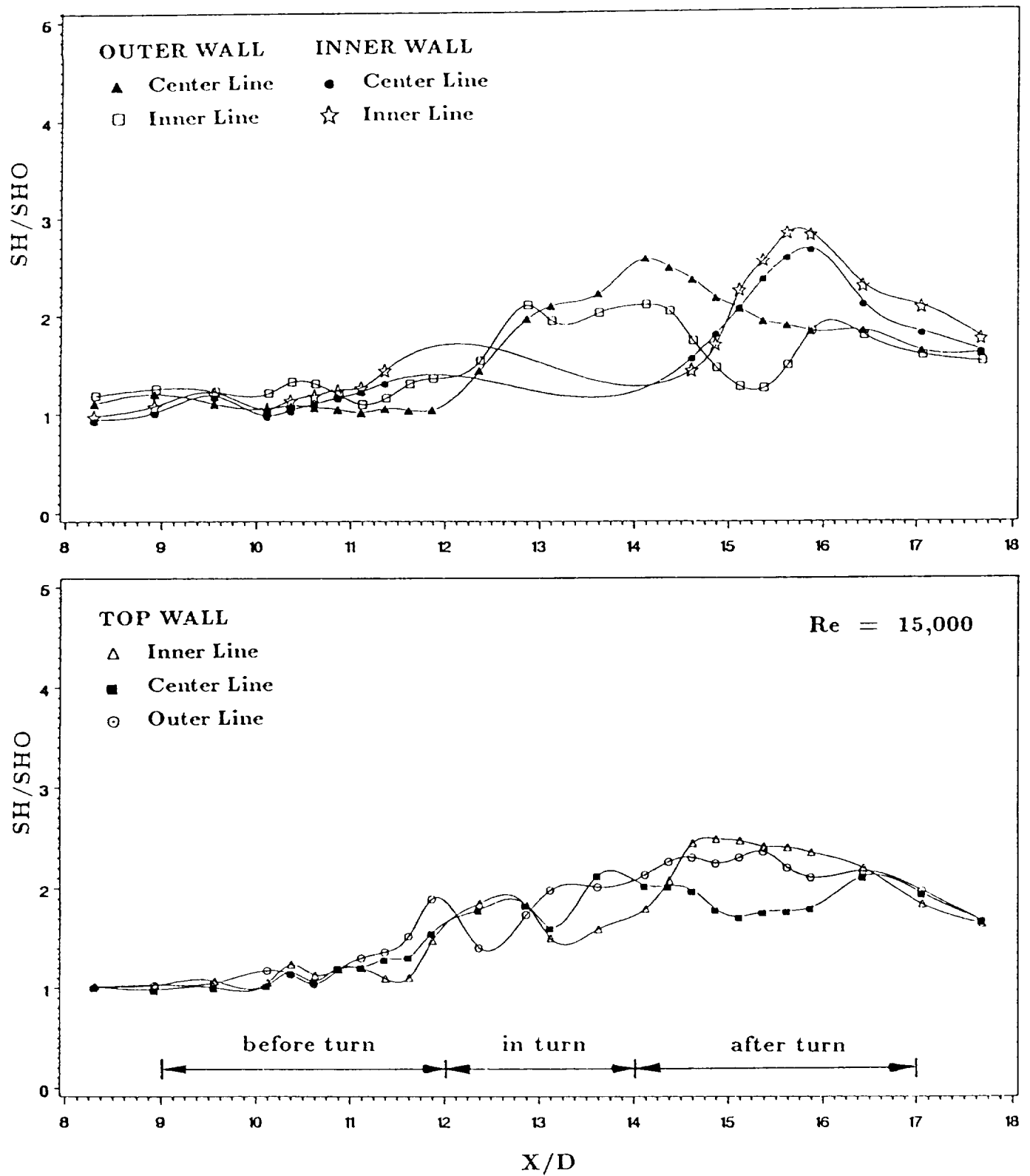


Fig. 5. The Local Sherwood No. Ratio for Smooth Channel with $Re=15,000$

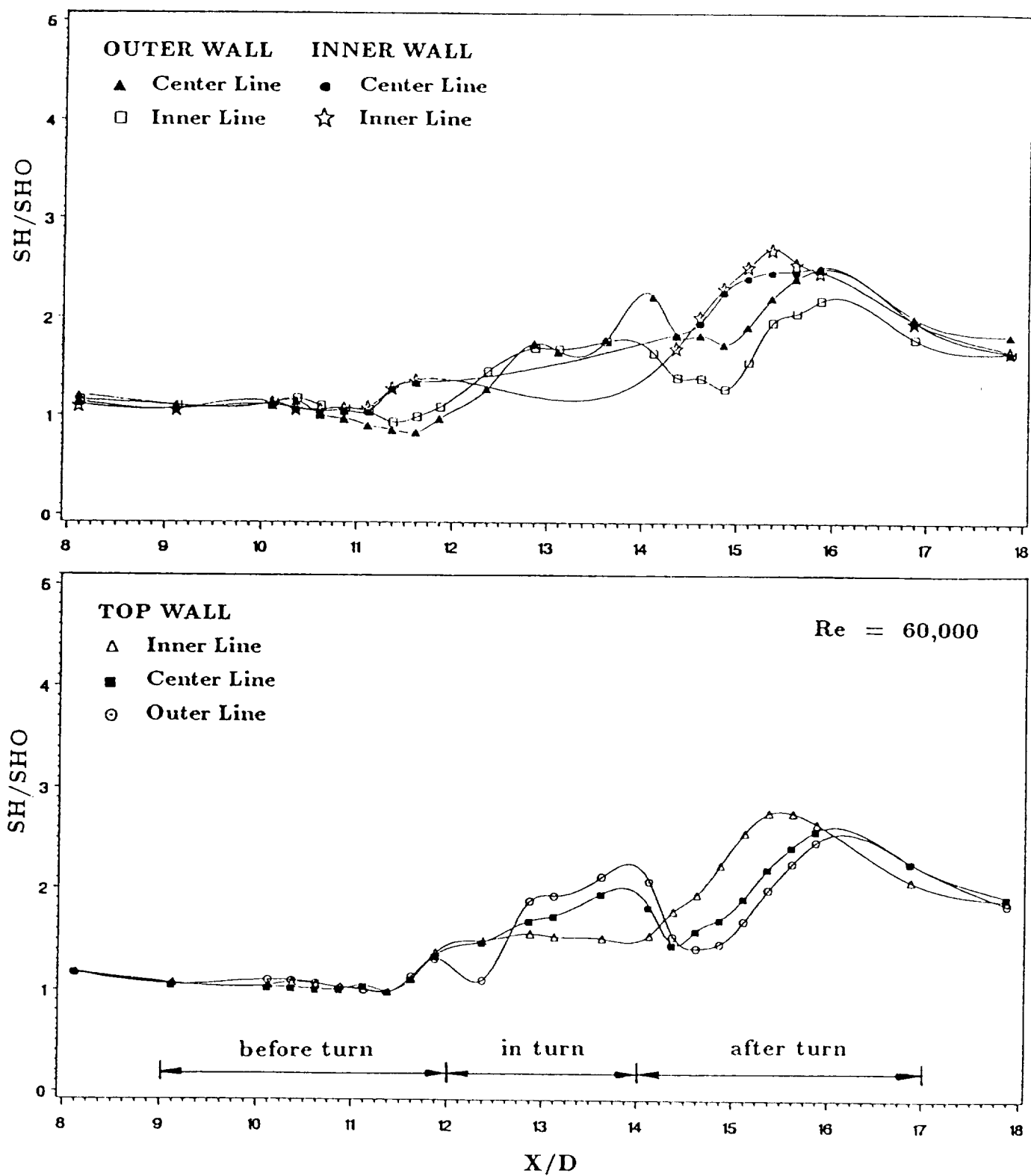


Fig. 6. The Local Sherwood No. Ratio for Smooth Channel with $Re=60,000$

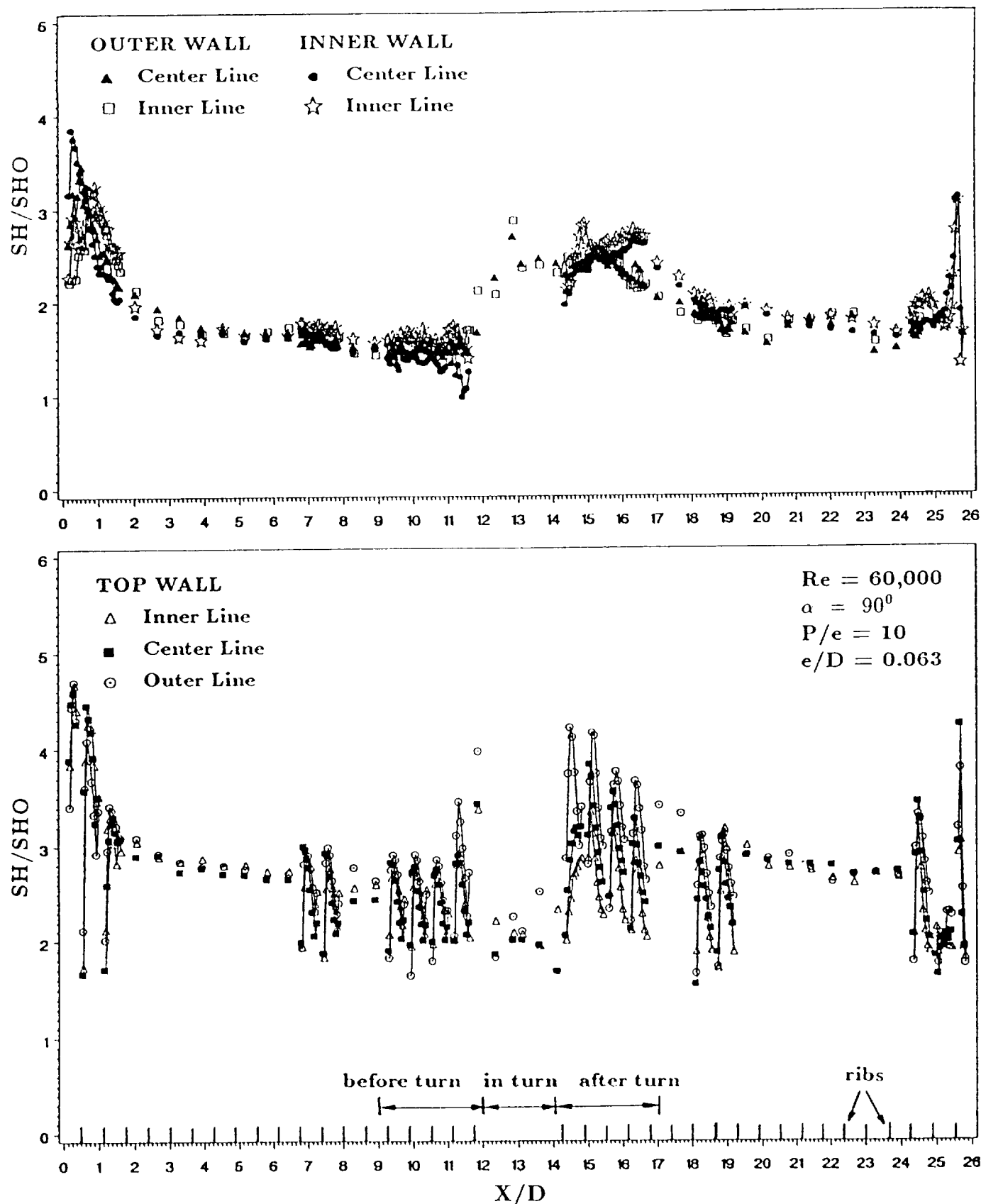


Fig. 7. The Local Sherwood No. Ratio for Ribbed Channel
with $e/D=0.063$, $P/e=10$, and $Re=60,000$

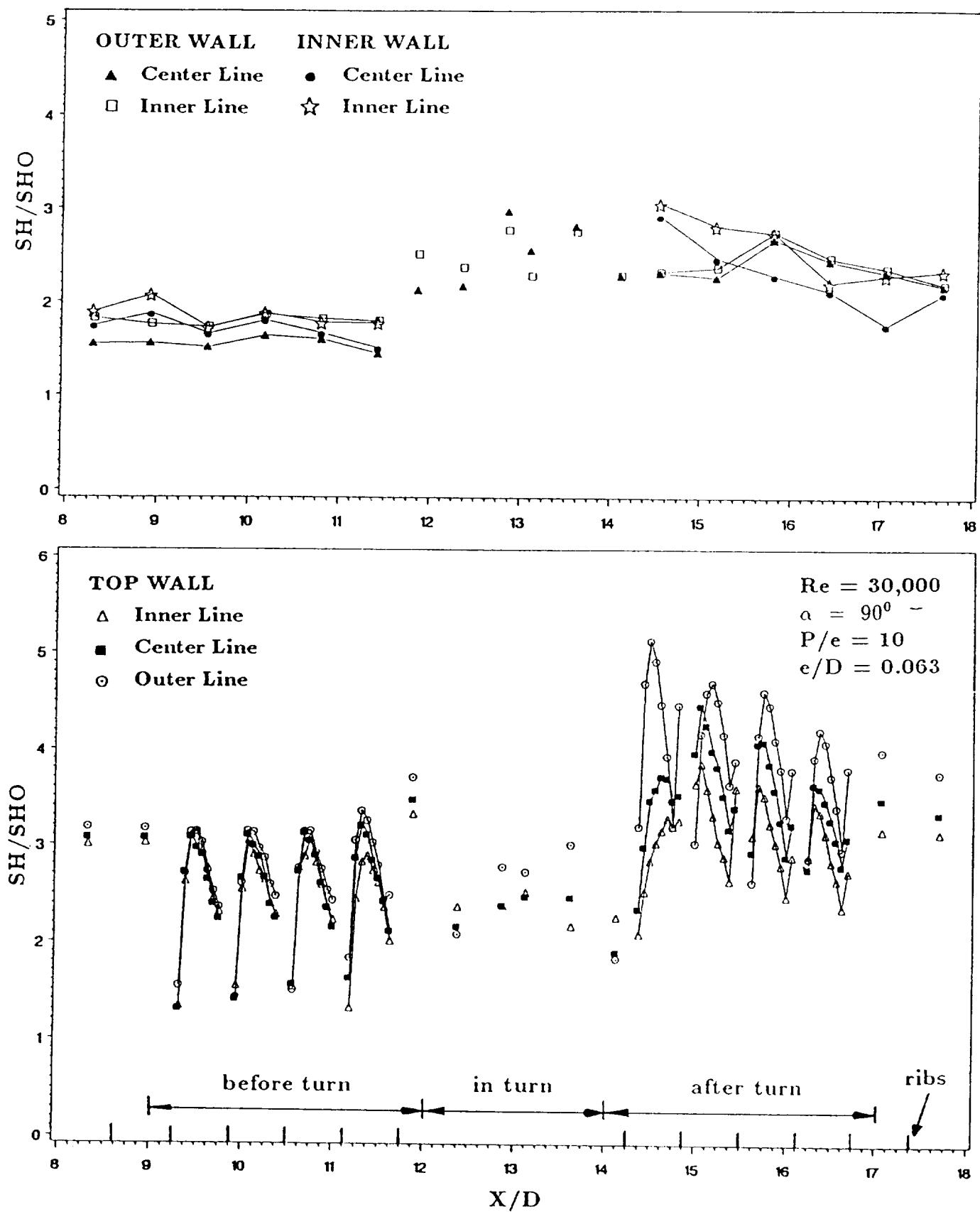


Fig. 8. The Local Sherwood No. Ratio for Ribbed Channel
 with $e/D=0.063$, $P/e=10$, and $Re=30,000$

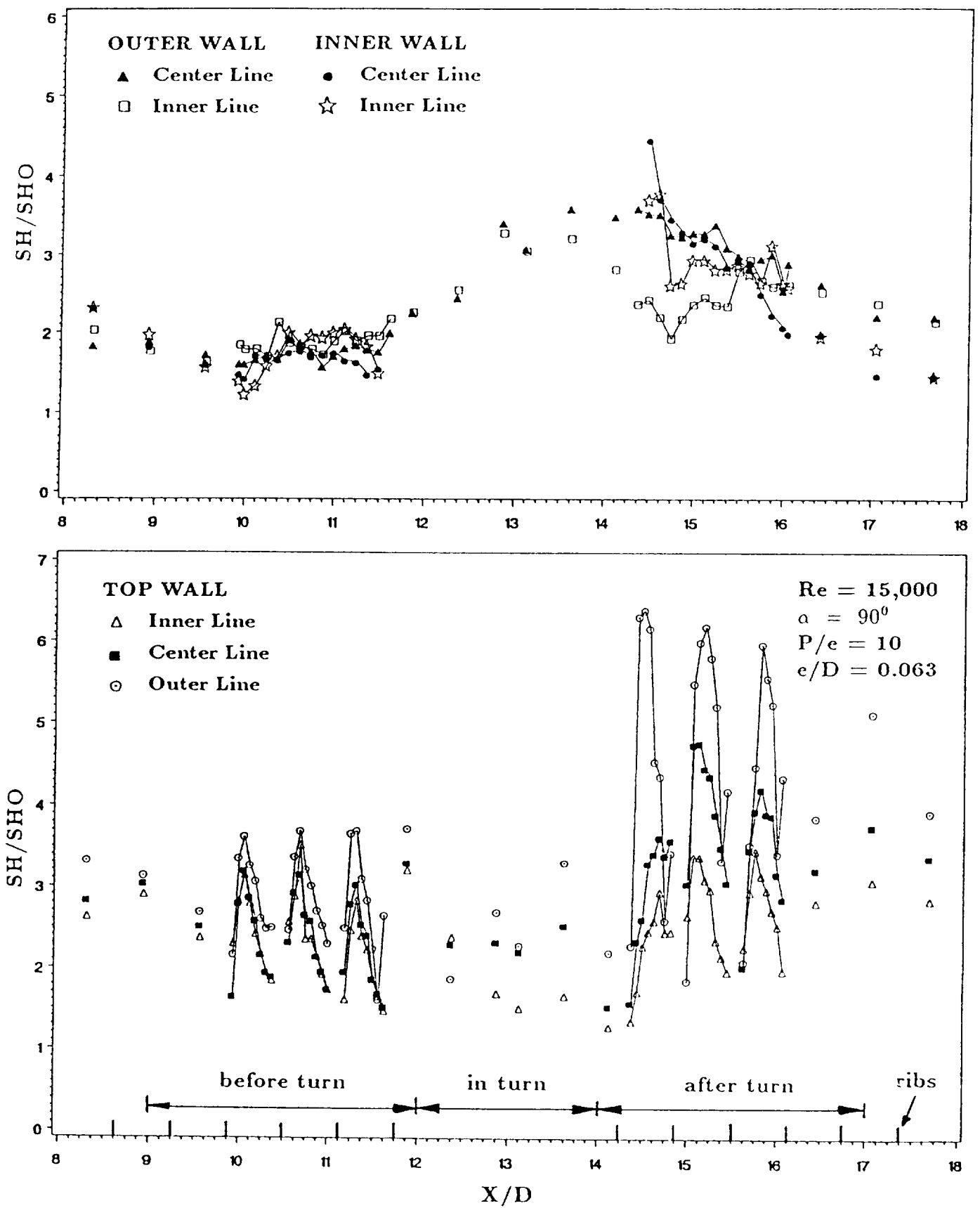


Fig. 9. The Local Sherwood No. Ratio for Ribbed Channel
 with $e/D=0.063$, $P/e=10$, and $Re=15.000$

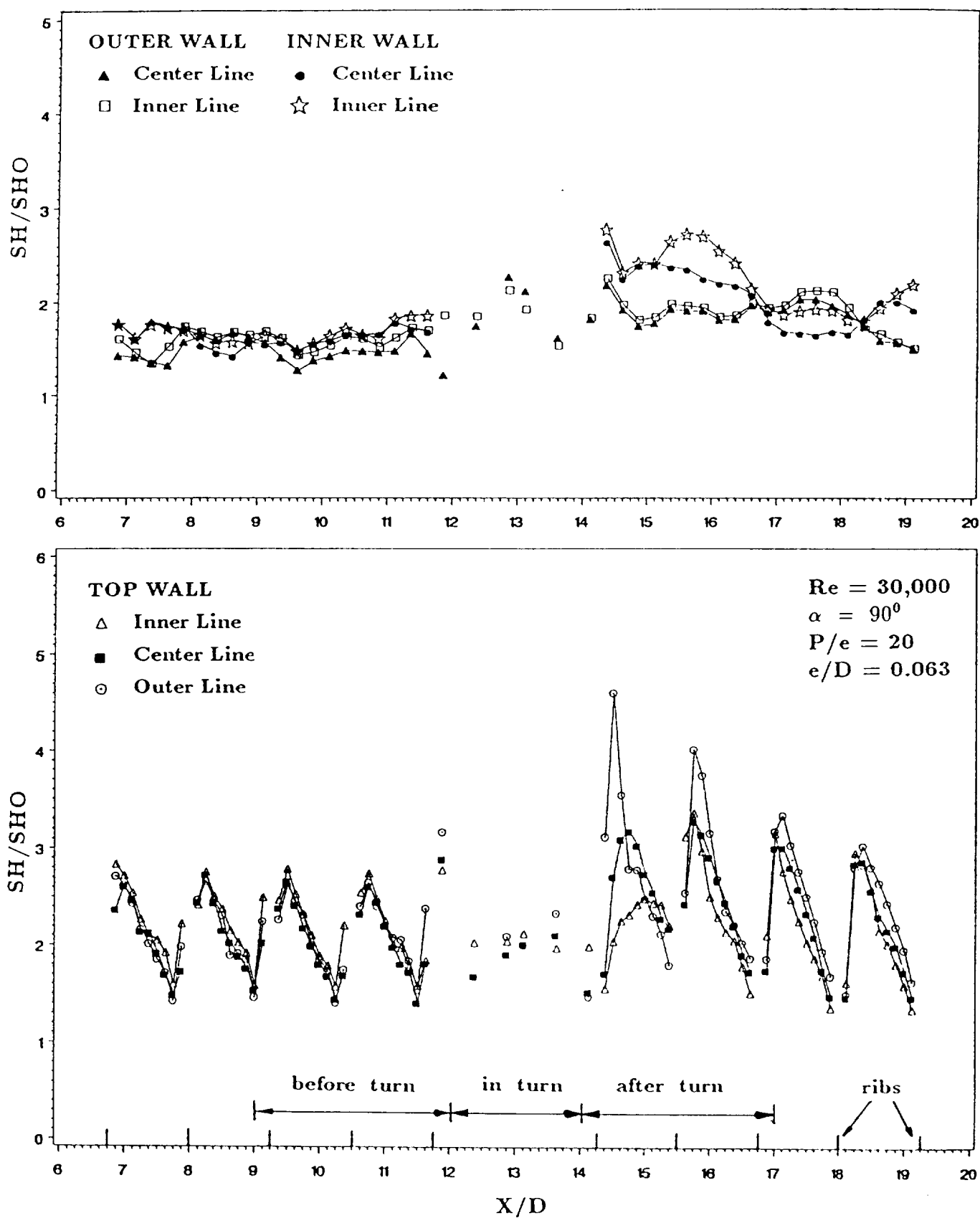


Fig. 10. The Local Sherwood No. Ratio for Ribbed Channel
with $e/D=0.063$, $P/e=20$, and $Re=30,000$

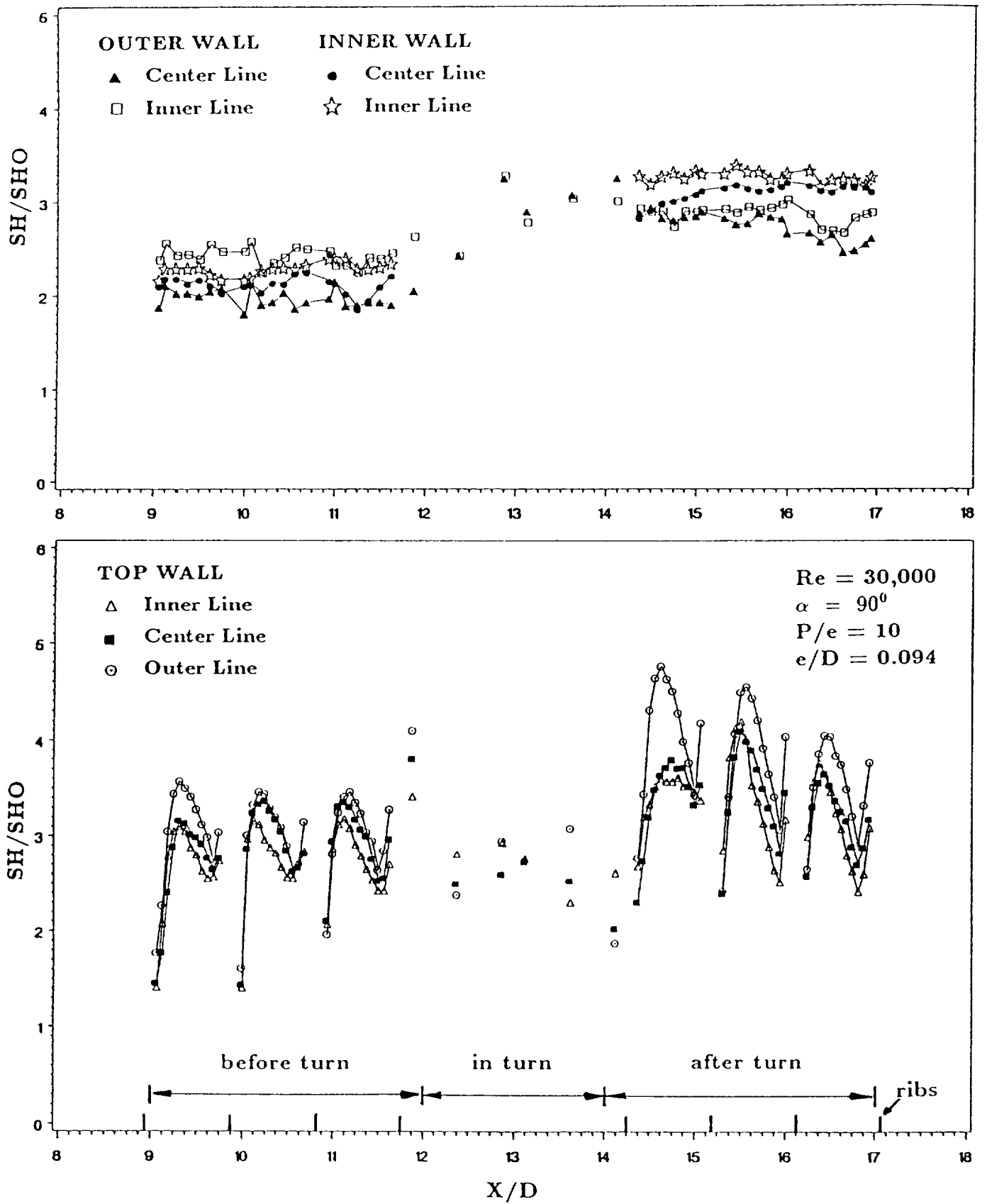


Fig. 11. The Local Sherwood No. Ratio for Ribbed Channel
 with $e/D=0.094$, $P/e=10$, and $Re=30,000$

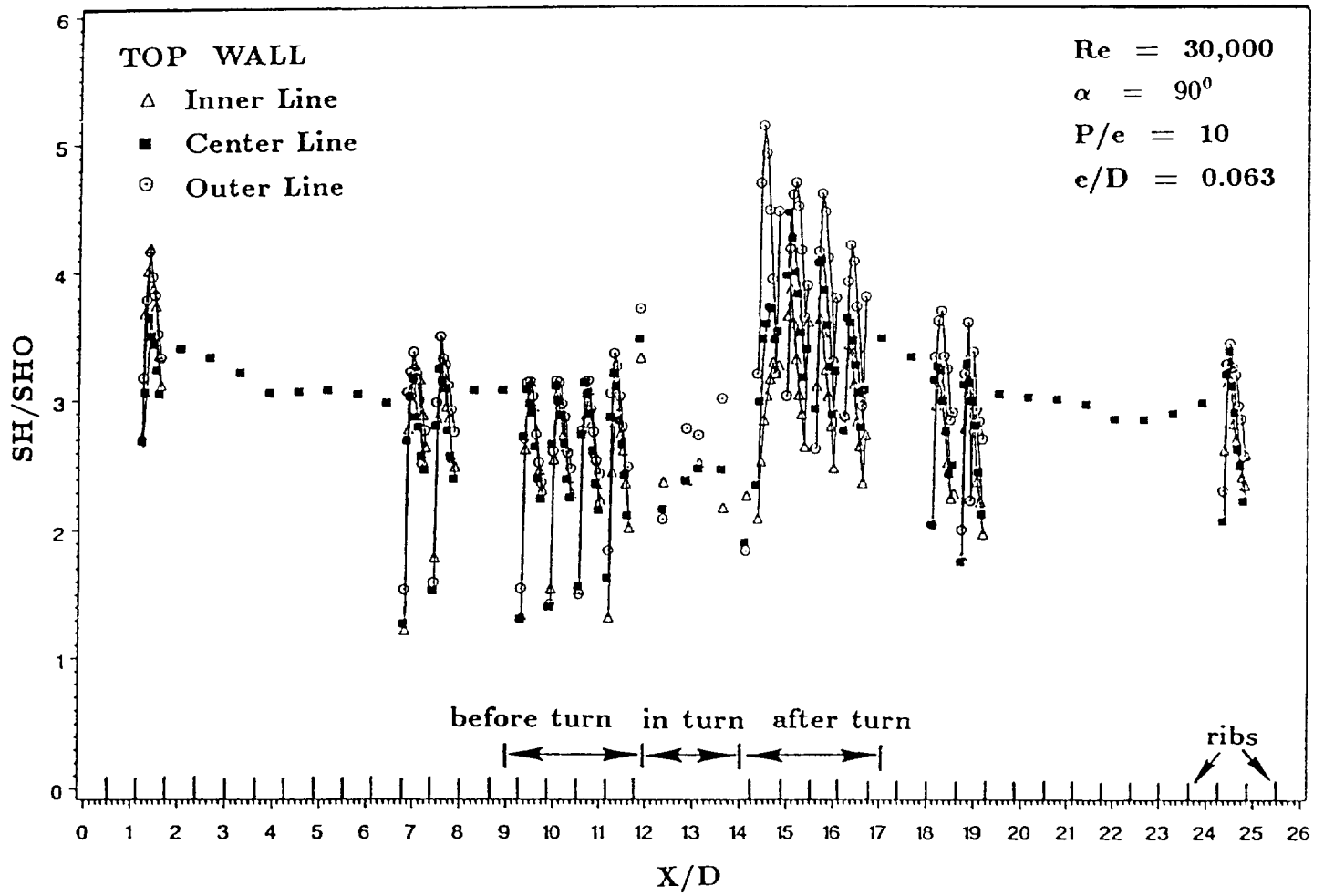


Fig. 12. The local Sherwood no. ratio with $\alpha = 90^\circ$ and $Re=30,000$

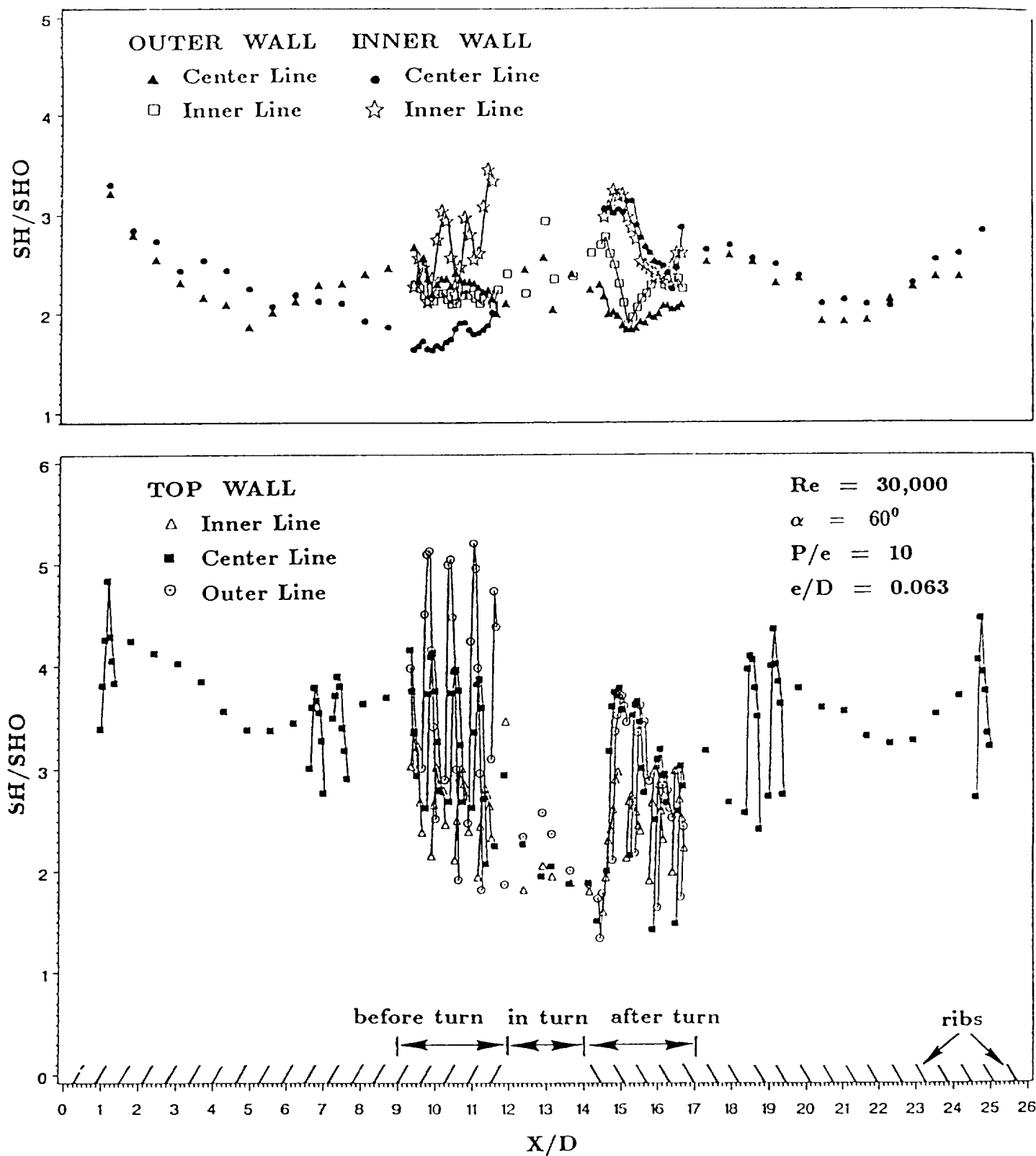


Fig. 13. The local Sherwood no. ratio with $\alpha = 60^\circ$ and $Re=30,000$

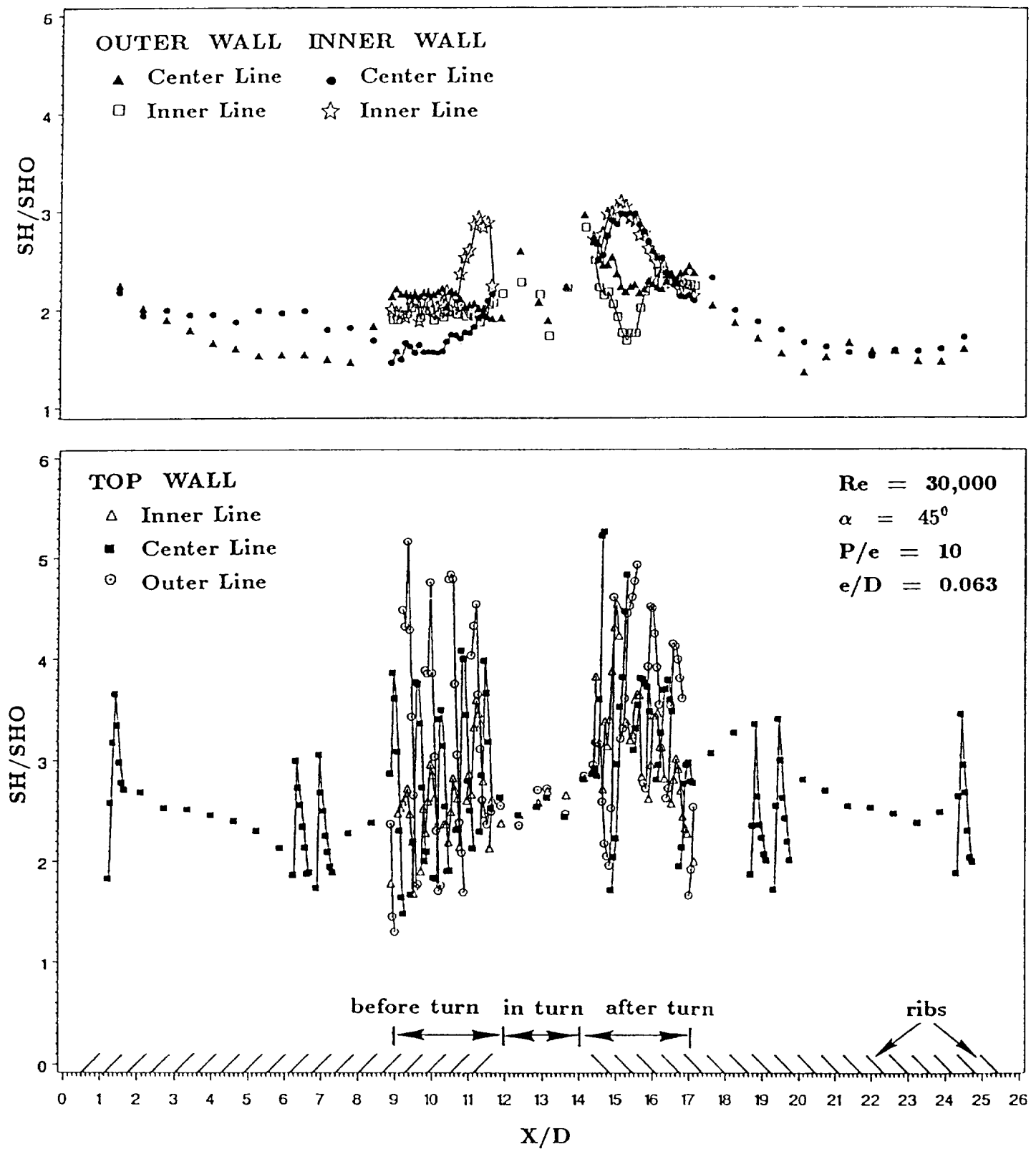
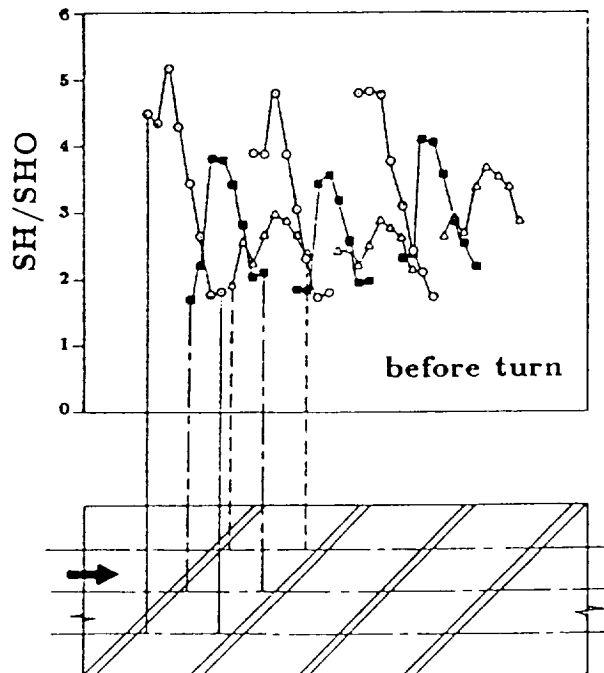
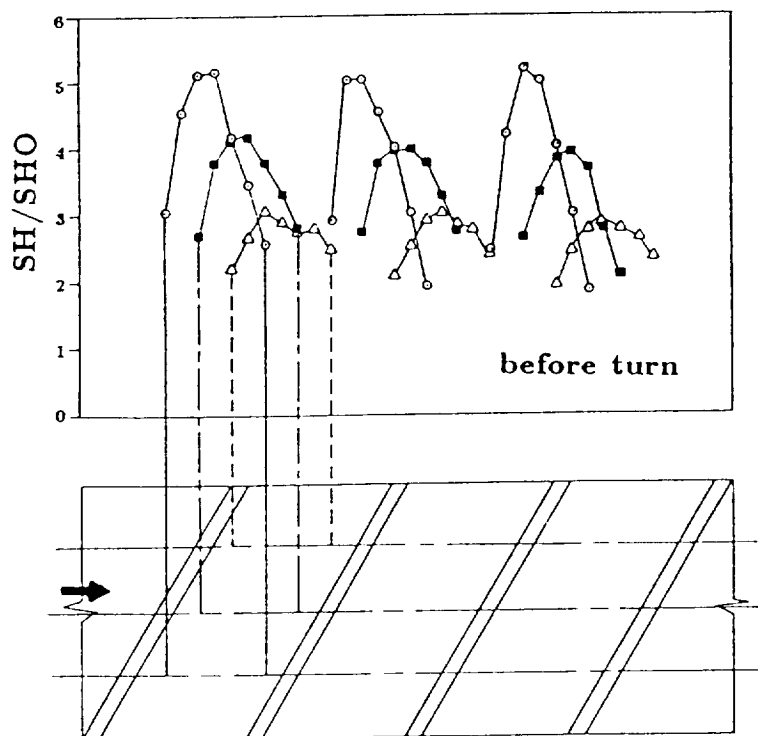
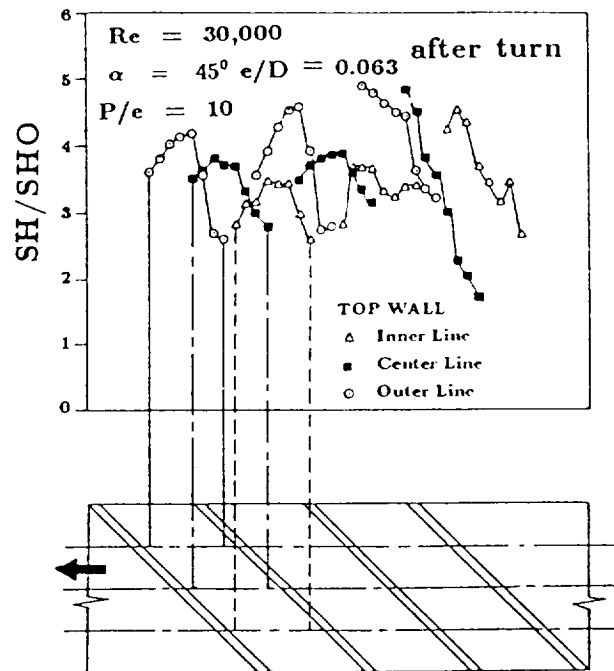
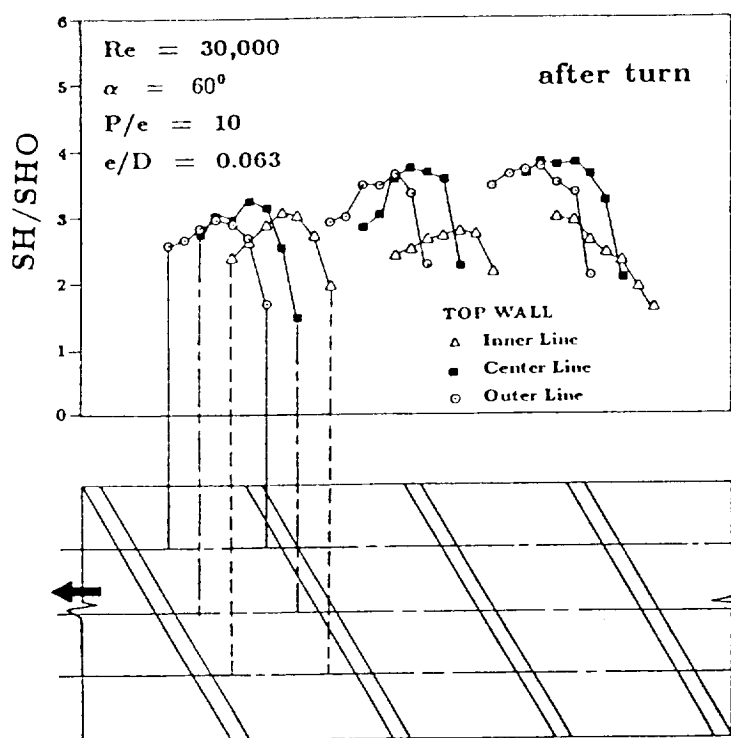


Fig. 14. The local Sherwood no. ratio with $\alpha = 45^\circ$ and $Re=30,000$



(a)

(b)

Fig. 15. The detailed Sherwood no. ratios on the top wall with $Re=30,000$, (a) $\alpha = 60^\circ$; (b) $\alpha = 45^\circ$

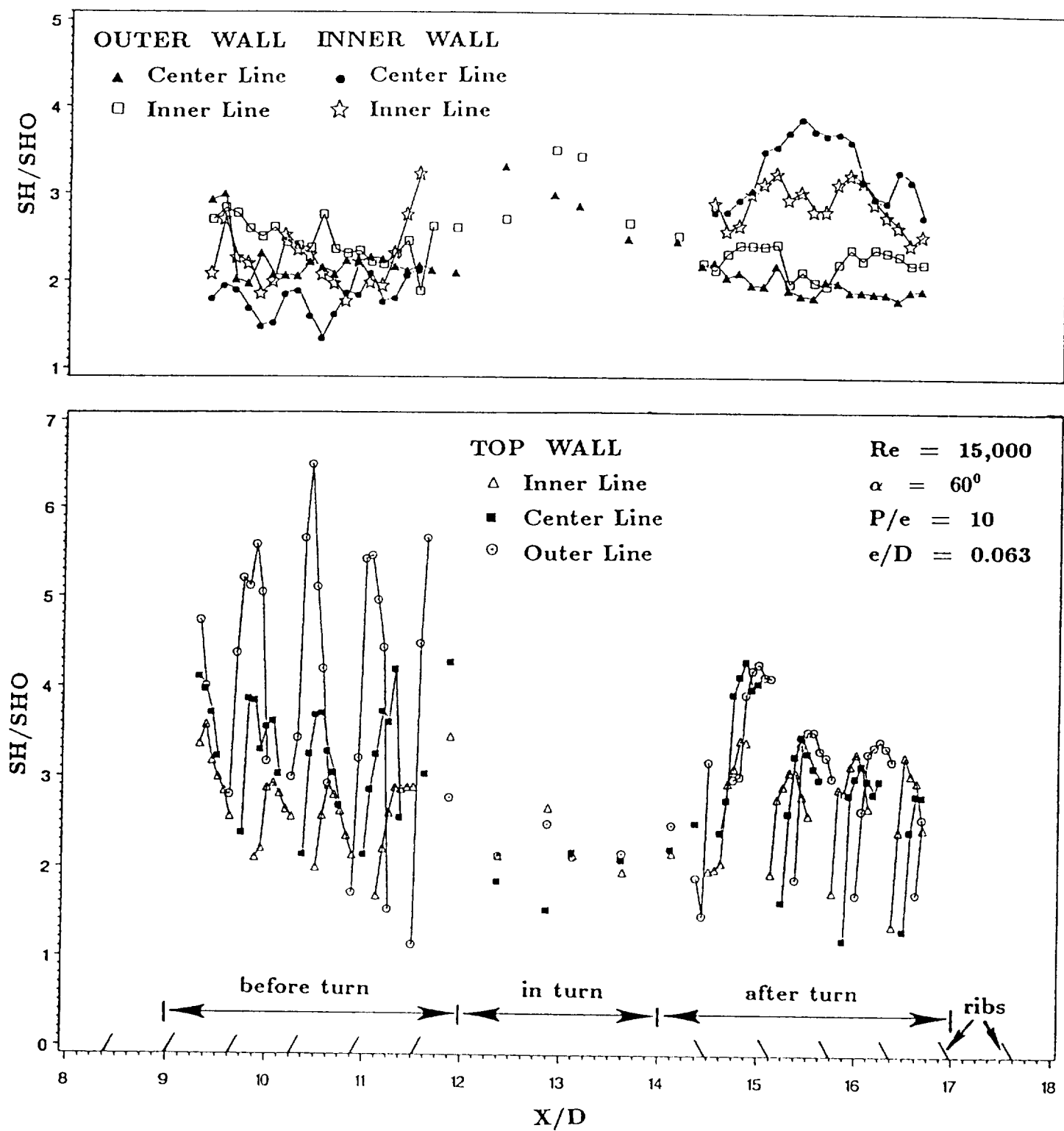


Fig. 16. The local Sherwood no. ratio with $\alpha = 60^\circ$ and $Re=15,000$

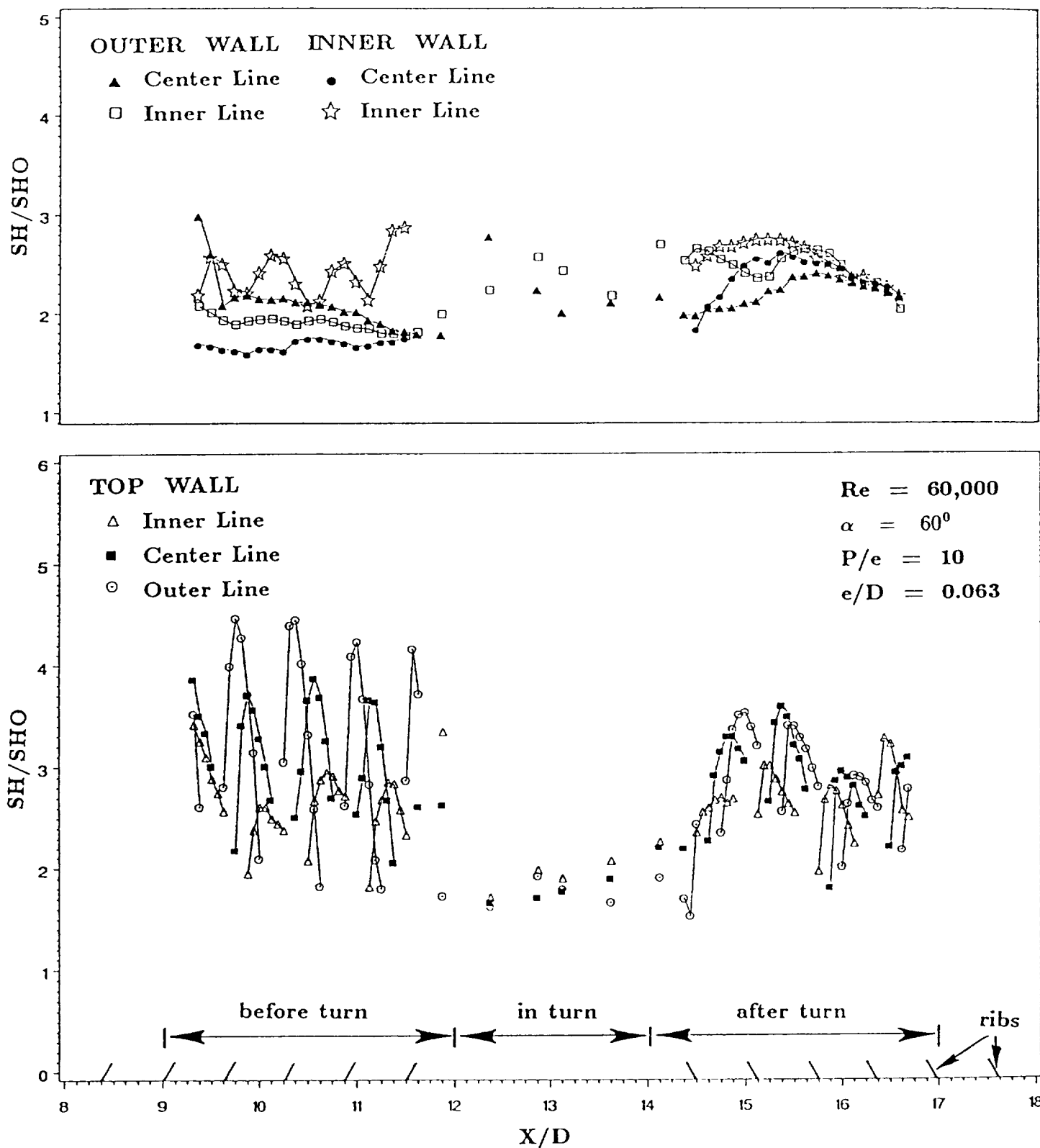


Fig. 17. The local Sherwood no. ratio with $\alpha = 60^\circ$ and $Re=60,000$

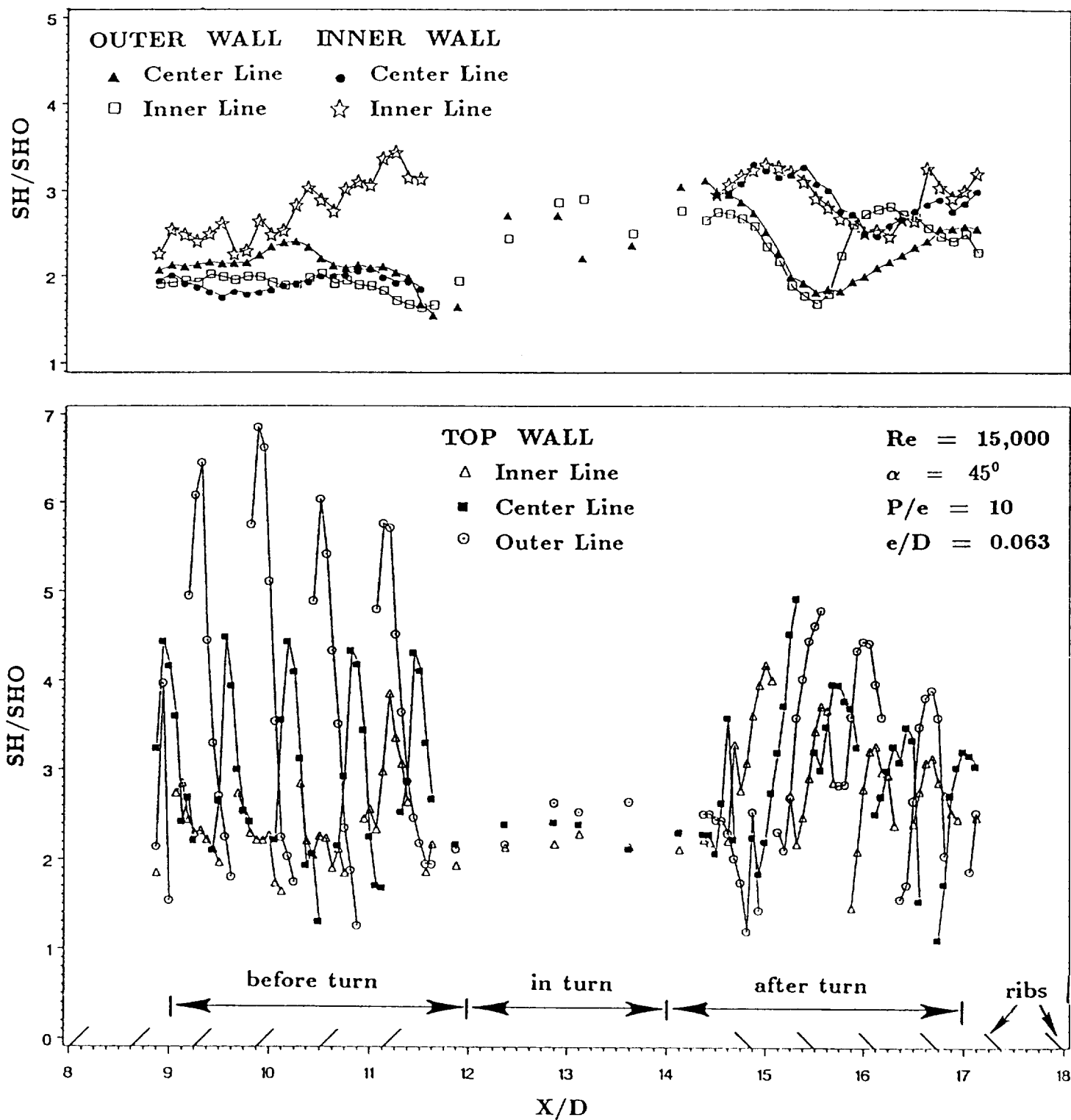


Fig. 18. The local Sherwood no. ratio with $\alpha = 45^\circ$ and $Re=15,000$

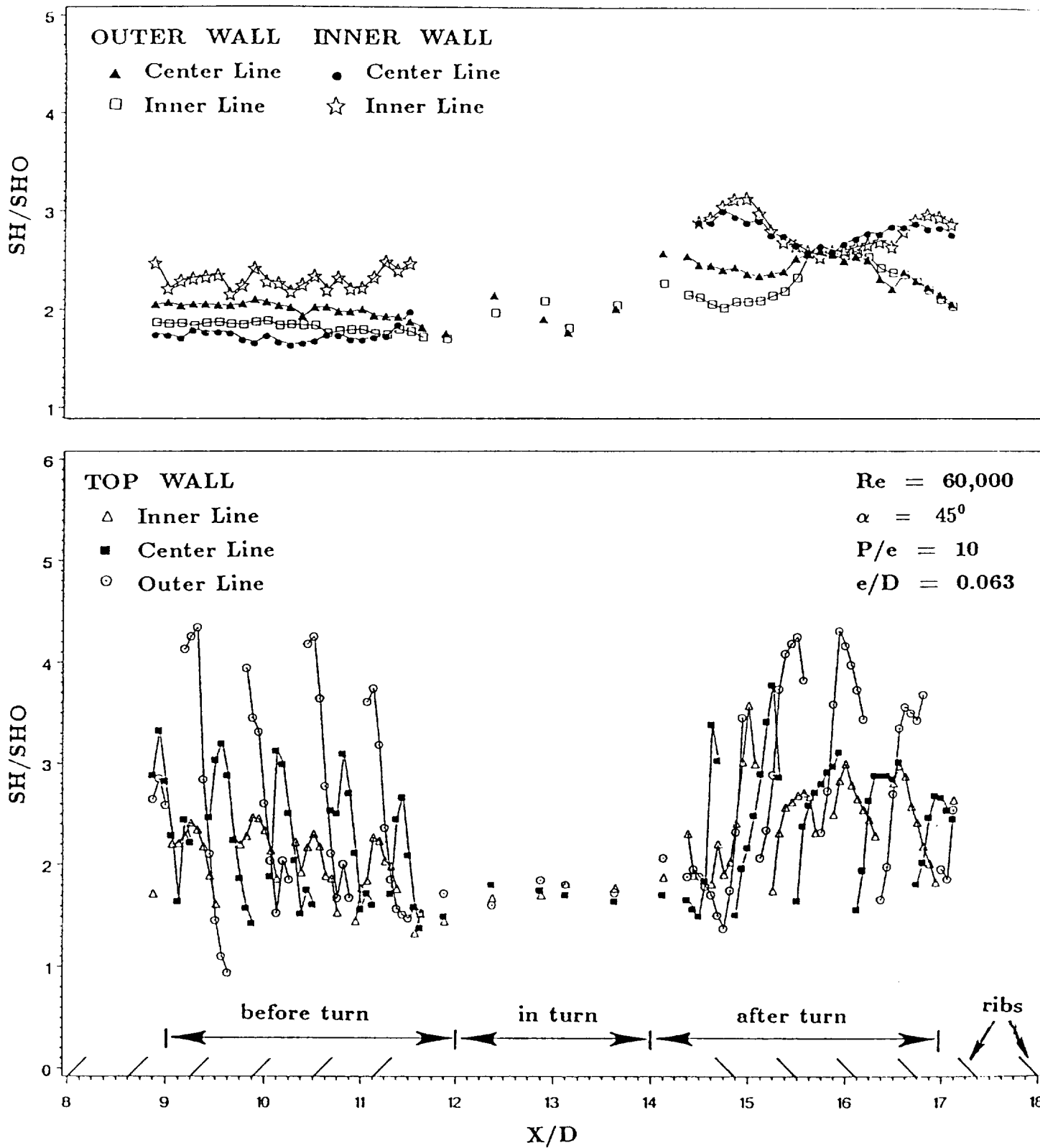


Fig. 19. The local Sherwood no. ratio with $\alpha = 45^\circ$ and $Re=60,000$

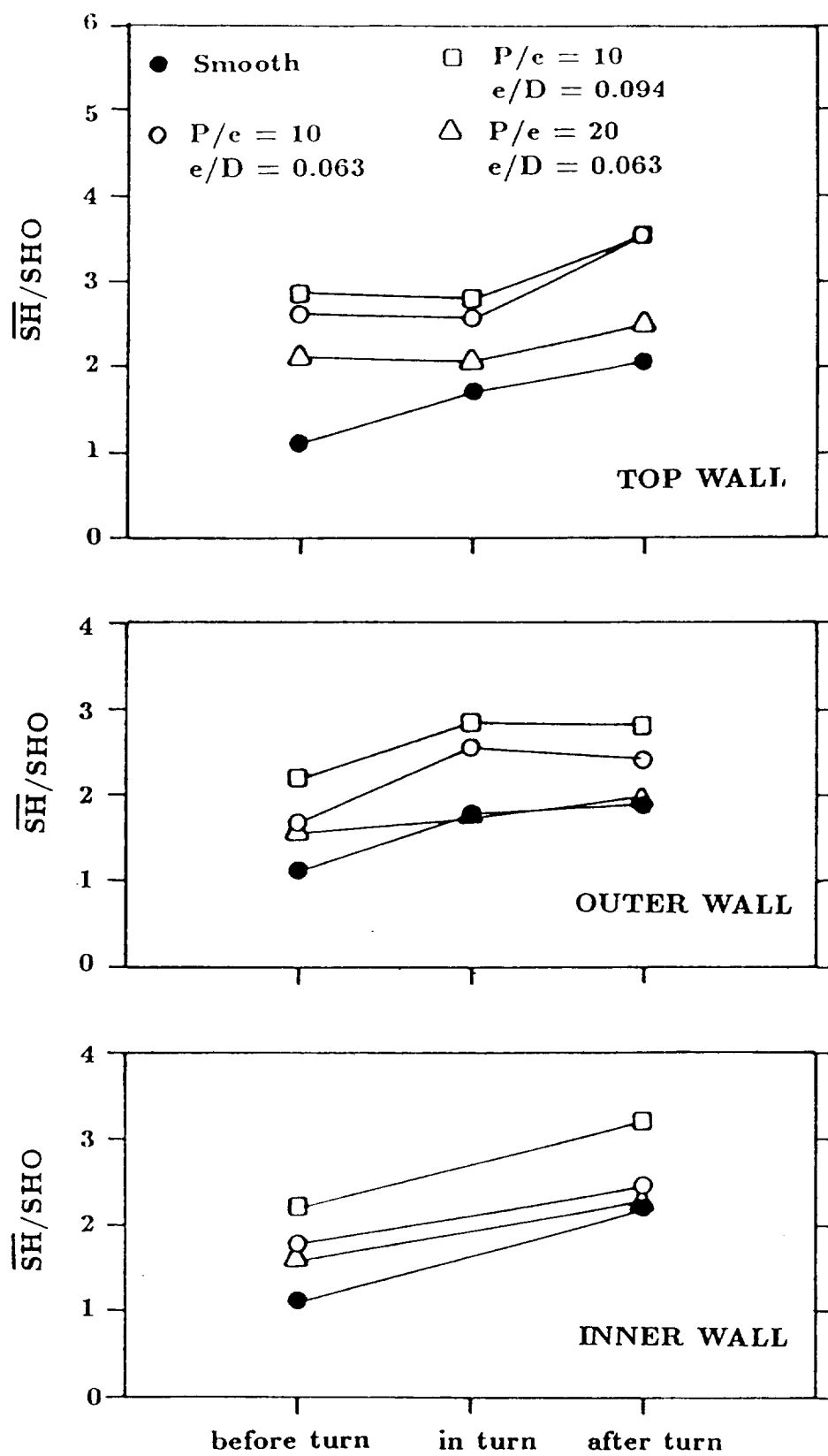


Fig. 20. The Average Sherwood No. Ratio on Each of the Channel Surfaces with $Re=30,000$

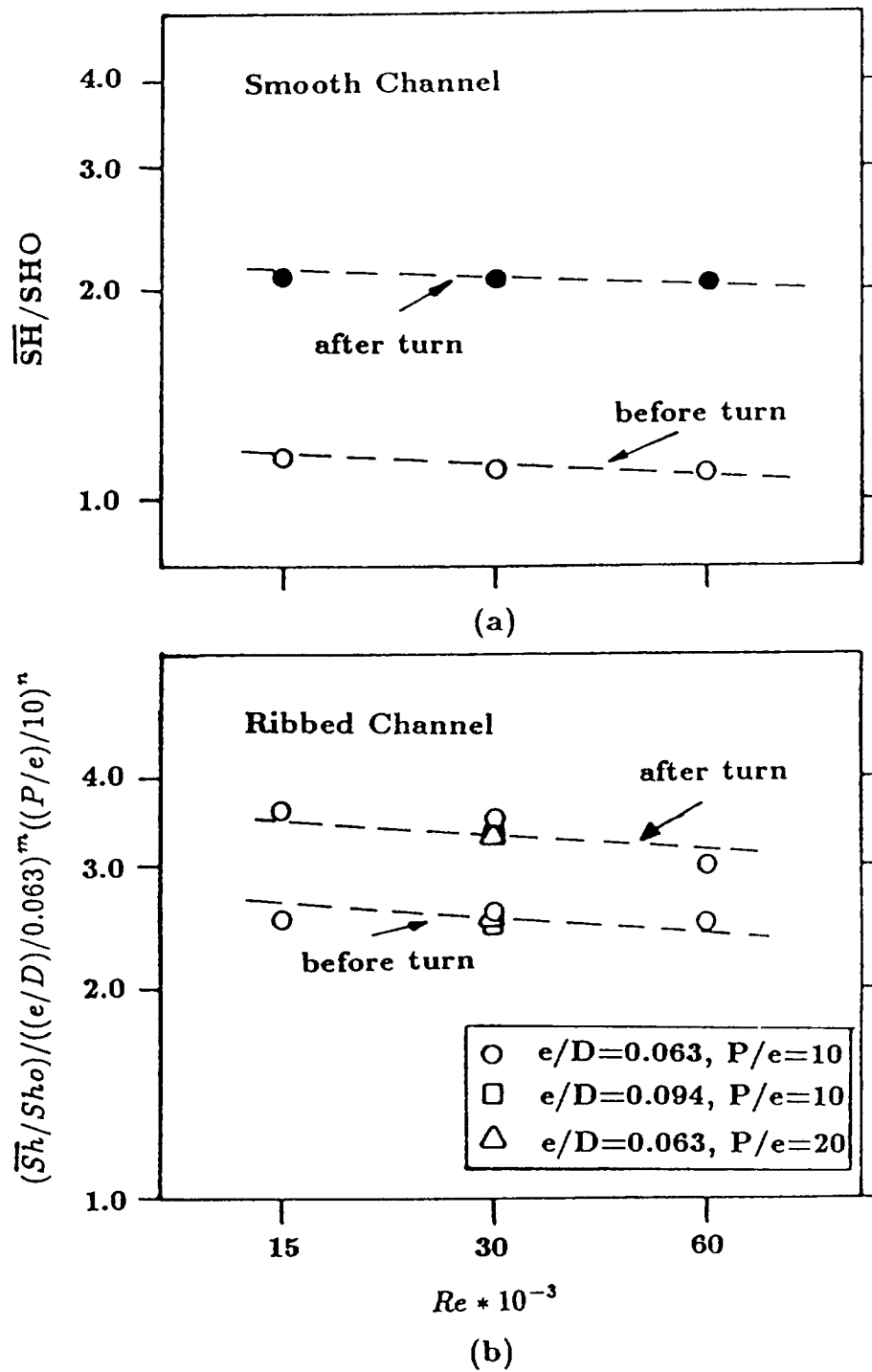


Fig. 21. Correlations of the Average Sherwood No. Ratio on the Top Wall

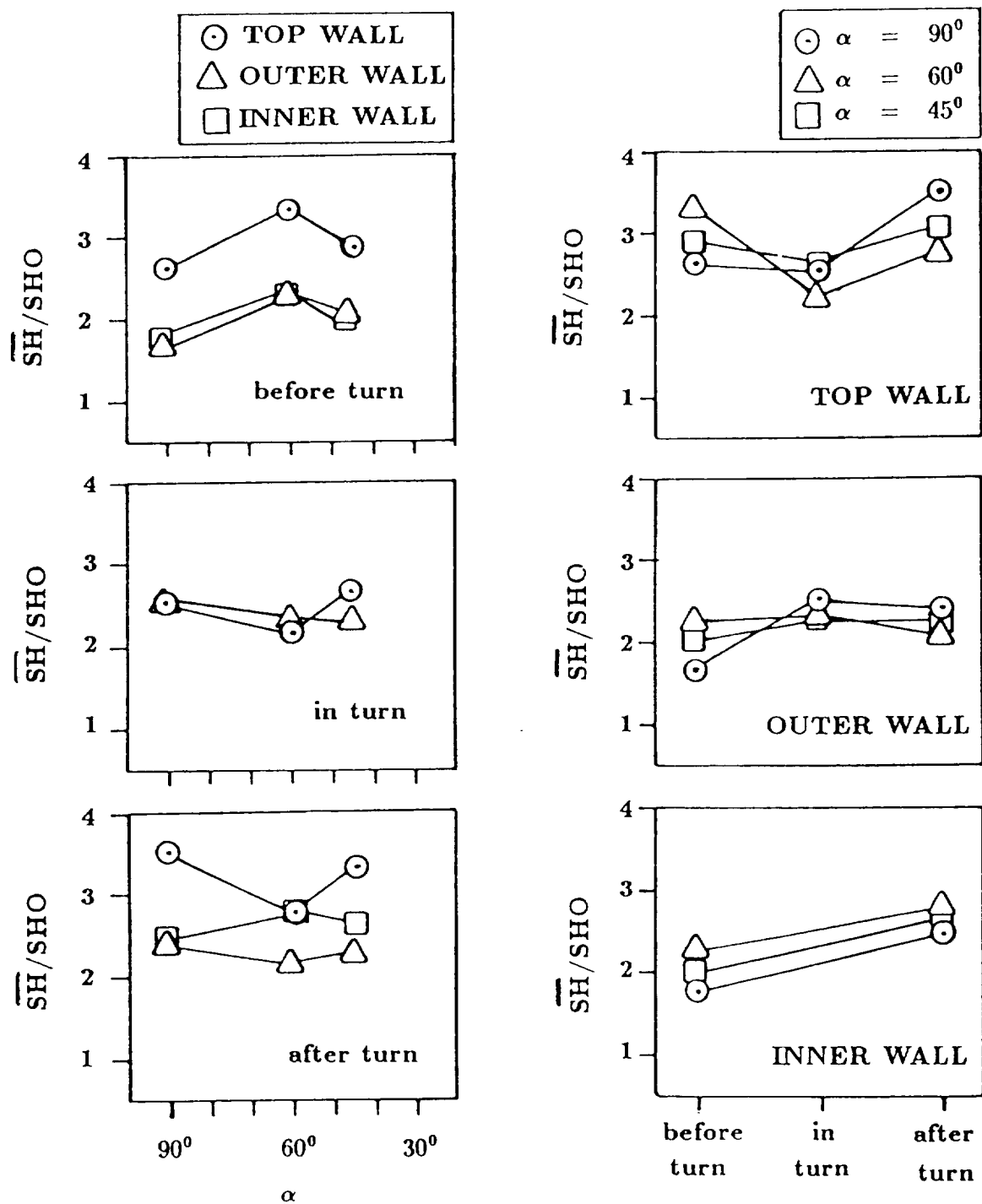


Fig. 22. The average Sherwood no. ratio on each of the channel surfaces with $Re=30,000$

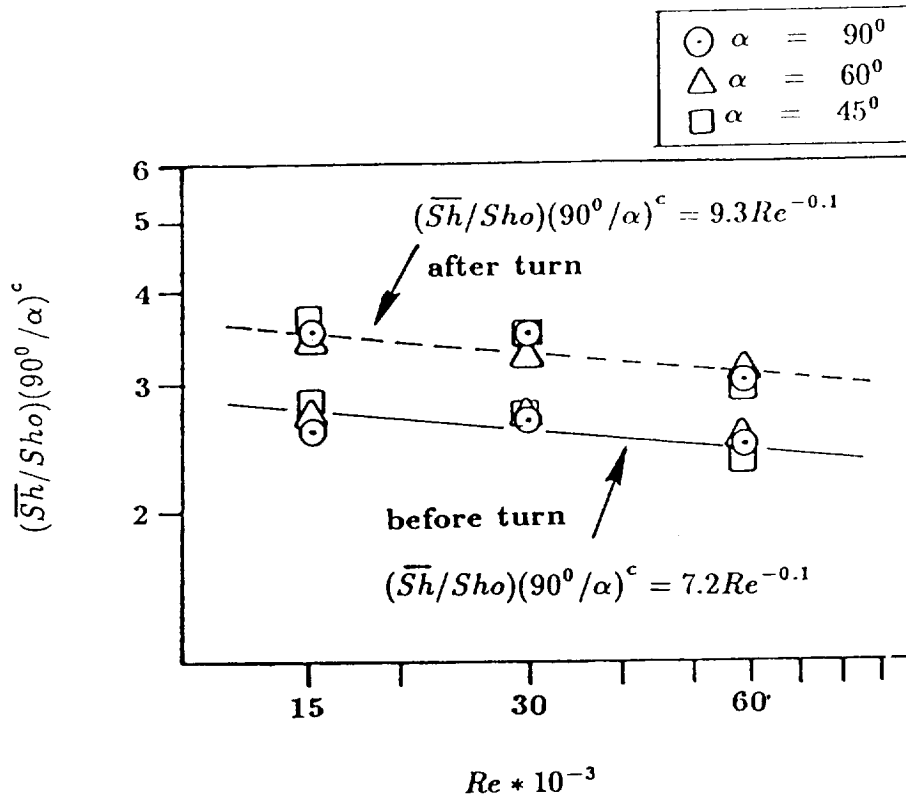


Fig. 23(a). Correlations of the average Sherwood no. ratio on the top wall with rib angles

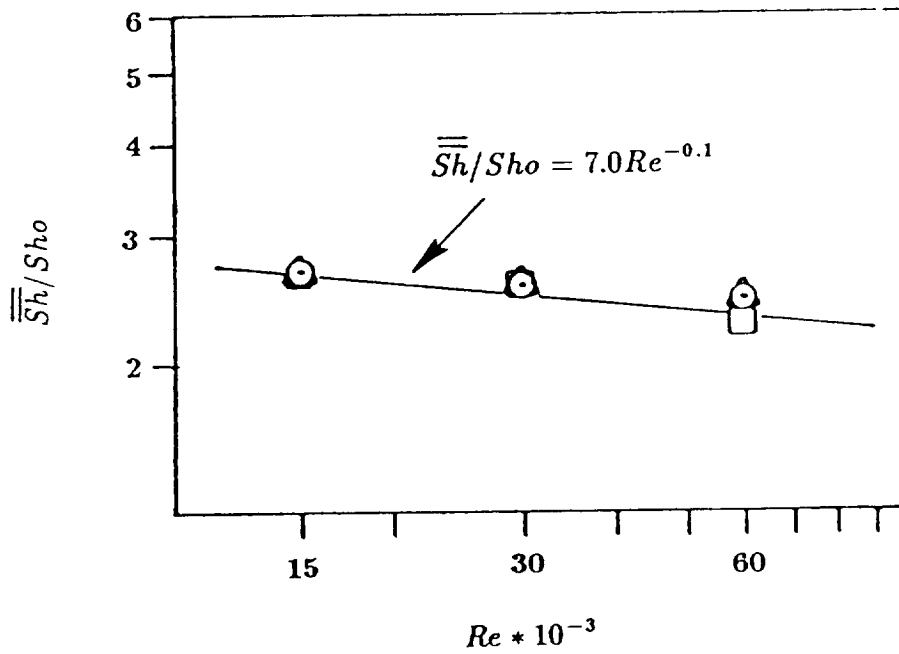


Fig. 23(b). Correlations of the overall average Sherwood no. ratio on all surfaces with rib angles

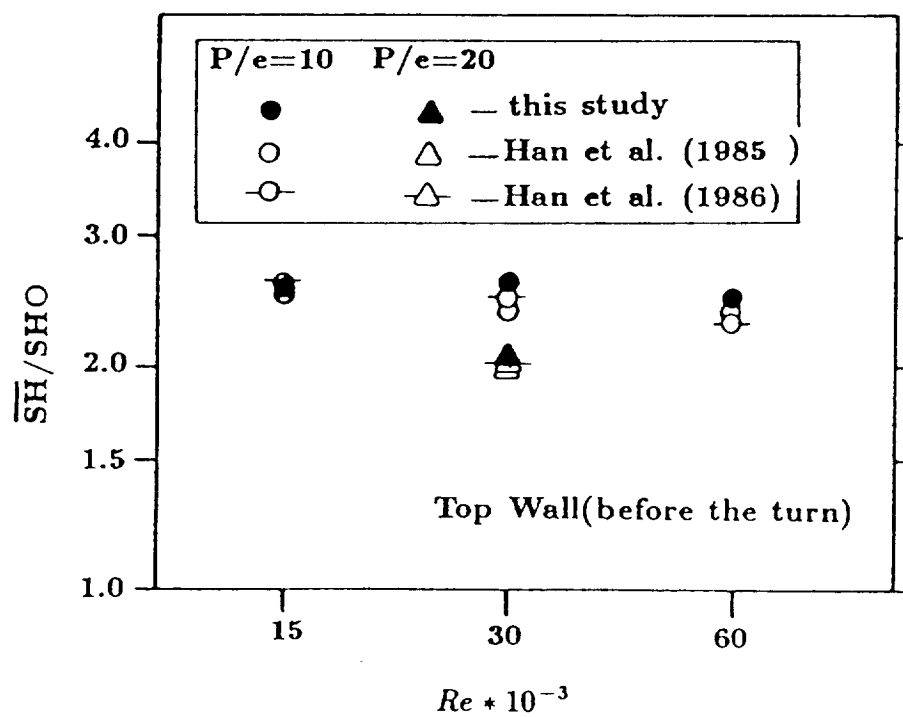
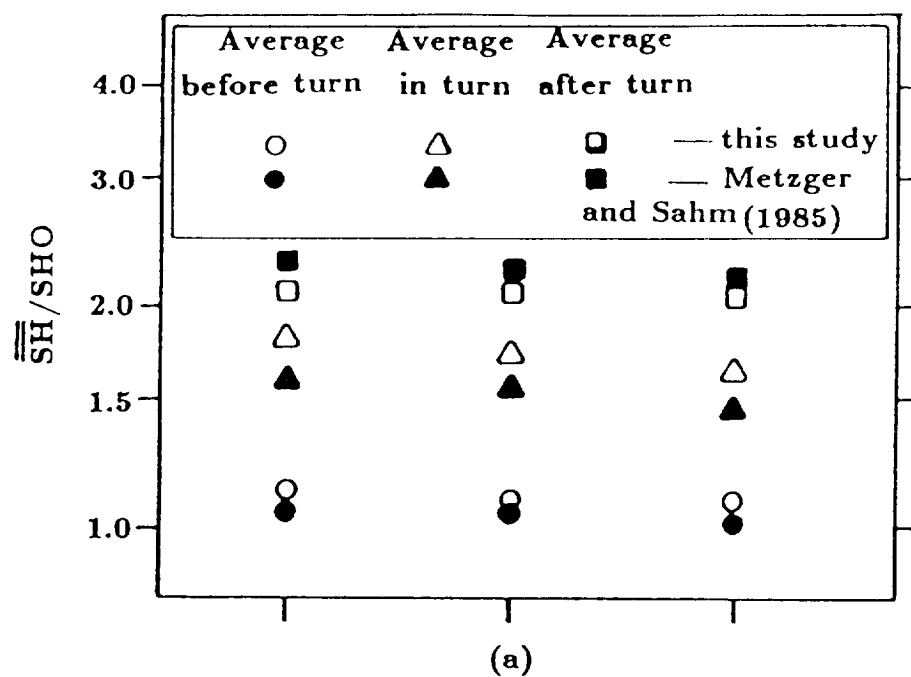


Fig. 24. Comparison between the present results and the published heat transfer data

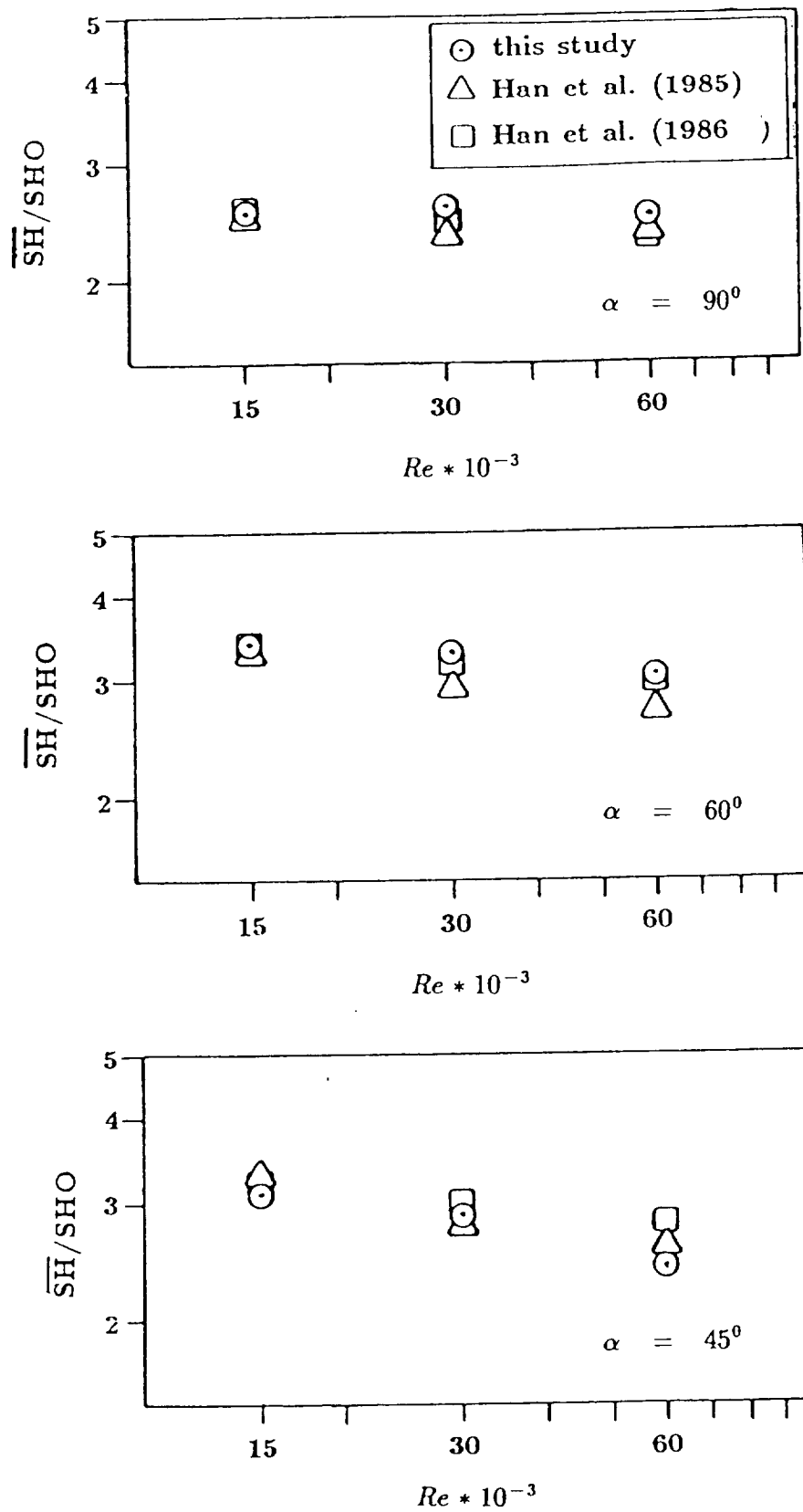
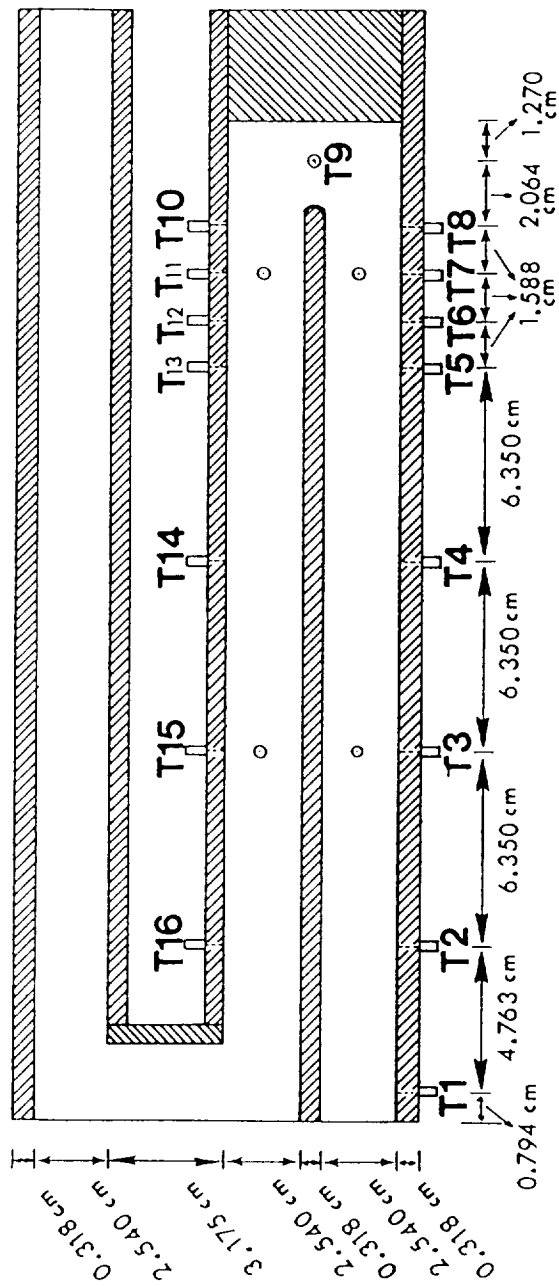


Fig. 25. Comparison between the present results on the top wall(before the turn) and the published heat transfer data

TOP VIEW



SIDE VIEW

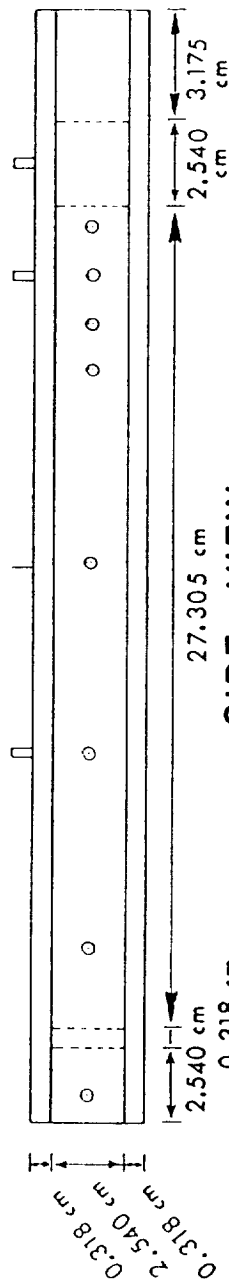


Fig. 26. Schematics of the test section for the pressure drop experiments.

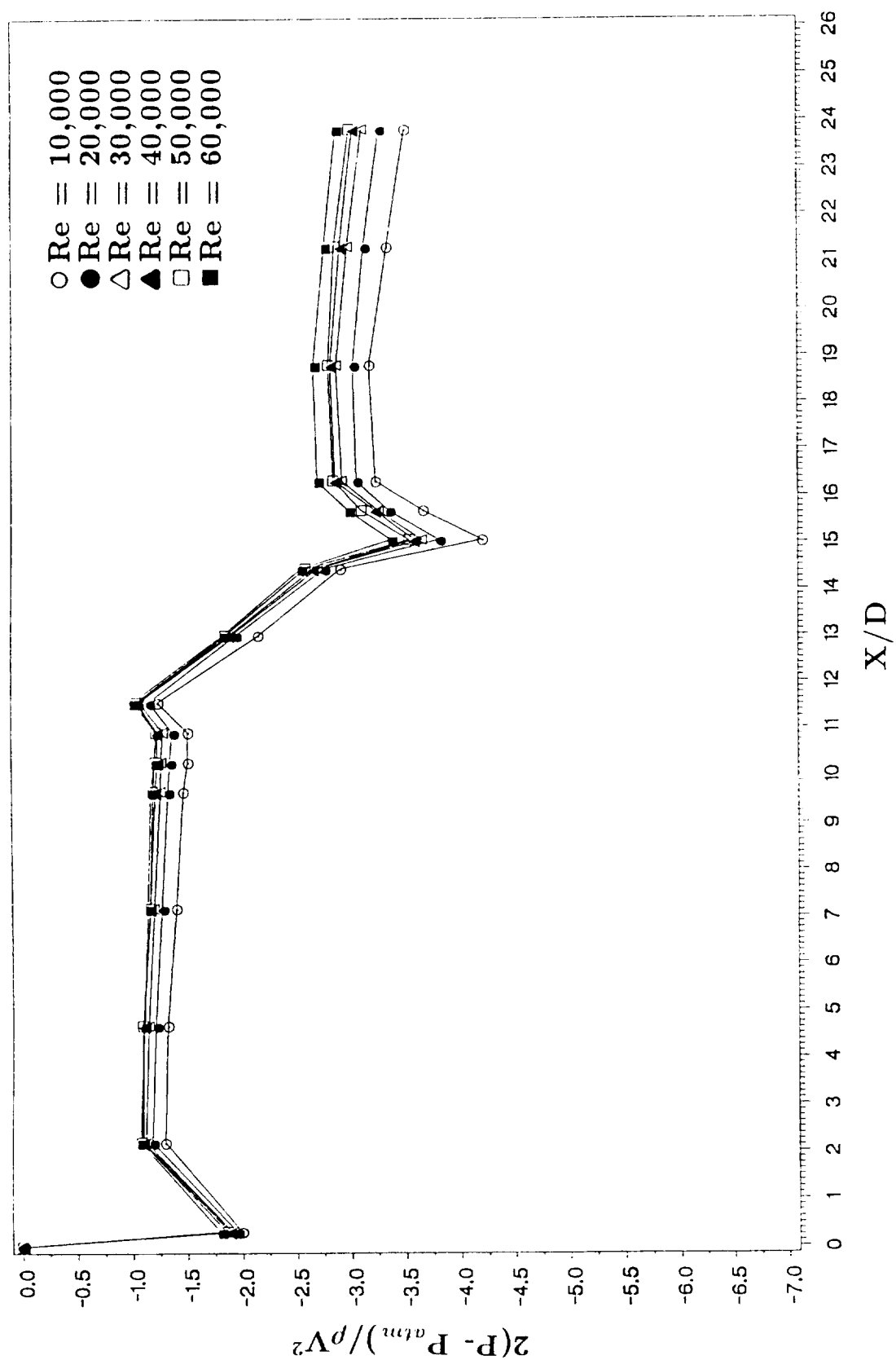


Fig. 27. Dimensionless pressure drop for smooth channel.

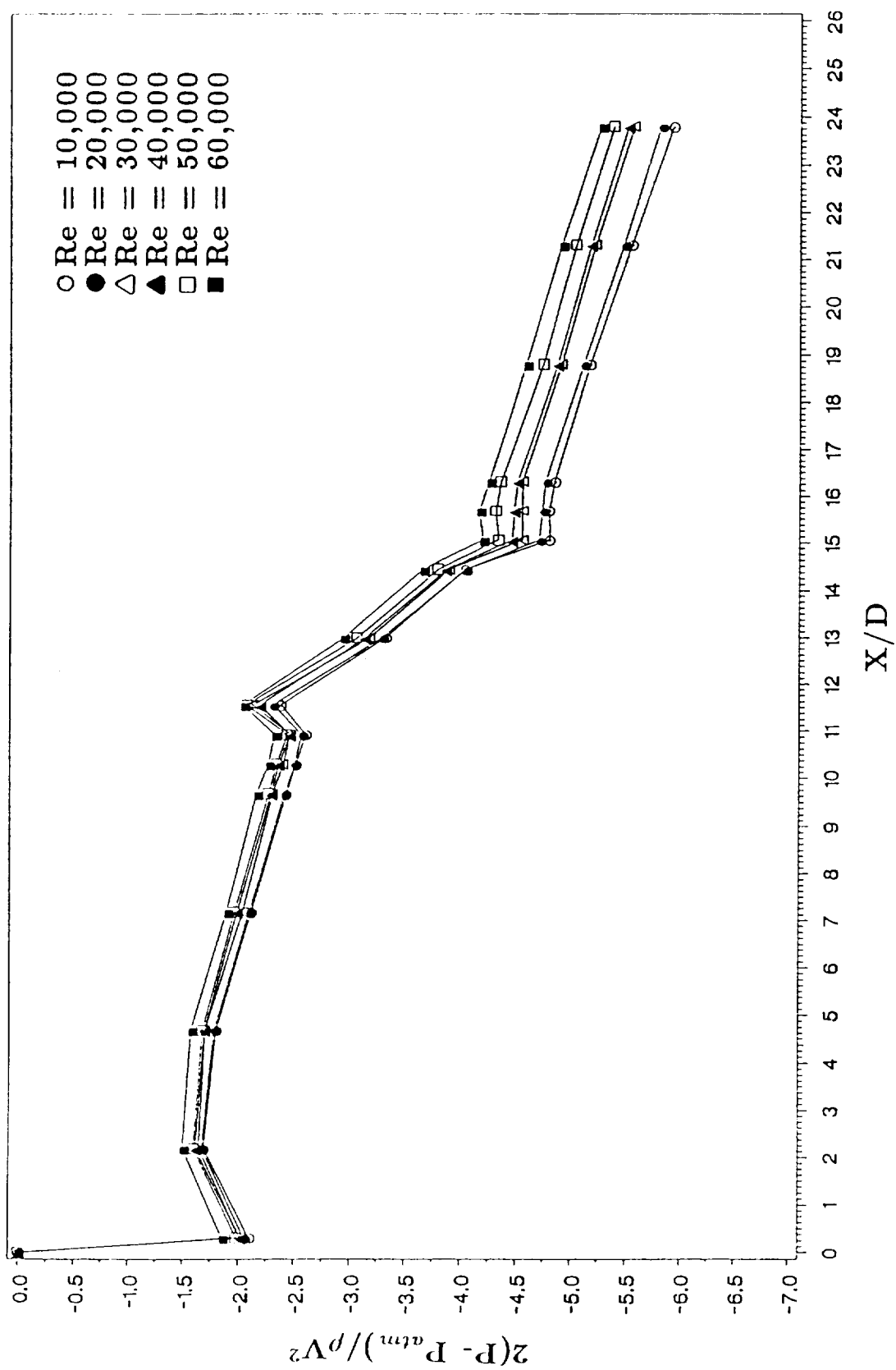


Fig. 28. Dimensionless pressure drop for rough channel
with $P/e=10$, $e/D=0.063$, and $\alpha = 90^\circ$

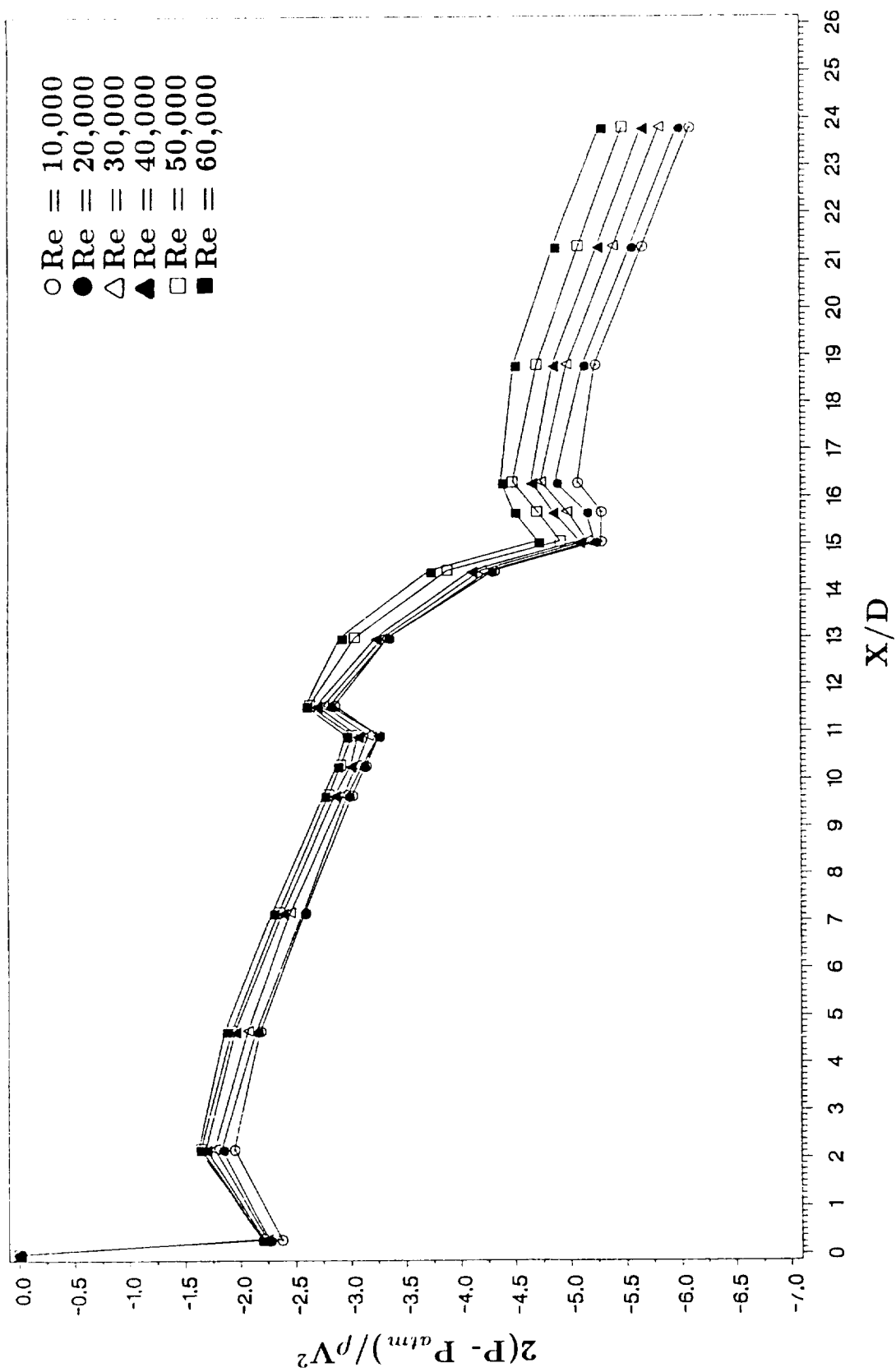


Fig. 29. Dimensionless pressure drop for rough channel
with $P/e=10$, $e/D=0.063$, and $\alpha = 60^\circ$.

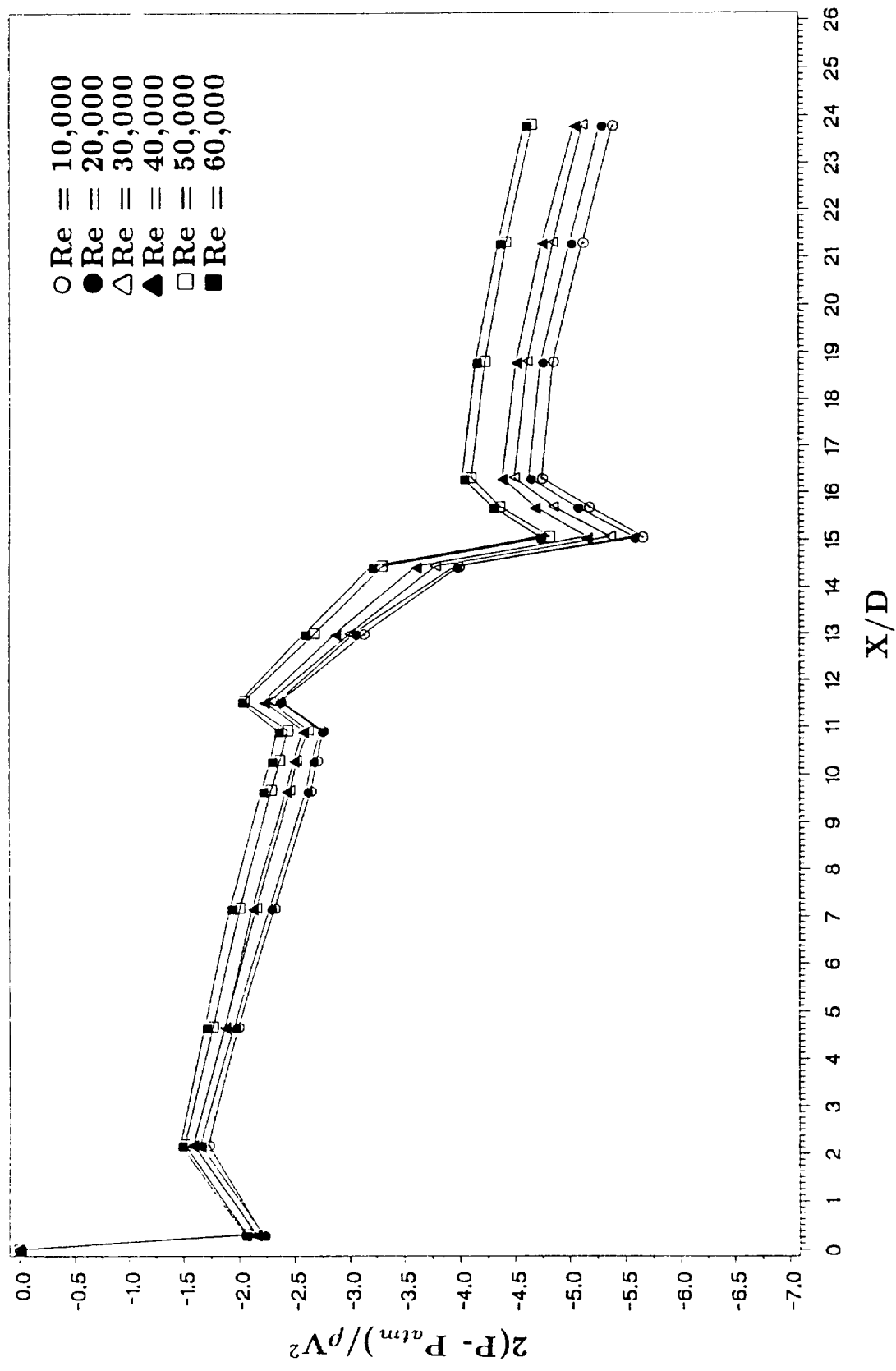


Fig. 30. Dimensionless pressure drop for rough channel
with $P/e=10$, $e/D=0.063$, and $\alpha = 45^\circ$.

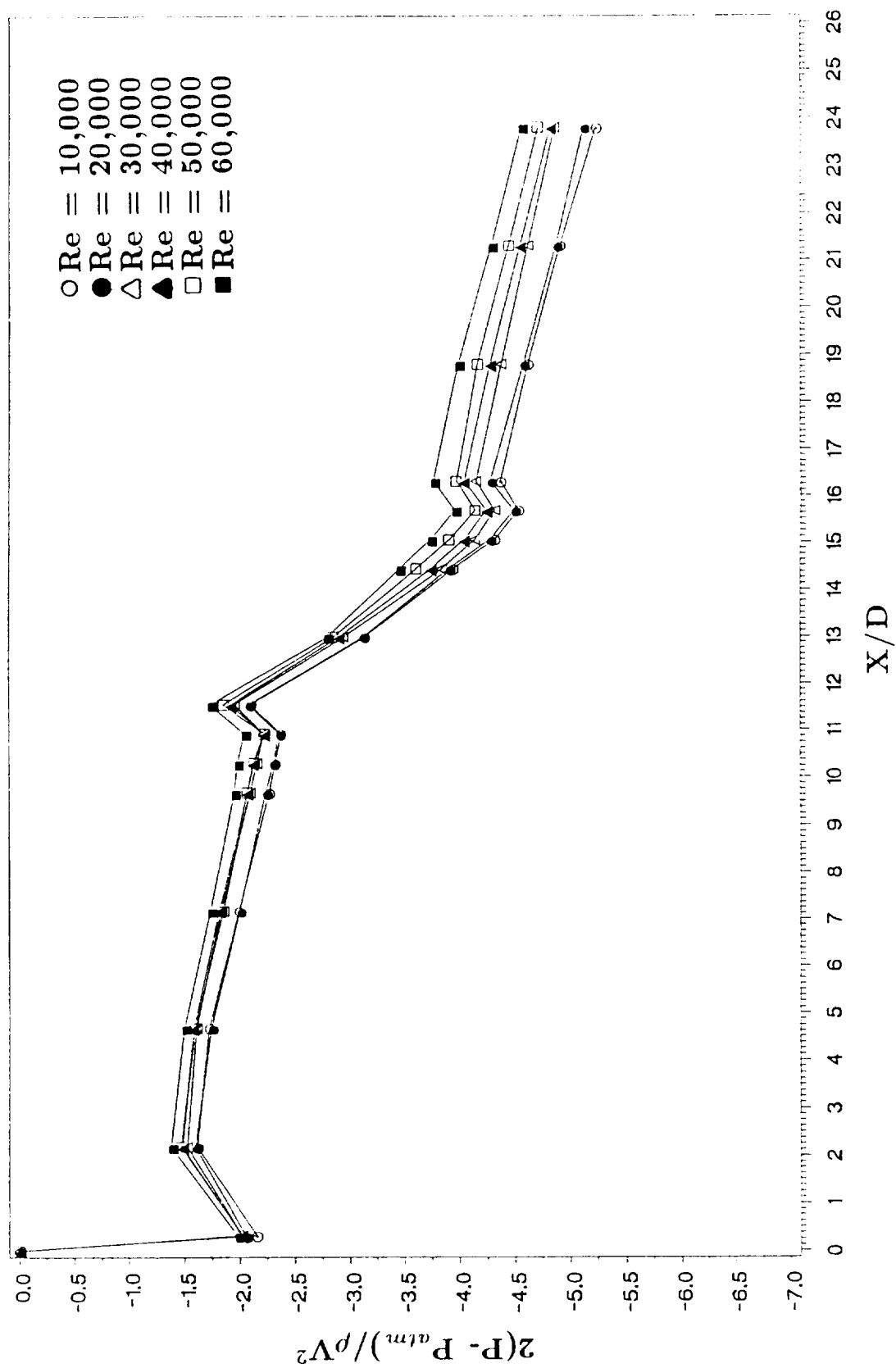


Fig. 31. Dimensionless pressure drop for rough channel
with $P/e=20$, $e/D=0.063$, and $\alpha = 90^\circ$.

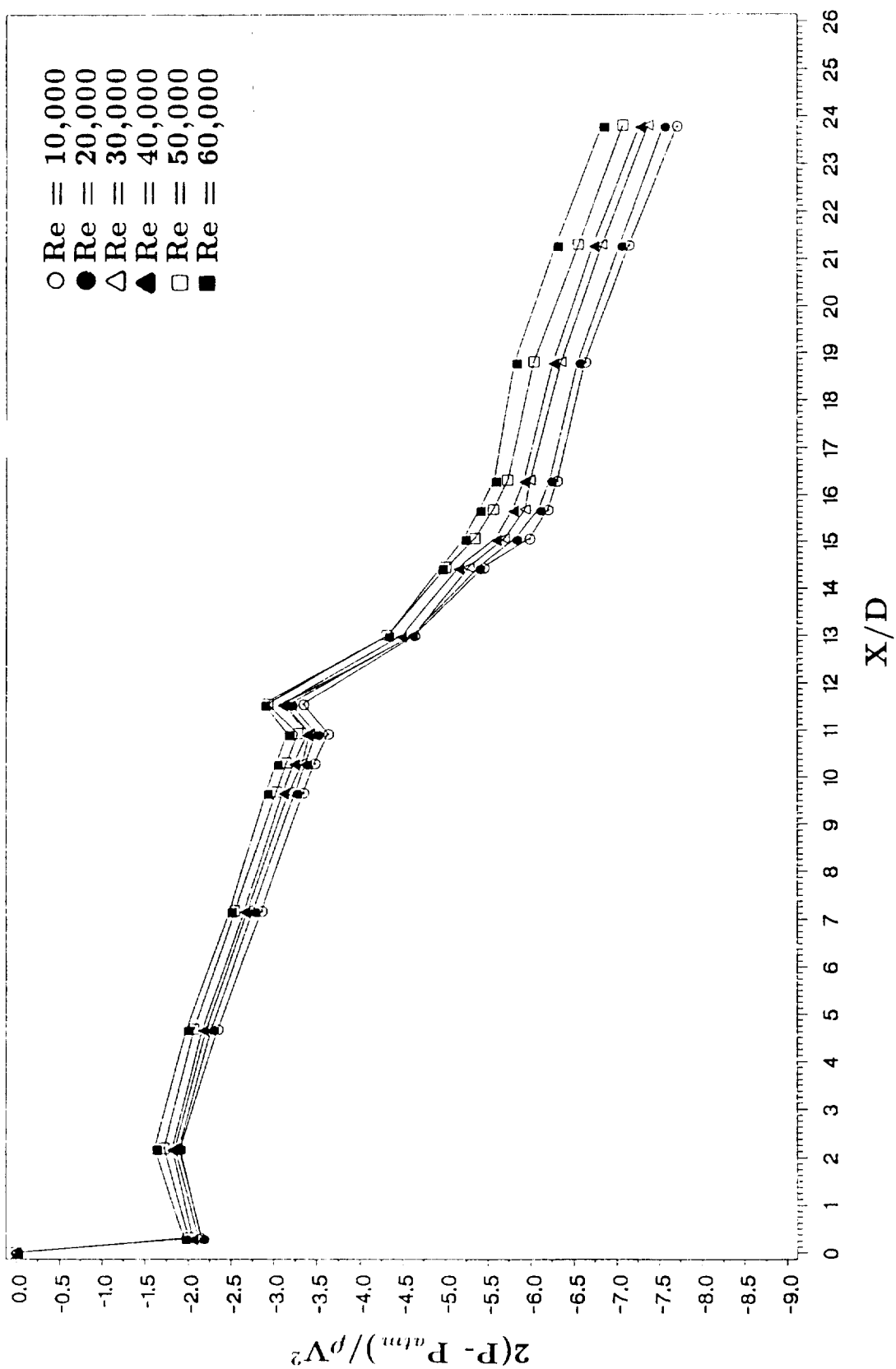


Fig. 32. Dimensionless pressure drop for rough channel
with $P/e=10$, $e/D=0.094$, and $\alpha = 90^\circ$.

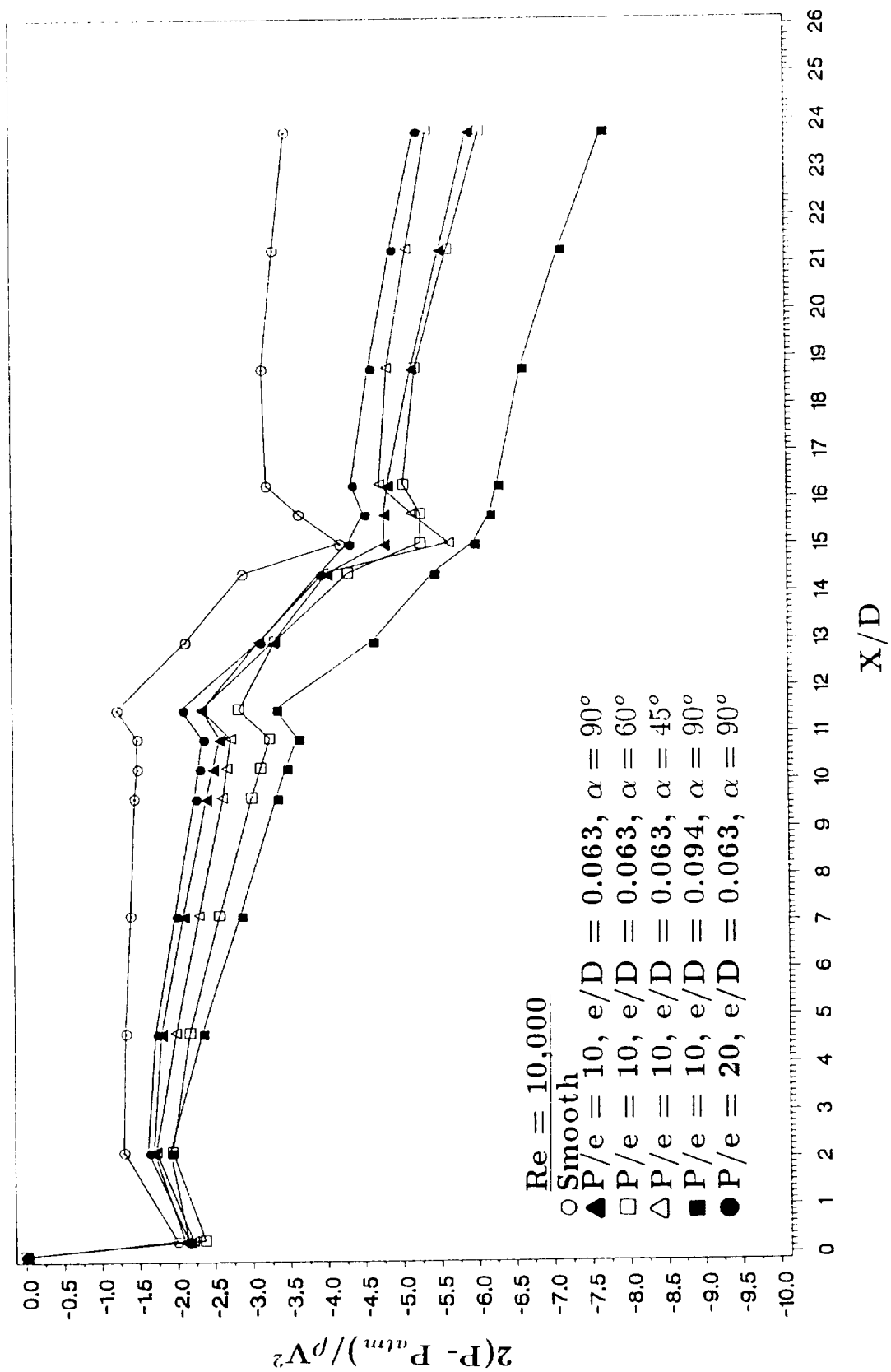


Fig. 33. Dimensionless pressure drop for rough channel
with $Re=10,000$.

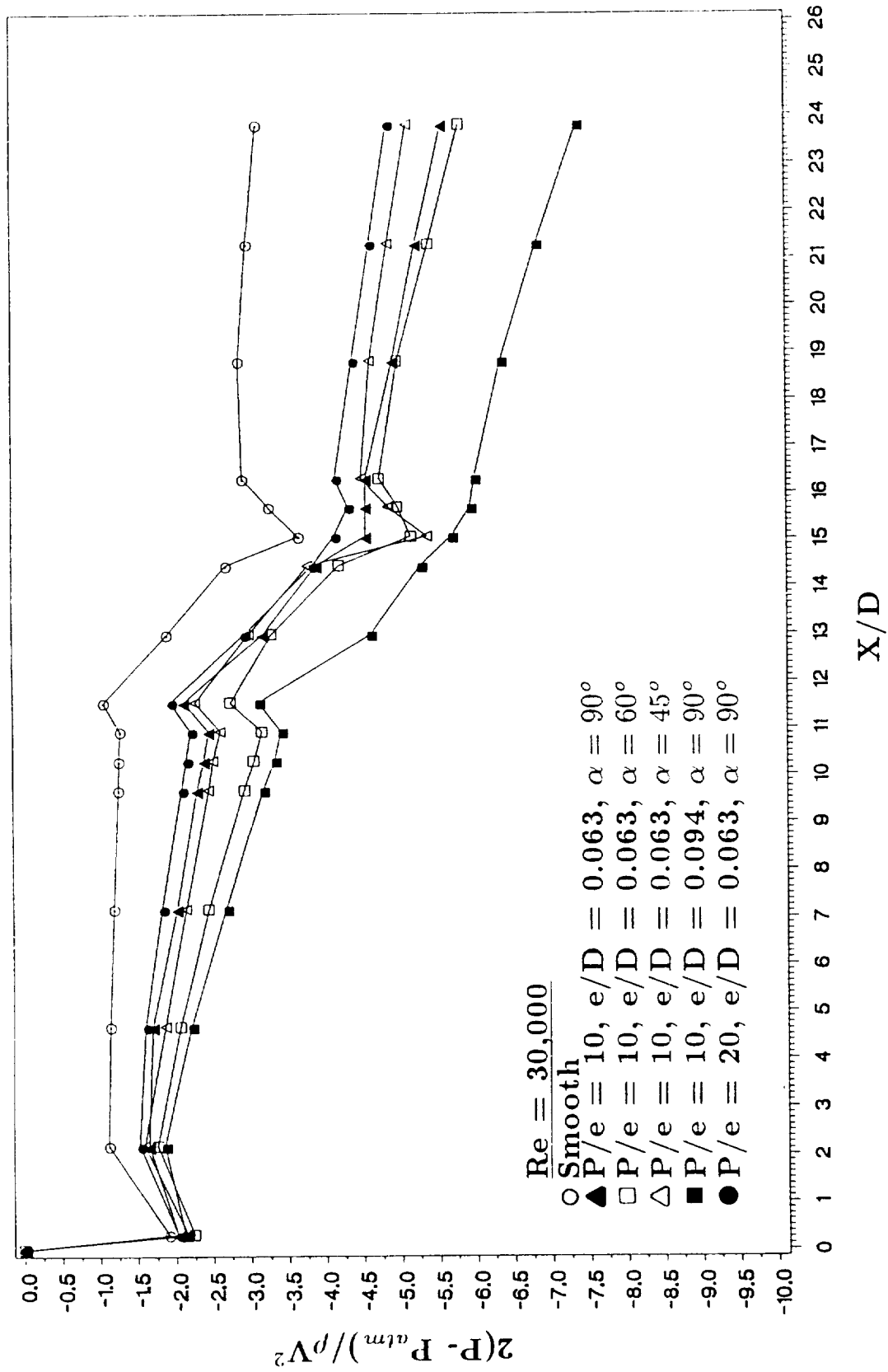


Fig. 34. Dimensionless pressure drop for rough channel
with $Re=30,000$.

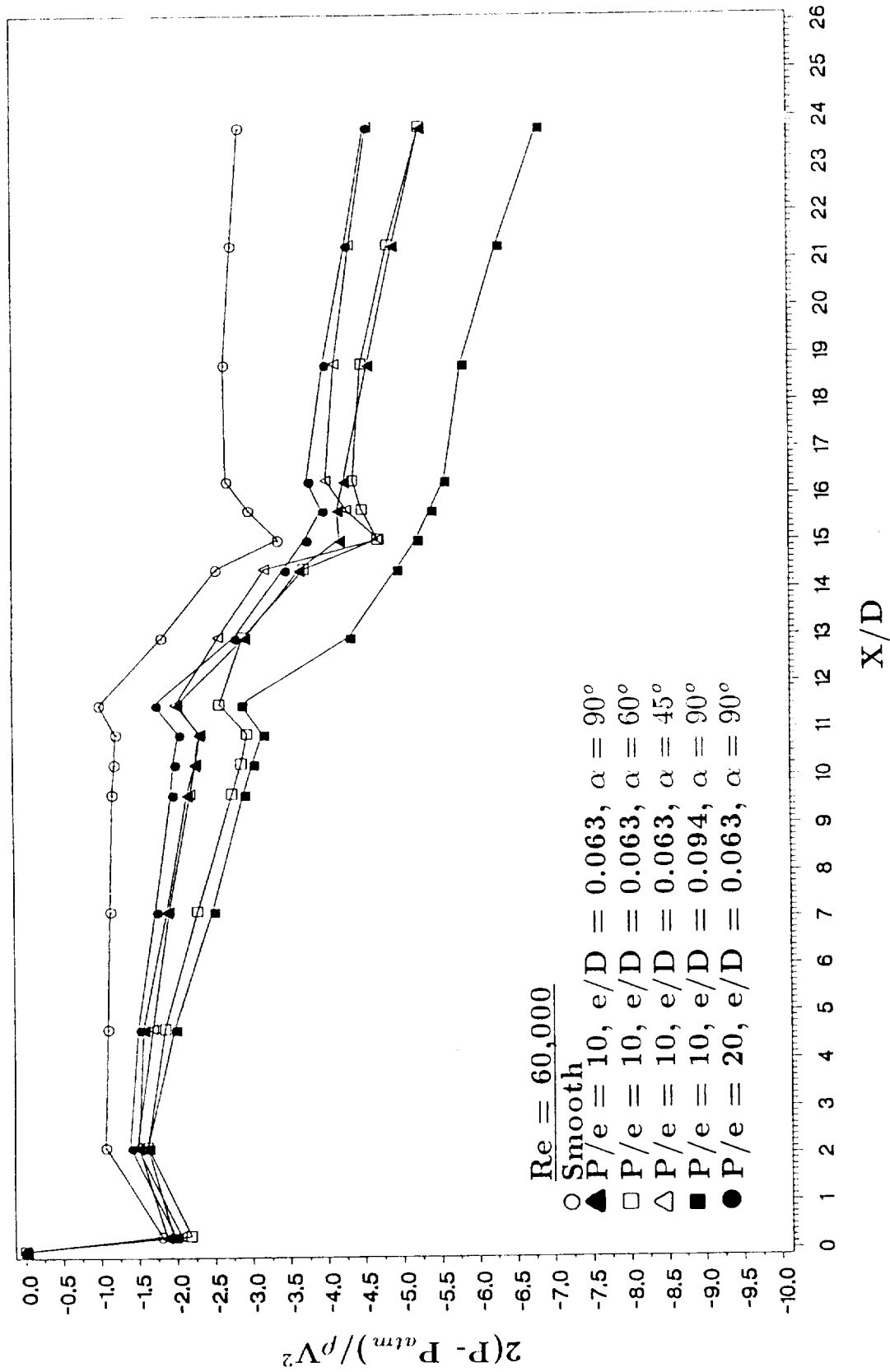


Fig. 35. Dimensionless pressure drop for rough channel
with Re=60,000.

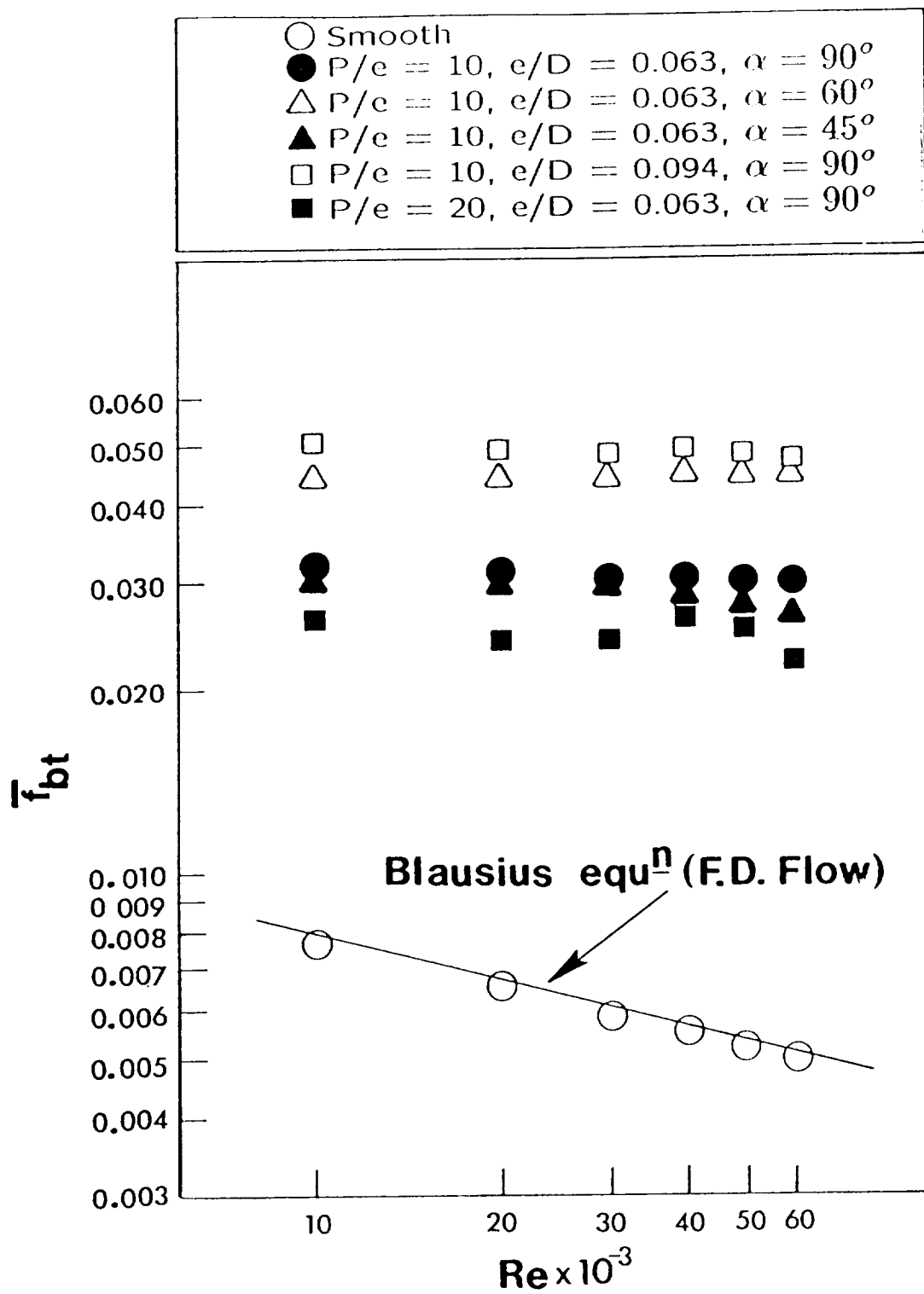


Fig. 36. Average fully-developed friction factor in the before-turn region.

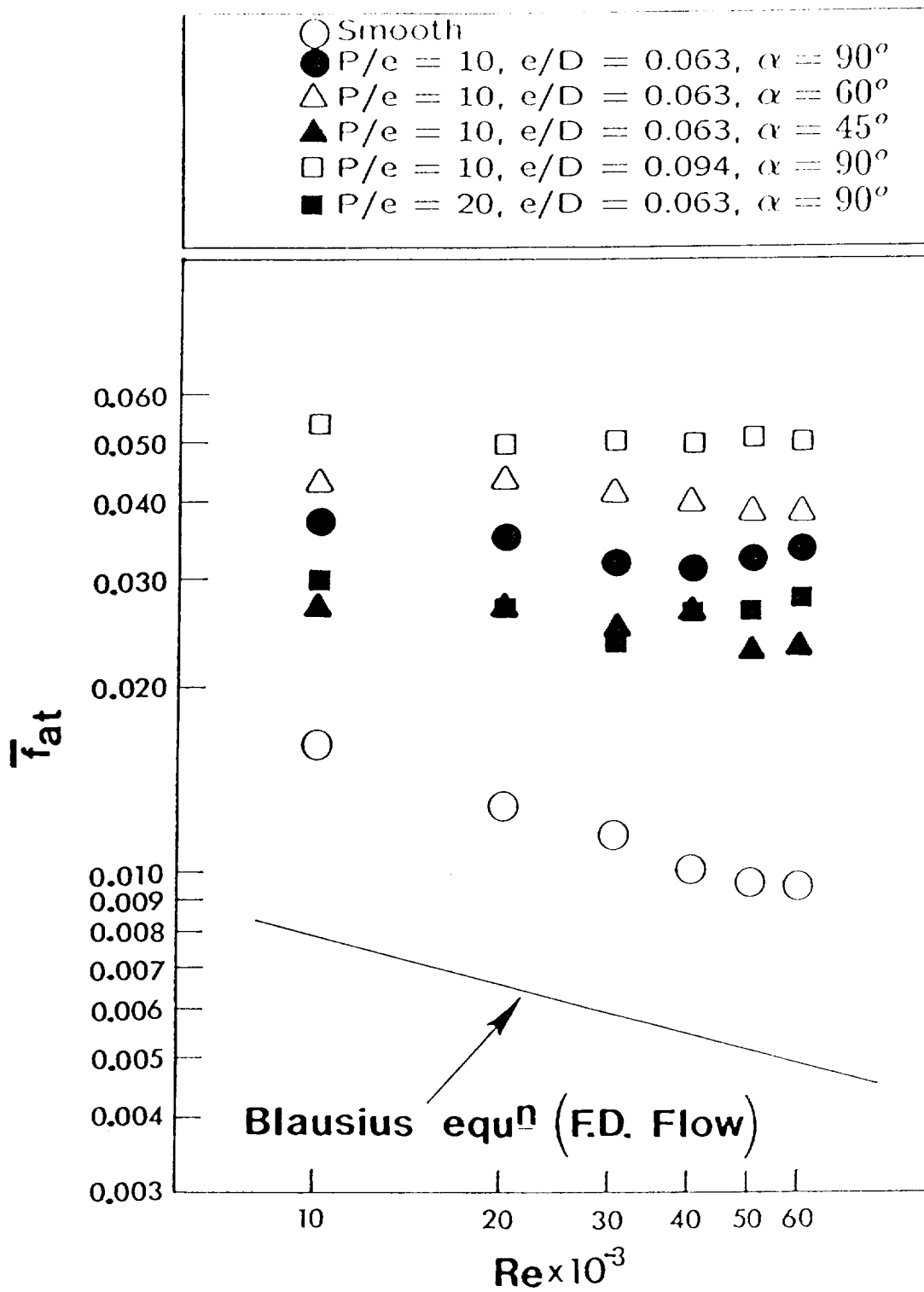


Fig. 37. Average fully-developed friction factor in the after-turn region.

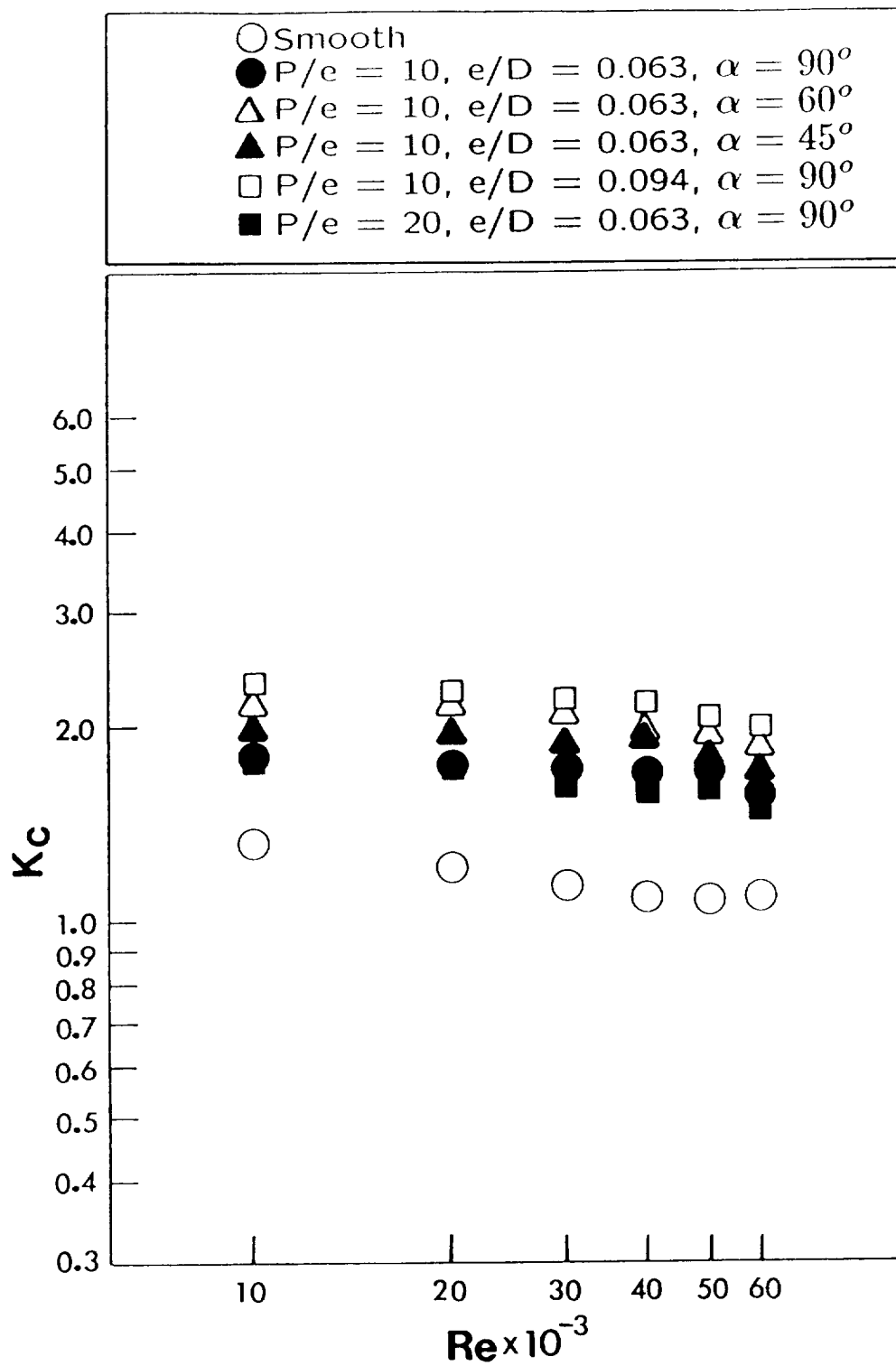


Fig. 38. Loss coefficient in the entrance region.

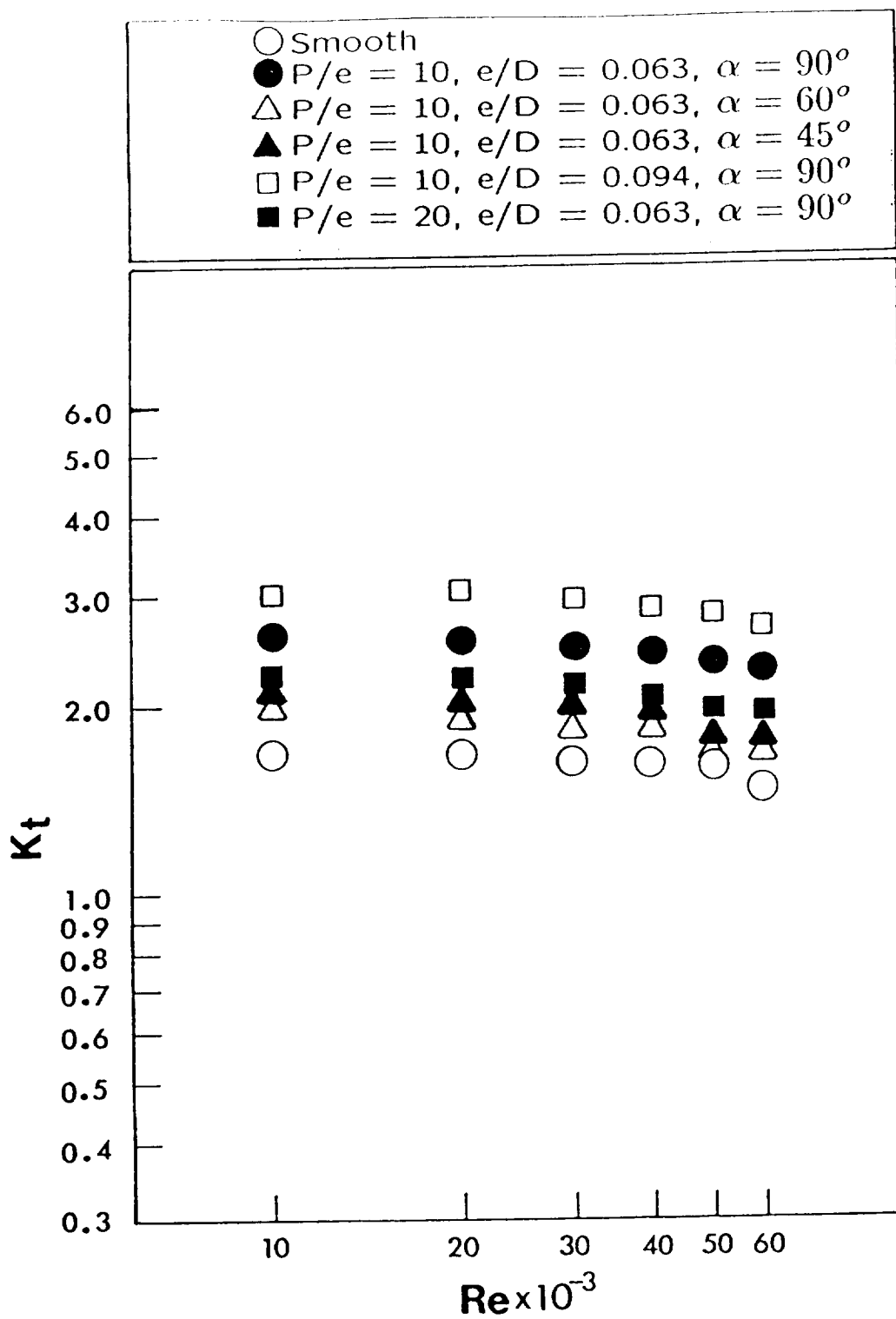


Fig. 39. Loss coefficient in the turn region.

APPENDIX A

NATURAL CONVECTION LOSS

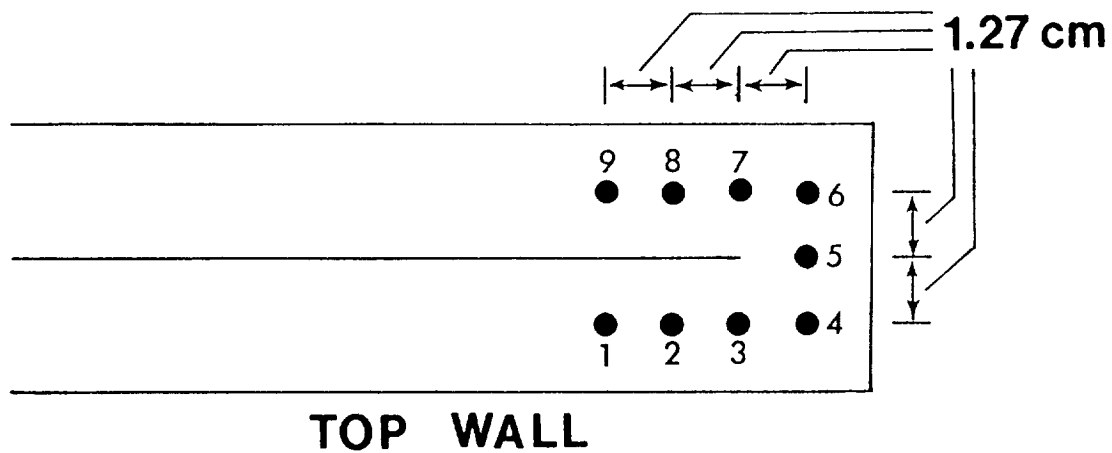
PRECEDING PAGE BLANK NOT FILLED

The mass transfer from a surface has direct relationship with the local *Sherwood number* and the local heat transfer coefficient. Therefore, in a mass transfer experiment, it becomes very critical to account for the exact transfer of mass taking place during the test run only.

In the present investigation, the naphthalene coated plates were sealed in air-tight plastic bags when they were not in use. But during assembling and disassembling the test apparatus, the naphthalene plates were in the open for about 30 minutes each time. The main factor to consider is the time during which the surface contour measurements were performed before and after the test runs. Depending upon the geometry of the plate, i.e. Top Plate (big) or the Side Plate (small); Smooth Plate or Rough Plate; Rib placement at right angle(90°) or acute angle(60° or 45°), the time taken in the measurement and in turn the mass transfer by natural convection will be different in each case. The time taken in the measurement of different surfaces was recorded. The maximum time (about 2 hours) was recorded for the top plate with ribs at an angle-of-attack of 60° and 45° , as the local contour measurement at the grid stations was more complicated.

In order to account for this mass transfer due to natural convection in data analysis of the *Sherwood number*, separate experiments were conducted to record the depth change of the naphthalene surfaces with respect to time. The fresh naphthalene coated Top Plate was kept open on the measurement table in the laboratory for 2 hrs. The depth was measured and recorded

at nine locations(as shown in the figure below) at an interval of 30 minutes. These locations were selected to cover all the three important regions, i.e. before-turn, in-turn, and after-turn. The depth change at these points with respect to time is given in the table on page 89.



A plot between the depth change (ΔZ) versus duration of time (Δt) was drawn and shown in the figure on page 88. The curve fit through the data points gives two equations (1) and (2) to account for the depth change for two different time periods.

$$\Delta Z = (\Delta t - 10)/10000 \quad \text{for } \Delta t \leq 70 \quad (1)$$

$$\Delta Z = (18 + 0.6\Delta t)/10000 \quad \text{for } \Delta t > 70 \quad (2)$$

Using these equations, depending on the time for which each plate was in the open, the correction for depth change was taken care of in the data analysis.

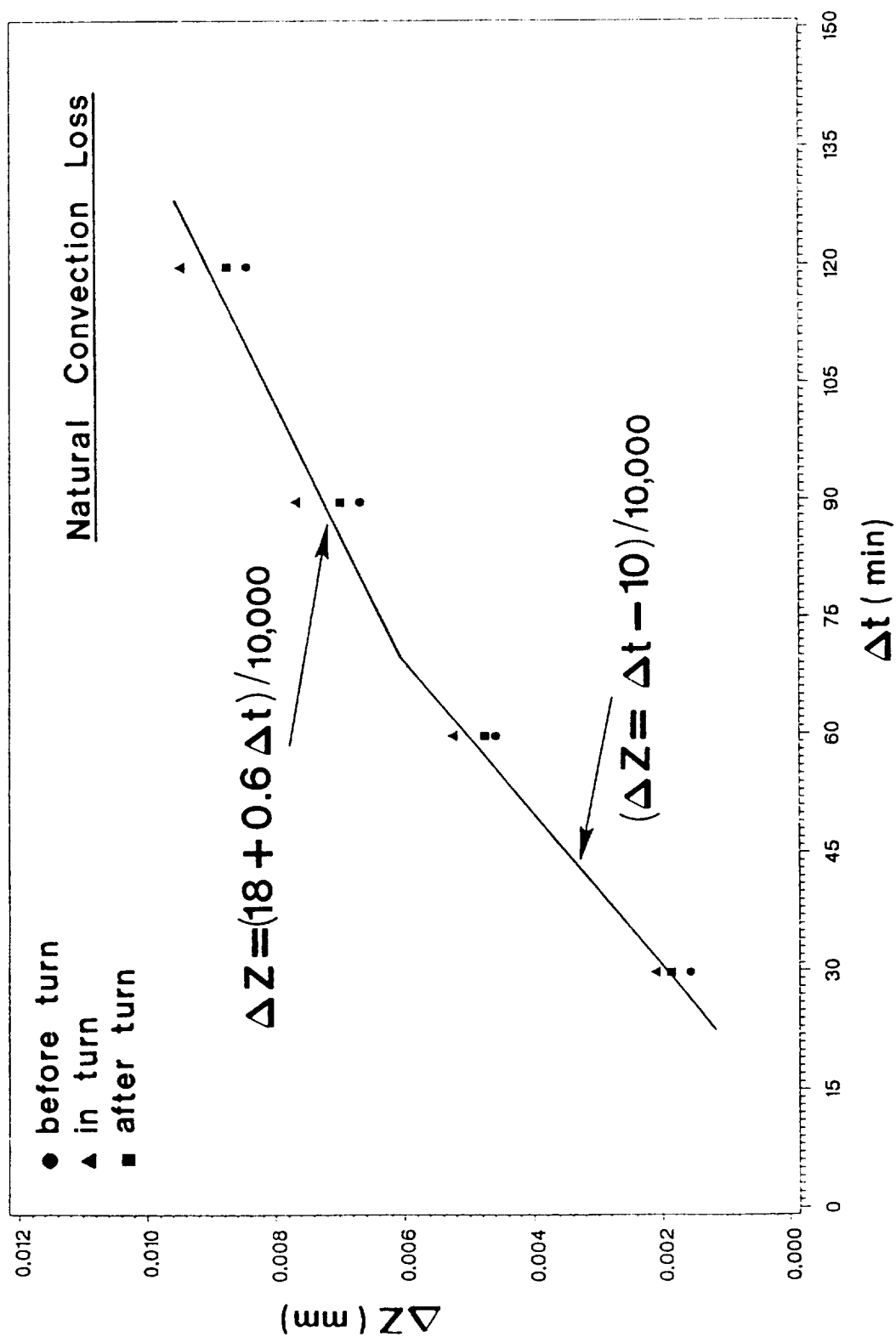
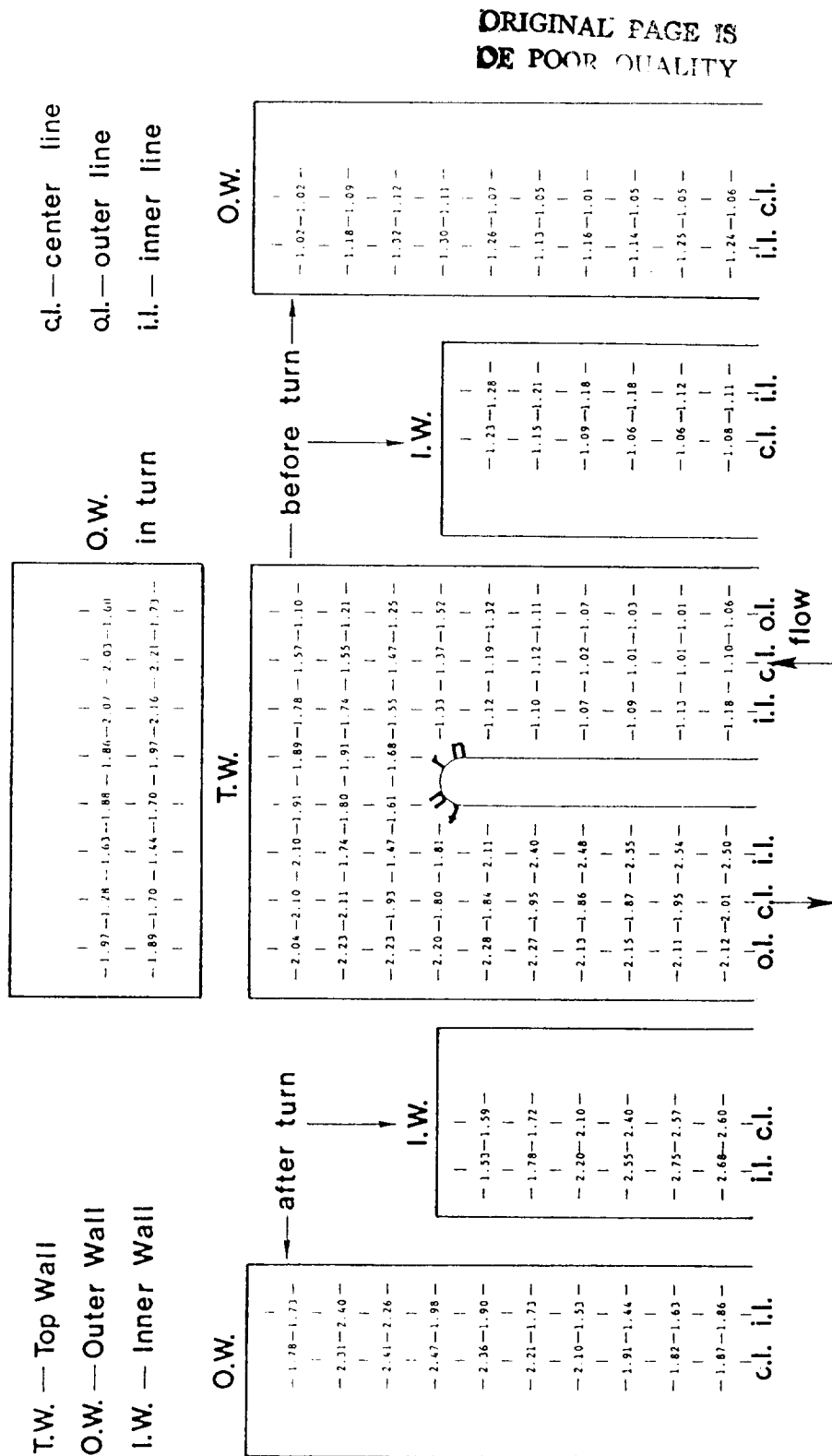


TABLE FOR NATURAL CONVECTION DEPTH CHANGE ΔZ

LOCATION/ Δt	30 min.	60 min.	90 min.	120 min.
1	0.0019	0.0045	0.0067	0.0085
2	0.0013	0.0044	0.0064	0.0082
3	0.0016	0.0050	0.0071	0.0088
4	0.0018	0.0051	0.0074	0.0093
5	0.0020	0.0052	0.0078	0.0094
6	0.0026	0.0055	0.0079	0.0098
7	0.0017	0.0052	0.0076	0.0093
8	0.0019	0.0044	0.0066	0.0084
9	0.0021	0.0048	0.0069	0.0087

APPENDIX B

HEAT/MASS TRANSFER DATA



Sh/Sh_0 for $Re=30,000$ Smooth Channel



I.W. – Inner Wall

O.W.

in turn

—after turn

I.W.

C.I. 11.
-2.00 -2.5

259-279-267-285-

1-25

Call flow

1.W.

1.091
2.76

— 1.87 — 1.55 —

100

iii.

ORIGINAL PAGE IS
OF POOR QUALITY.

Sh/Sh₀ for Re=30,000, P/e=10, e/D=0.063, $\alpha=60^\circ$

Table 1. AVERAGE REGIONAL SH/SH₀ RATIOS

Re x10 ⁻³	P/e	e/D	α	TW1	TW2	TW3	OW1	OW2	OW3	OW4	OW5	IW1	IW2
15	–	–	–	1.14	1.82	2.08	1.16	1.16	2.10	2.25	1.81	1.15	2.16
30	–	–	–	1.09	1.73	2.07	1.13	1.13	1.82	2.17	1.86	1.12	2.18
60	–	–	–	1.08	1.69	2.07	1.04	1.12	1.66	1.93	1.86	1.13	2.20
15	10	0.063	90°	2.53	2.40	3.53	1.82	2.09	3.01	3.49	2.72	1.73	2.74
30	10	0.063	90°	2.61	2.55	3.50	1.67	2.13	2.56	2.77	2.39	1.78	2.44
60	10	0.063	90°	2.48	2.23	2.99	1.52	1.82	2.54	2.44	2.35	1.48	2.53
15	10	0.063	60°	3.37	2.31	2.91	2.37	2.27	3.11	2.63	2.10	2.05	3.00
30	10	0.063	60°	3.29	2.17	2.75	2.24	2.12	2.37	2.57	2.15	2.25	2.76
60	10	0.063	60°	3.03	1.92	2.80	2.00	2.03	2.35	2.43	2.33	2.05	2.46
15	10	0.063	45°	3.07	2.80	2.93	2.00	2.28	1.96	3.60	2.39	2.35	2.93
30	10	0.063	45°	2.86	2.63	3.14	2.03	2.12	2.10	2.86	2.25	1.98	2.61
60	10	0.063	45°	2.29	1.87	2.62	1.91	1.69	2.00	2.35	2.33	2.03	2.80
30	20	0.063	90°	2.12	2.06	2.49	1.55	1.62	2.05	1.29	1.94	1.61	2.21
30	10	0.094	90°	2.85	2.80	3.50	2.20	2.29	2.88	3.31	2.80	2.20	3.20

Re : REYNOLDS NUMBER

P/e : PITCH-TO-RIB HEIGHT RATIO

e/D : RIB HEIGHT-TO-HYDRAULIC DIAMETER RATIO

α : RIB ANGLE-OF-ATTACK

REGIONS:

TW1 : TOP WALL BEFORE-TURN (X/D=9.0 to 12.0)

TW2 : TOP WALL IN-TURN (X/D=12.0 to 14.0)

TW3 : TOP WALL AFTER-TURN (X/D=14.0 to 17.0)

OW1 : OUTER WALL BEFORE-TURN (X/D=9.0 to 12.0)

OW2 : OUTER WALL IN-TURN (X/D=12.0 to 12.5)

OW3 : OUTER WALL IN-TURN (X/D=12.5 to 13.5)

OW4 : OUTER WALL IN-TURN (X/D=13.5 to 14.0)

OW5 : OUTER WALL AFTER-TURN (X/D=14.0 to 17.0)

IW1 : INNER WALL BEFORE-TURN (X/D=9.0 to 12.0)

IW2 : INNER WALL AFTER-TURN (X/D=14.0 to 17.0)

C 2

Smooth Channel: $Re = 15,000$

Sh/Sh_0

	TOP		WALL
X/D	O.L.	C.L.	I.L.
	BEFORE		TURN
8.313	1.014	1.014	1.023
8.938	1.033	0.9846	1.030
9.563	1.054	1.006	1.073
10.125	1.178	1.030	1.057
10.375	1.140	1.159	1.239
10.625	1.042	1.069	1.133
10.875	1.186	1.212	1.187
11.125	1.306	1.213	1.202
11.375	1.366	1.295	1.098
11.625	1.523	1.318	1.106
	IN		TURN
11.875	1.900	1.562	1.477
12.375	1.407	1.787	1.853
12.875	1.738	1.836	1.834
13.125	1.985	1.612	1.500
13.625	2.014	2.130	1.596
14.125	2.132	2.031	1.796
	AFTER		TURN
14.375	2.260	2.025	2.080
14.625	2.301	1.982	2.442
14.875	2.244	1.789	2.483
15.125	2.300	1.716	2.465
15.375	2.356	1.763	2.408
15.625	2.201	1.772	2.398
15.875	2.106	1.805	2.349
16.438	2.166	2.114	2.193
17.063	1.976	1.947	1.840
17.688	1.672	1.673	1.644

OUTER WALL AND INNER WALL				

X/D	I.L.	C.L.	I.L.	C.L.

BEFORE TURN				

	OUTER	WALL	INNER	WALL

8.313	1.186	1.105	0.983	0.946
8.938	1.256	1.204	1.087	1.021
9.563	1.233	1.104	1.218	1.182
10.125	1.213	1.057	1.061	0.989
10.375	1.327	1.089	1.147	1.045
10.625	1.310	1.073	1.195	1.109
10.875	1.197	1.050	1.251	1.172
11.125	1.100	1.021	1.278	1.235
11.375	1.165	1.060	1.455	1.326
11.625	1.311	1.044		

IN TURN				

11.875	1.365	1.047		
12.375	1.548	1.450		
12.875	2.116	1.983		
13.125	1.960	2.113		
13.625	2.041	2.240		
14.125	2.123	2.598		

AFTER TURN				

14.375	2.058	2.505		
14.625	1.752	2.380	1.457	1.586
14.875	1.474	2.194	1.725	1.832
15.125	1.285	2.083	2.281	2.102
15.375	1.268	1.956	2.584	2.397
15.625	1.502	1.911	2.867	2.618
15.875	1.860	1.852	2.847	2.697
16.438	1.810	1.861	2.326	2.138
17.063	1.607	1.650	2.110	1.843
17.688	1.540	1.631	1.787	1.651

Smooth Channel: $Re = 30,000$

Sh/Sh_0

TOP WALL

X/D	O.L.	C.L.	I.L.
	BEFORE	TURN	
1.125	2.559	2.731	2.819
2.125	1.523	1.499	1.647
3.125	1.357	1.328	1.429
4.125	1.234	1.251	1.259
5.125	1.203	1.193	1.156
6.125	1.222	1.158	1.080
7.125	1.171	1.070	1.121
8.125	1.122	1.012	1.063
9.125	1.081	1.008	1.044
10.125	1.116	1.049	1.099
10.375	1.058	1.095	1.183
10.625	1.007	1.009	1.132
10.875	1.025	1.014	1.093
11.125	1.068	1.015	1.068
11.375	1.107	1.122	1.103
11.625	1.319	1.186	1.124
	IN	TURN	
11.875	1.521	1.368	1.333
12.375	1.104	1.548	1.549
12.875	1.891	1.911	1.681
13.125	1.911	1.797	1.609
13.625	2.043	2.110	1.471
14.125	2.196	1.800	1.810

	AFTER	TURN	

14.375	2.282	1.840	2.108
14.625	2.267	1.951	2.403
14.875	2.126	1.860	2.478
15.125	2.150	1.870	2.550
15.375	2.106	1.954	2.538
15.625	2.117	2.008	2.499
15.875	2.015	2.074	2.389
16.875	1.765	1.864	1.775
17.875	1.675	1.642	1.463
18.875	1.523	1.387	1.282
19.875	1.337	1.220	1.158
20.875	1.187	1.174	1.075
21.875	1.070	1.062	1.018
22.875	1.045	1.055	1.010
23.875	1.019	1.052	1.012
24.875	1.431	1.380	1.634

OUTER WALL		AND	INNER WALL	

X/D	I.L.	C.L.	I.L.	C.L.

BEFORE TURN				

	OUTER	WALL	INNER	WALL

1.125	2.333	2.289	2.490	2.056
2.125	1.900	1.700	1.840	1.655
3.125	1.600	1.500	1.548	1.442
4.125	1.410	1.300	1.387	1.264
5.125	1.326	1.260	1.201	1.256
6.125	1.150	1.206	1.202	1.103
7.125	1.136	1.145	1.217	1.077
8.125	1.150	1.097	1.060	1.064
9.125	1.173	1.125	1.055	1.072
10.125	1.213	1.113	1.130	1.106
10.375	1.238	1.064	1.107	1.084
10.625	1.252	1.045	1.117	1.064
10.875	1.136	1.045	1.183	1.061
11.125	1.158	1.008	1.176	1.089
11.375	1.128	1.049	1.207	1.154
11.625	1.261	1.071	1.281	1.228

IN TURN				

11.875	1.297	1.108		
12.375	1.375	1.308		
12.875	1.970	1.855		
13.125	1.700	1.883		
13.625	1.810	1.878		
14.125	1.984	2.472		

		AFTER	TURN	

14.375	1.900	2.359	1.532	1.594
14.625	1.732	2.205	1.779	1.718
14.875	1.530	2.097	2.201	2.102
15.125	1.437	1.912	2.546	2.403
15.375	1.630	1.816	2.747	2.574
15.625	1.863	1.869	2.684	2.596
15.875	2.123	2.151	2.620	2.592
16.875	1.784	1.923	2.028	1.983
17.875	1.578	1.630	1.823	1.778
18.875	1.496	1.597	1.455	1.517
19.875	1.408	1.436	1.281	1.208
20.875	1.345	1.424	1.080	1.135
21.875	1.176	1.232	1.170	1.174
22.875	0.9526	0.9493	1.167	1.245
23.875	1.066	1.188	1.499	1.643
24.875			1.465	1.259

Smooth Channel: $Re = 60,000$

Sh/Sh_0

	TOP		WALL
X/D	O.L.	C.L.	I.L.
	BEFORE	TURN	
8.125	1.174	1.191	1.179
9.125	1.061	1.061	1.075
10.125	1.105	1.035	1.051
10.375	1.100	1.027	1.081
10.625	1.074	1.014	1.063
10.875	1.027	1.013	1.037
11.125	1.001	1.050	1.012
	IN	TURN	
11.375	0.9806	0.9919	0.9865
11.625	1.147	1.117	1.115
11.875	1.315	1.350	1.377
12.375	1.106	1.482	1.492
12.875	1.882	1.688	1.562
13.125	1.933	1.735	1.535
13.625	2.122	1.958	1.518
14.125	2.076	1.825	1.549
	AFTER	TURN	
14.375	1.540	1.462	1.779
14.625	1.426	1.602	1.947
14.875	1.471	1.706	2.239
15.125	1.688	1.916	2.558
15.375	1.994	2.207	2.755
15.625	2.259	2.425	2.754
15.875	2.472	2.583	2.649
16.875	2.261	2.265	2.076
17.875	1.845	1.924	1.887

OUTER WALL		AND	INNER WALL	

X/D	I.L.	C.L.	I.L.	C.L.

BEFORE TURN				

	OUTER	WALL	INNER	WALL

8.125	1.150	1.200	1.102	1.130
9.125	1.095	1.100	1.065	1.061
10.125	1.130	1.127	1.127	1.101
10.375	1.169	1.139	1.071	1.065
10.625	1.094	1.004	1.058	1.035
10.875	1.068	0.964	1.076	1.046
11.125	1.032	0.900	1.084	1.041
11.375	0.930	0.851	1.285	1.276
11.625	0.983	0.830	1.367	1.338

IN TURN				

11.875	1.082	0.970		
12.375	1.447	1.274		
12.875	1.690	1.745		
13.125	1.683	1.659		
13.625	1.765	1.784		
14.125	1.645	2.223		

AFTER TURN				

14.375	1.390	1.828	1.708	1.842
14.625	1.384	1.831	2.027	1.964
14.875	1.275	1.737	2.319	2.275
15.125	1.551	1.921	2.527	2.417
15.375	1.960	2.212	2.703	2.471
15.625	2.052	2.407	2.560	2.476
15.875	2.180	2.498	2.471	2.524
16.875	1.788	2.007	1.969	1.966
17.875	1.652	1.824	1.670	1.656

Rough Channel: $Re=15,000$, $P/e=10$, $e/D=0.063$, $\alpha = 90^\circ$

Sh/Sh_0

TOP WALL

X/D	C.L.	C.L.	I.L.
	BEFORE	TURN	
8.313	3.322	2.835	2.625
8.938	3.131	3.045	2.898
9.563	2.686	2.520	2.367
9.938	2.165	1.656	2.300
10.000	3.355	2.802	2.820
10.063	3.620	3.200	3.141
10.125	3.261	2.874	2.794
10.188	3.067	2.593	2.414
10.250	2.611	2.170	2.166
10.313	2.483	1.956	1.942
10.375	2.498	1.906	1.848
10.438	RIB	RIB	RIB
10.500	RIB	RIB	RIB
10.563	2.470	2.325	2.571
10.625	3.374	2.936	2.878
10.688	3.691	3.156	3.521
10.750	3.206	2.661	2.354
10.813	3.013	2.588	2.357
10.875	2.703	2.148	2.134
10.938	2.522	1.969	1.922
11.000	2.300	1.747	1.732
11.063	RIB	RIB	RIB
11.125	RIB	RIB	RIB
11.188	2.497	1.967	1.609
11.250	3.660	2.797	2.461
11.313	3.694	3.037	2.829
11.375	3.097	2.547	2.393
11.438	2.832	2.411	2.226
11.500	2.237	1.881	1.856
11.563	1.612	1.693	1.647
11.625	2.649	1.528	1.471

	IN TURN		
11.875	3.723	3.308	3.200
12.375	1.874	2.303	2.378
12.875	2.692	2.329	1.688
13.125	2.282	2.213	1.507
13.625	3.300	2.537	1.658
14.125	2.194	1.537	1.273
	AFTER TURN		
14.375	2.282	1.583	1.342
14.438	6.306	2.345	1.710
14.500	6.383	2.619	2.271
14.563	6.161	3.301	2.449
14.625	4.536	3.427	2.585
14.688	4.353	3.628	2.936
14.750	2.592	3.401	2.439
14.813	3.426	3.591	2.446
14.875	RIB	RIB	RIB
14.938	RIB	RIB	RIB
15.000	1.853	3.051	2.646
15.063	5.480	4.741	3.376
15.125	5.989	4.763	3.374
15.188	6.186	4.460	3.091
15.250	5.799	4.363	2.970
15.313	5.203	3.907	2.339
15.375	3.325	3.503	2.139
15.438	4.181	3.066	1.961
15.500	RIB	RIB	RIB
15.563	RIB	RIB	RIB
15.625	2.079	2.029	2.250
15.688	3.525	3.474	2.933
15.750	4.472	3.952	3.454
15.813	5.958	4.213	3.135
15.875	5.543	3.916	2.957
15.938	5.226	3.893	2.702
16.000	3.415	3.166	2.512
16.063	4.335	2.856	1.970
16.438	3.855	3.216	2.810
17.063	5.107	3.755	3.065
17.688	3.915	3.376	2.837

OUTER WALL		AND	INNER WALL	

X/D	I.L.	C.L.	I.L.	C.L.

BEFORE TURN				

	OUTER	WALL	INNER	WALL

8.313	2.019	1.826	2.320	2.313
8.938	1.761	1.884	1.981	1.828
9.563	1.640	1.717	1.580	1.607
9.938	1.840	1.604	1.401	1.486
10.000	1.780	1.599	1.231	1.425
10.125	1.791	1.654	1.340	1.720
10.250	1.692	1.709	1.590	1.674
10.375	2.118	1.666	1.708	1.662
10.500	1.869	1.907	2.002	1.749
10.625	1.827	1.843	1.838	1.770
10.750	1.794	1.756	1.966	1.703
10.875	1.718	1.572	1.941	1.722
11.000	1.890	1.701	2.003	1.752
11.125	2.010	1.800	2.046	1.655
11.250	1.892	1.833	1.926	1.633
11.375	1.956	1.780	1.838	1.482
11.500	1.955	1.758	1.505	1.555
11.625	2.168	1.993		

		IN	TURN	

11.875	2.255	2.243		
12.375	2.544	2.439		
12.875	3.275	3.400		
13.125	3.047	3.073		
13.625	3.209	3.586		
14.125	2.805	3.484		

		AFTER	TURN	

14.375	2.357	3.586		
14.500	2.416	3.520	3.707	4.447
14.625	2.188	3.509	3.783	3.711
14.750	1.925	3.250	2.613	3.463
14.875	2.166	3.224	2.641	3.299
15.000	2.352	3.272	2.936	3.154
15.125	2.445	3.271	2.934	3.207
15.250	2.345	3.378	2.814	3.120
15.375	2.329	3.083	2.822	2.846
15.500	2.780	2.981	2.872	2.918
15.625	2.926	2.887	2.768	2.814
15.750	2.661	2.938	2.644	2.494
15.875	2.581	2.991	3.123	2.229
16.000	2.588	2.527	2.638	2.071
16.063	2.607	2.876	2.581	1.991
16.438	2.512	2.615	1.963	1.987
17.063	2.365	2.200	1.811	1.477
17.688	2.134	2.194	1.463	1.476

Rough Channel: $Re=30,000$, $P/e=10$, $e/D=0.063$, $\alpha = 90^\circ$

$$\text{Sh}/\text{Sh}_0$$

TOP WALL

X/D	O.L.	C.L.	I.L.
	BEFORE	TURN	
0.563	1.369	0.9620	0.9345
0.625	1.609	1.431	1.782
0.688	2.014	1.930	2.302
0.750	2.399	2.154	2.676
0.813	2.265	1.812	2.277
0.875	1.965	1.828	2.345
0.938	1.649	1.358	2.164
1.000	2.194	2.710	3.014
1.063	RIB	RIB	RIB
1.125	RIB	RIB	RIB
1.188	2.026	1.441	1.181
1.250	3.179	2.708	3.677
1.313	3.788	3.079	4.013
1.375	4.170	3.662	4.198
1.438	3.972	3.517	3.876
1.500	3.827	3.449	3.736
1.563	3.517	3.253	3.344
1.625	3.331	3.067	3.117
2.063		3.415	
2.688		3.347	
3.313		3.230	
3.938		3.071	
4.563		3.078	
5.188		3.093	
5.813		3.059	
6.438		2.996	
6.813	1.539	1.288	1.219
6.875	3.055	2.703	2.774
6.938	3.212	3.038	3.076
7.000	3.369	3.181	3.271
7.063	3.156	2.882	3.231
7.125	3.001	2.804	3.153
7.188	2.511	2.587	2.883
7.250	2.764	2.481	2.638
7.313	RIB	RIB	RIB
7.375	RIB	RIB	RIB
7.438	1.598	1.545	1.787

7.500	2.982	2.814	2.851
7.563	3.491	3.252	3.284
7.625	3.317	3.159	3.177
7.688	3.268	3.100	2.947
7.750	3.109	2.780	2.860
7.813	2.927	2.584	2.559
7.875	2.755	2.412	2.487
8.313		3.087	
8.938		3.087	
9.313	1.549	1.324	1.337
9.375	2.704	2.735	2.622
9.438	3.133	3.095	3.103
9.500	3.144	2.985	3.132
9.563	3.025	2.913	2.944
9.625	2.735	2.655	2.755
9.688	2.529	2.417	2.466
9.750	2.369	2.262	2.316
9.813	RIB	RIB	RIB
9.875	RIB	RIB	RIB
9.938	1.426	1.420	1.543
10.000	2.611	2.675	2.549
10.063	3.147	3.118	3.043
10.125	3.134	3.009	2.902
10.188	2.970	2.895	2.729
10.250	2.870	2.681	2.638
10.313	2.597	2.408	2.402
10.375	2.480	2.273	2.290
10.438	RIB	RIB	RIB
10.500	RIB	RIB	RIB
10.563	1.504	1.580	1.538
10.625	2.764	2.744	2.761
10.688	3.148	3.142	2.886
10.750	3.149	3.057	3.073
10.813	2.927	2.908	2.820
10.875	2.756	2.628	2.595
10.938	2.540	2.380	2.361
11.000	2.442	2.174	2.240
11.063	RIB	RIB	RIB
11.125	RIB	RIB	RIB
11.188	1.846	1.642	1.320
11.250	3.052	2.884	2.450
11.313	3.359	3.219	2.826
11.375	3.257	3.120	2.890
11.438	3.028	2.856	2.738
11.500	2.796	2.674	2.614
11.563	2.439	2.442	2.365
11.625	2.495	2.135	2.018

	IN	TURN	

11.875	3.710	3.485	3.322
12.375	2.094	2.185	2.373
12.875	2.781	2.403	2.384
13.125	2.730	2.493	2.522
13.625	3.014	2.486	2.176
14.125	1.841	1.919	2.270

	AFTER	TURN	

14.375	3.201	2.366	2.094
14.438	4.692	3.000	2.531
14.500	5.132	3.483	2.843
14.563	4.919	3.600	3.031
14.625	4.479	3.734	3.156
14.688	3.940	3.716	3.285
14.750	3.205	3.481	3.199
14.813	4.467	3.539	3.261
14.875	RIB	RIB	RIB
14.938	RIB	RIB	RIB
15.000	3.034	3.980	3.647
15.063	4.178	4.474	3.855
15.125	4.601	4.276	3.586
15.188	4.697	4.004	3.311
15.250	4.507	3.836	3.038
15.313	4.167	3.531	2.891
15.375	3.638	3.184	2.643
15.438	3.888	3.406	3.599
15.500	RIB	RIB	RIB
15.563	RIB	RIB	RIB
15.625	2.630	2.947	3.103
15.688	4.156	4.080	3.619
15.750	4.610	4.099	3.514
15.813	4.464	3.865	3.229
15.875	4.107	3.590	3.026
15.938	3.799	3.267	2.795
16.000	3.297	2.902	2.480
16.063	3.788	3.237	2.888
16.125	RIB	RIB	RIB
16.188	RIB	RIB	RIB
16.250	2.877	2.777	2.884
16.313	3.919	3.648	3.423
16.375	4.206	3.610	3.343
16.438	4.076	3.471	3.120
16.500	3.723	3.280	2.831
16.563	3.397	3.069	2.644

16.625	2.955	2.803	2.367
16.688	3.799	3.093	2.728
17.063		3.490	
17.688		3.342	
18.125	2.041	2.066	2.081
18.188	3.329	3.168	2.955
18.250	3.611	3.265	3.142
18.313	3.690	3.238	3.021
18.375	3.335	3.007	2.770
18.438	3.236	2.775	2.523
18.500	2.847	2.451	2.252
18.563	2.905	2.519	2.286
18.625	RIB	RIB	RIB
18.688	RIB	RIB	RIB
18.750	2.006	1.768	1.797
18.813	3.199	3.128	2.784
18.875	3.599	3.288	3.155
18.938	2.238	3.141	3.012
19.000	3.367	3.008	2.846
19.063	2.927	2.817	2.376
19.125	2.837	2.467	2.223
19.188	2.703	2.140	1.968
19.563		3.058	
20.188		3.034	
20.813		3.019	
21.438		2.977	
22.063		2.864	
22.688		2.860	
23.313		2.908	
23.938		2.992	
24.375	2.312	2.087	2.618
24.438	3.274	3.209	3.133
24.500	3.435	3.385	3.278
24.563	3.255	3.123	2.815
24.625	3.189	2.917	2.697
24.688	2.957	2.638	2.500
24.750	2.854	2.519	2.412
24.813	2.579	2.245	2.350
24.875	RIB	RIB	RIB
24.938	RIB	RIB	RIB
25.000	2.540	2.464	2.528
25.063	2.188	2.138	2.232
25.125	2.410	2.329	2.361
25.188	2.389	2.302	2.096
25.250	2.311	2.255	1.883
25.313	2.419	2.389	1.851
25.375	2.382	2.799	2.328
25.438	3.084	2.903	2.421

OUTER WALL		AND	INNER WALL	

X/D	I.L.	C.L.	I.L.	C.L.

BEFORE TURN				

OUTER WALL		INNER WALL		

8.313	1.822	1.552	1.894	1.740
8.938	1.760	1.558	2.072	1.872
9.563	1.729	1.513	1.719	1.654
10.188	1.862	1.639	1.883	1.800
10.813	1.819	1.603	1.780	1.666
11.438	1.798	1.445	1.777	1.507

IN TURN				

11.875	2.511	2.128		
12.375	2.374	2.172		
12.875	2.775	2.982		
13.125	2.288	2.561		
13.625	2.759	2.819		
14.125	2.297	2.289		

AFTER TURN				

14.563	2.335	2.323	3.062	2.925
15.188	2.380	2.277	2.818	2.480
15.813	2.754	2.678	2.747	2.295
16.438	2.481	2.450	2.214	2.123
17.063	2.370	2.326	2.293	1.762
17.688	2.201	2.185	2.347	2.110

Rough Channel: $Re=60,000$, $P/e=10$, $e/D=0.063$, $\alpha = 90^\circ$

Sh/Sh₀

	TOP WALL		
X/D	O.L.	C.L.	I.L.
	BEFORE	TURN	
0.188	3.414	3.906	3.839
0.250	4.438	4.495	4.602
0.313	4.700	4.604	4.668
0.375	4.301	4.281	4.403
0.438	RIB	RIB	RIB
0.500	RIB	RIB	RIB
0.563	2.124	1.677	1.729
0.625	3.613	3.597	3.888
0.688	4.088	4.466	4.251
0.750	3.905	4.337	4.256
0.813	3.686	4.194	4.217
0.875	3.340	3.935	3.839
0.938	2.930	3.261	3.472
1.000	3.373	3.526	3.521
1.063	RIB	RIB	RIB
1.125	RIB	RIB	RIB
1.188	2.023	1.722	2.124
1.250	2.966	2.611	3.193
1.313	3.422	3.088	3.307
1.375	3.376	3.255	3.250
1.438	3.265	3.318	3.039
1.500	3.216	3.167	2.817
1.563	3.062	3.078	3.142
1.625	3.092	3.094	2.960
2.063	3.093	2.915	3.050
2.688	2.934	2.925	2.890
3.313	2.843	2.742	2.836
3.938	2.785	2.783	2.869
4.563	2.797	2.722	2.800
5.188	2.757	2.712	2.805
5.813	2.675	2.665	2.733
6.438	2.714	2.665	2.734
6.813	1.931	2.003	1.941
6.875	2.816	3.017	2.576
6.938	2.915	2.983	2.901
7.000	2.913	2.786	2.834
7.063	2.763	2.559	2.787
7.125	2.577	2.322	2.583
7.188	2.313	2.072	2.394

7.250	2.521	2.212	2.517
7.313	RIB	RIB	RIB
7.375	RIB	RIB	RIB
7.438	1.872	1.889	1.824
7.500	2.829	2.947	2.551
7.563	2.993	2.925	2.772
7.625	2.915	2.698	2.752
7.688	2.642	2.419	2.567
7.750	2.470	2.244	2.375
7.813	2.289	2.096	2.157
7.875	2.402	2.212	2.512
8.313	2.776	2.444	2.563
8.938	2.638	2.452	2.594
9.313	1.824	1.918	2.066
9.375	2.750	2.844	2.669
9.438	2.915	2.820	2.772
9.500	2.858	2.650	2.681
9.563	2.701	2.431	2.542
9.625	2.466	2.216	2.363
9.688	2.228	2.041	2.167
9.750	2.386	2.242	2.441
9.813	RIB	RIB	RIB
9.875	RIB	RIB	RIB
9.938	1.643	1.976	1.941
10.000	2.702	2.737	2.567
10.063	2.919	2.795	2.793
10.125	2.855	2.551	2.684
10.188	2.634	2.376	2.519
10.250	2.391	2.195	2.344
10.313	2.226	2.025	2.078
10.375	2.498	2.188	2.543
10.438	RIB	RIB	RIB
10.500	RIB	RIB	RIB
10.563	1.793	2.010	1.969
10.625	2.700	2.702	2.605
10.688	2.863	2.766	2.748
10.750	2.787	2.609	2.633
10.813	2.616	2.416	2.453
10.875	2.437	2.204	2.329
10.938	2.325	2.028	2.075
11.000	2.328	2.167	2.292
11.063	RIB	RIB	RIB
11.125	RIB	RIB	RIB
11.188	2.060	2.019	2.020
11.250	3.118	2.834	2.800
11.313	3.462	2.921	2.931
11.375	3.257	2.839	2.801
11.438	2.985	2.609	2.668
11.500	2.665	2.334	2.403
11.563	2.271	2.083	2.084
11.625	2.722	2.214	2.035

	----- IN TURN -----		
11.875	3.977	3.452	3.377
12.375	1.833	1.877	2.214
12.875	2.262	2.027	2.089
13.125	2.108	2.029	2.074
13.625	2.525	1.978	1.946
14.125	1.683	1.701	2.332
	----- AFTER TURN -----		
14.375	2.878	2.076	2.010
14.438	3.745	2.549	2.306
14.500	4.217	2.865	2.445
14.563	4.116	3.041	2.678
14.625	3.756	3.168	2.711
14.688	3.361	3.208	2.777
14.750	3.013	3.122	2.845
14.813	3.406	3.217	2.876
14.875	RIB	RIB	RIB
14.938	RIB	RIB	RIB
15.000	2.810	3.127	2.879
15.063	3.665	3.852	3.351
15.125	4.165	3.731	3.135
15.188	4.135	3.431	2.870
15.250	3.746	3.201	2.614
15.313	3.393	2.948	2.461
15.375	3.084	2.783	2.331
15.438	3.007	2.633	2.276
15.500	RIB	RIB	RIB
15.563	RIB	RIB	RIB
15.625	2.343	2.482	2.497
15.688	3.152	3.409	3.133
15.750	3.635	3.575	3.141
15.813	3.765	3.436	2.975
15.875	3.668	3.224	2.759
15.938	3.417	2.988	2.566
16.000	3.195	2.854	2.330
16.063	3.071	2.730	2.222
16.125	RIB	RIB	RIB
16.188	RIB	RIB	RIB
16.250	2.219	2.146	2.111
16.313	3.131	3.037	2.828
16.375	3.671	3.299	2.849
16.438	3.630	3.026	2.750
16.500	3.389	2.832	2.529
16.563	3.162	2.690	2.288
16.625	2.778	2.515	2.109
16.688	2.643	2.422	2.039
17.063	3.421	3.011	2.786

17.688	3.336	2.950	2.942
18.125	1.661	1.563	1.837
18.188	2.584	2.449	2.764
18.250	3.104	2.844	3.080
18.313	3.113	2.725	2.908
18.375	2.978	2.592	2.569
18.438	2.703	2.449	2.239
18.500	2.499	2.272	2.032
18.563	2.358	2.145	1.898
18.625	RIB	RIB	RIB
18.688	RIB	RIB	RIB
18.750	1.728	1.895	1.709
18.813	2.872	2.753	2.522
18.875	3.048	3.106	3.126
18.938	3.119	2.833	3.177
19.000	2.951	2.611	2.979
19.063	2.763	2.457	2.491
19.125	2.602	2.367	2.190
19.188	2.468	2.192	1.879
19.563	2.917	2.915	3.006
20.188	2.872	2.857	2.776
20.813	2.913	2.821	2.767
21.438	2.762	2.813	2.734
22.063	2.622	2.804	2.655
22.688	2.690	2.710	2.602
23.313	2.716	2.714	2.702
23.938	2.680	2.740	2.663
24.375	1.776	2.073	2.071
24.438	2.979	2.919	2.910
24.500	3.320	3.458	3.233
24.563	3.268	3.288	2.760
24.625	3.073	2.938	2.309
24.688	2.830	2.518	2.094
24.750	2.601	2.217	1.930
24.813	2.495	2.042	1.885
24.875	RIB	RIB	RIB
24.938	RIB	RIB	RIB
25.000	2.022	1.847	2.130
25.063	1.756	1.653	1.864
25.125	1.960	1.922	1.931
25.188	2.070	2.021	2.062
25.250	2.053	1.936	1.963
25.313	2.297	2.049	2.087
25.375	2.299	2.018	1.915
25.438	2.268	2.099	1.913
25.500	RIB	RIB	RIB
25.563	RIB	RIB	RIB
25.625	3.188	3.049	2.924
25.688	3.786	4.248	3.046
25.750	2.544	2.278	1.913
25.813	1.751	1.945	1.816

OUTER WALL		AND	INNER WALL	

X/D	I.L.	C.L.	I.L.	C.L.

BEFORE TURN				

	OUTER	WALL	INNER	WALL

0.188	2.215	2.634	2.283	3.182
0.250	2.243	2.858	2.676	3.868
0.313	2.329	3.186	2.937	3.766
0.375	2.262	2.938	2.893	3.685
0.438	2.511	3.161	2.781	3.529
0.500	2.580	3.338	2.656	3.425
0.563	2.640	3.467	2.783	3.332
0.625	2.574	3.075	2.661	3.224
0.688	2.880	3.269	3.153	3.137
0.750	2.825	3.022	3.233	3.040
0.813	2.929	2.977	3.222	2.820
0.875	2.978	2.853	3.187	2.661
0.938	2.999	2.798	3.267	2.528
1.000	2.932	2.706	3.032	2.417
1.063	2.906	2.522	3.058	2.339
1.125	2.888	2.546	3.002	2.416
1.188	2.790	2.556	2.898	2.337
1.250	2.734	2.465	2.830	2.327
1.313	2.614	2.475	2.812	2.281
1.375	2.577	2.304	2.646	2.292
1.438	2.514	2.278	2.629	2.130
1.500	2.465	2.258	2.610	2.062
1.563	2.414	2.196	2.546	2.034
1.625	2.340	2.176	2.553	2.059
2.063	2.127	2.098	1.973	1.869
2.688	1.813	1.944	1.727	1.666
3.313	1.768	1.846	1.640	1.698
3.938	1.664	1.734	1.605	1.677
4.563	1.663	1.712	1.732	1.689
5.188	1.644	1.671	1.661	1.592
5.813	1.681	1.663	1.659	1.621
6.438	1.723	1.675	1.660	1.627
6.813	1.651	1.558	1.786	1.701
6.875	1.654	1.564	1.782	1.664
6.938	1.650	1.594	1.738	1.705
7.000	1.615	1.587	1.718	1.670
7.063	1.587	1.525	1.744	1.671
7.125	1.641	1.544	1.699	1.652
7.188	1.640	1.621	1.752	1.667

7.250	1.636	1.594	1.721	1.628
7.313	1.618	1.603	1.769	1.652
7.375	1.615	1.600	1.765	1.653
7.438	1.699	1.633	1.709	1.627
7.500	1.671	1.596	1.702	1.585
7.563	1.555	1.551	1.738	1.583
7.625	1.555	1.550	1.701	1.554
7.688	1.547	1.526	1.707	1.545
7.750	1.563	1.508	1.692	1.568
7.813	1.603	1.588	1.748	1.596
7.875	1.616	1.540	1.664	1.525
8.313	1.446	1.522	1.616	1.474
8.938	1.423	1.539	1.574	1.502
9.313	1.591	1.439	1.610	1.401
9.375	1.517	1.561	1.519	1.350
9.438	1.528	1.510	1.635	1.442
9.500	1.550	1.412	1.596	1.415
9.563	1.519	1.470	1.568	1.339
9.625	1.613	1.492	1.568	1.288
9.688	1.555	1.553	1.671	1.464
9.750	1.557	1.505	1.615	1.402
9.813	1.582	1.458	1.627	1.386
9.875	1.605	1.461	1.692	1.386
9.938	1.580	1.440	1.675	1.461
10.000	1.556	1.425	1.607	1.417
10.063	1.531	1.470	1.669	1.475
10.125	1.523	1.485	1.634	1.409
10.188	1.535	1.510	1.573	1.365
10.250	1.536	1.534	1.572	1.367
10.313	1.495	1.483	1.721	1.352
10.375	1.514	1.485	1.605	1.363
10.438	1.581	1.468	1.602	1.387
10.500	1.528	1.549	1.592	1.412
10.563	1.556	1.456	1.583	1.421
10.625	1.542	1.406	1.520	1.401
10.688	1.416	1.466	1.603	1.365
10.750	1.451	1.510	1.530	1.336
10.813	1.469	1.450	1.501	1.266
10.875	1.519	1.413	1.546	1.277
10.938	1.521	1.492	1.600	1.316
11.000	1.516	1.475	1.623	1.463
11.063	1.540	1.451	1.713	1.468
11.125	1.614	1.567	1.721	1.350
11.188	1.574	1.504	1.752	1.545
11.250	1.569	1.460	1.582	1.225
11.313	1.581	1.530	1.711	1.335
11.375	1.553	1.632	1.534	1.209
11.438	1.519	1.520	1.494	1.000
11.500	1.579	1.519	1.472	1.063
11.563	1.687	1.472	1.506	1.090
11.625	1.692	1.448	1.400	1.266

		IN	TURN	

11.875	2.116	1.671		
12.375	2.075	2.267		
12.875	2.872	2.708		
13.125	2.364	2.418		
13.625	2.393	2.472		
14.125	2.306	2.416		

		AFTER	TURN	

14.375	2.383	2.292	2.366	1.980
14.438	2.475	2.288	2.143	2.114
14.500	2.433	2.258	2.182	2.093
14.563	2.474	2.250	2.213	2.287
14.625	2.479	2.382	2.376	2.310
14.688	2.466	2.339	2.485	2.378
14.750	2.433	2.354	2.561	2.407
14.813	2.477	2.392	2.712	2.404
14.875	2.359	2.339	2.824	2.427
14.938	2.399	2.382	2.849	2.447
15.000	2.349	2.339	2.682	2.444
15.063	2.446	2.370	2.570	2.496
15.125	2.478	2.487	2.607	2.439
15.188	2.533	2.473	2.605	2.481
15.250	2.627	2.554	2.582	2.544
15.313	2.541	2.482	2.558	2.505
15.375	2.518	2.481	2.527	2.455
15.438	2.576	2.447	2.619	2.473
15.500	2.555	2.452	2.630	2.531
15.563	2.543	2.424	2.650	2.522
15.625	2.427	2.380	2.669	2.497
15.688	2.459	2.468	2.585	2.455
15.750	2.471	2.434	2.593	2.484
15.813	2.467	2.420	2.654	2.527
15.875	2.417	2.383	2.694	2.503
15.938	2.410	2.353	2.666	2.533
16.000	2.297	2.303	2.674	2.488
16.063	2.256	2.335	2.732	2.567
16.125	2.248	2.284	2.710	2.548
16.188	2.315	2.285	2.700	2.579
16.250	2.152	2.243	2.688	2.596
16.313	2.170	2.239	2.735	2.649
16.375	2.159	2.235	2.789	2.706
16.438	2.125	2.396	2.723	2.655
16.500	2.164	2.206	2.728	2.642
16.563	2.130	2.337	2.715	2.637
16.625	2.148	2.177	2.721	2.630
16.688	2.173	2.162	2.713	2.637
17.063	2.039	2.032	2.422	2.364

17.688	1.864	1.986	2.274	2.171
18.125	1.849	1.864	2.086	2.014
18.188	1.774	1.840	2.001	1.983
18.250	1.800	1.840	2.065	1.972
18.313	1.817	1.812	1.970	1.917
18.375	1.840	1.873	1.986	1.954
18.438	1.795	1.808	2.057	1.943
18.500	1.835	1.828	1.985	1.895
18.563	1.818	1.854	2.011	1.850
18.625	1.844	1.816	1.976	1.896
18.688	1.761	1.801	1.863	1.827
18.750	1.774	1.800	1.851	1.846
18.813	1.726	1.776	1.837	1.838
18.875	1.762	1.680	1.850	1.909
18.938	1.680	1.703	1.846	1.905
19.000	1.625	1.652	1.855	1.894
19.063	1.805	1.692	1.865	1.887
19.125	1.791	1.681	1.939	1.889
19.188	1.770	1.762	1.856	1.909
19.563	1.680	1.651	1.953	1.943
20.188	1.571	1.535	1.893	1.849
20.813	1.763	1.717	1.809	1.750
21.438	1.779	1.789	1.783	1.713
22.063	1.831	1.731	1.830	1.686
22.688	1.837	1.814	1.796	1.658
23.313	1.535	1.434	1.729	1.630
23.938	1.611	1.469	1.647	1.601
24.375	1.855	1.641	1.769	1.743
24.438	1.791	1.602	1.883	1.725
24.500	1.742	1.582	1.948	1.685
24.563	1.779	1.629	1.936	1.713
24.625			1.925	1.662
24.688			2.022	1.729
24.750			1.963	1.761
24.813			1.984	1.760
24.875			2.041	1.752
24.938			1.946	1.743
25.000			1.930	1.695
25.063			1.864	1.795
25.125			1.784	1.751
25.188			1.790	1.822
25.250			1.768	1.803
25.313			1.698	1.875
25.375			1.722	2.051
25.438			1.801	2.232
25.500			1.923	2.115
25.563			2.277	2.450
25.625			2.754	3.076
25.688			3.077	3.113
25.750			1.325	1.883
25.813			1.654	1.628

Rough Channel: $Re=15,000$, $P/e=10$, $e/D=0.063$, $\alpha = 60^\circ$

Sh/Sh₀

	TOP WALL		
X/D	O.L.	C.L.	I.L.
	BEFORE	TURN	
8.063	4.004	4.034	3.288
8.688	2.671	3.289	2.646
9.313	4.736	4.129	3.364
9.375	4.005	3.991	3.575
9.438	RIB	3.726	3.173
9.500	RIB	3.240	2.994
9.563	RIB	RIB	2.837
9.625	2.802	RIB	2.554
9.688	4.373	RIB	RIB
9.750	5.204	2.391	RIB
9.813	5.118	3.885	RIB
9.875	5.578	3.863	2.105
9.938	5.050	3.316	2.211
10.000	3.172	3.567	2.872
10.063	RIB	3.629	2.924
10.125	RIB	3.043	2.810
10.188	RIB	RIB	2.633
10.250	2.995	RIB	2.551
10.313	3.434	RIB	RIB
10.375	5.655	2.159	RIB
10.438	6.496	3.264	RIB
10.500	5.108	3.701	1.992
10.563	4.202	3.720	2.564
10.625	2.923	3.294	2.896
10.688	RIB	3.055	2.793
10.750	RIB	2.693	2.617
10.813	RIB	RIB	2.349
10.875	1.715	RIB	2.133
10.938	3.205	RIB	RIB
11.000	5.424	2.159	RIB
11.063	5.462	2.871	RIB
11.125	4.964	3.262	1.673
11.188	4.436	3.744	2.209
11.250	1.527	3.619	2.599
11.313	RIB	4.213	2.877
11.375	RIB	2.562	2.857
11.438	RIB	RIB	2.878
11.500	1.135	RIB	2.879
11.563	4.481	RIB	RIB
11.625	5.657	3.048	RIB

	----- IN TURN -----		
11.875	2.769	4.290	3.446
12.375	2.140	1.863	2.125
12.875	2.485	1.539	2.658
13.125	2.124	2.195	2.141
13.625	2.170	2.108	1.956
14.125	2.474	2.228	2.165
	----- AFTER TURN -----		
14.375	1.895	2.511	RIB
14.438	1.463	RIB	RIB
14.500	3.171	RIB	1.969
14.563	RIB	RIB	1.988
14.625	RIB	2.414	2.058
14.688	RIB	2.762	2.929
14.750	2.984	3.942	3.103
14.813	3.016	4.140	3.413
14.875	3.923	4.307	3.393
14.938	4.193	4.000	RIB
15.000	4.266	4.063	RIB
15.063	4.123	RIB	RIB
15.125	4.113	RIB	1.938
15.188	RIB	RIB	2.764
15.250	RIB	1.631	2.898
15.313	RIB	2.625	3.063
15.375	1.884	3.257	3.053
15.438	3.369	3.476	2.794
15.500	3.516	3.290	2.586
15.563	3.516	3.124	RIB
15.625	3.308	2.999	RIB
15.688	3.235	RIB	RIB
15.750	3.005	RIB	1.727
15.813	RIB	RIB	2.874
15.875	RIB	1.207	2.842
15.938	RIB	2.828	3.135
16.000	1.703	3.017	3.271
16.063	2.646	3.153	3.125
16.125	3.276	2.986	2.674
16.188	3.350	2.838	RIB
16.250	3.414	2.985	RIB
16.313	3.340	RIB	RIB
16.375	3.191	RIB	1.353
16.438	RIB	RIB	2.416
16.500	RIB	1.314	3.238
16.563	RIB	2.432	3.037
16.625	1.719	2.822	2.952
16.688	2.554	2.811	2.444
17.313	2.018	2.736	3.101
17.938	2.784	3.196	3.197

OUTER WALL		AND	INNER WALL	

X/D	I.L.	C.L.	I.L.	C.L.

		BEFORE	TURN	

	OUTER	WALL	INNER	WALL

8.063	2.590	2.243	2.744	1.965
8.688	3.074	2.677	2.371	1.963
9.375	2.700	2.925	2.096	1.801
9.500	2.830	2.991	2.716	1.956
9.625	2.770	2.014	2.280	1.901
9.750	2.594	1.966	2.213	1.687
9.875	2.502	2.316	1.862	1.484
10.000	2.609	2.067	2.004	1.523
10.125	2.444	2.060	2.534	1.855
10.250	2.406	2.054	2.373	1.894
10.375	2.378	2.214	2.307	1.599
10.500	2.755	2.155	2.084	1.346
10.625	2.362	2.074	1.985	1.623
10.750	2.313	2.233	1.774	1.869
10.875	2.348	2.226	2.237	1.845
11.000	2.217	2.281	1.995	2.099
11.125	2.188	2.252	1.960	1.765
11.250	2.313	2.162	2.335	1.812
11.375	2.459	2.114	2.771	2.075
11.500	1.880	2.179	3.238	2.133
11.625	2.621	2.122		

		IN	TURN
11.875	2.606	2.095	
12.375	2.705	3.306	
12.875	3.490	2.983	
13.125	3.419	2.859	
13.625	2.667	2.493	
14.125	2.522	2.466	

		AFTER	TURN	
14.375	2.209	2.182		
14.500	2.128	2.224	2.904	2.804
14.625	2.324	2.051	2.595	2.812
14.750	2.419	2.105	2.655	2.945
14.875	2.413	1.964	3.016	3.049
15.000	2.407	1.957	3.131	3.505
15.125	2.431	2.186	3.245	3.557
15.250	1.977	1.908	2.954	3.723
15.375	2.114	1.838	3.037	3.879
15.500	1.992	1.819	2.819	3.737
15.625	1.953	2.009	2.819	3.686
15.750	2.205	1.990	3.131	3.707
15.875	2.374	1.887	3.234	3.613
16.000	2.251	1.888	3.151	3.163
16.125	2.380	1.870	2.910	2.965
16.250	2.341	1.861	2.762	2.922
16.375	2.301	1.789	2.644	3.269
16.500	2.197	1.895	2.442	3.162
16.625	2.210	1.907	2.545	2.759
17.313	2.376	2.134	2.004	2.157
17.938	1.867	2.055	2.211	2.312

Rough Channel: $Re=30,000$, $P/e=10$, $e/D=0.063$, $\alpha = 60^\circ$

Sh/Sh₀			

	TOP	WALL	

X/D	O.L.	C.L.	I.L.

	BEFORE	TURN	

0.375		1.767	
0.438		2.974	
0.500		4.108	
0.563		2.547	
0.625		2.245	
0.688		1.701	
0.750		2.114	
1.000		3.406	
1.063		3.828	
1.125		4.281	
1.188		4.859	
1.250		4.310	
1.313		4.071	
1.375		3.853	
1.813		4.265	
2.438		4.143	
3.063		4.044	
3.688		3.869	
4.313		3.576	
4.938		3.395	
5.563		3.390	
6.188		3.460	
6.625		3.029	
6.688		3.615	
6.750		3.807	
6.813		3.677	
6.875		3.564	
6.938		3.293	
7.000		2.791	
7.250		3.505	
7.313		3.731	
7.375		3.915	
7.438		3.820	
7.500		3.413	
7.563		3.197	
7.625		2.930	
8.063		3.649	
8.688		3.712	
9.313	3.982	4.177	3.035

9.375	3.028	3.775	3.361
9.438	RIB	3.380	3.173
9.500	RIB	2.960	3.226
9.563	RIB	RIB	2.690
9.625	3.020	RIB	2.395
9.688	4.515	RIB	RIB
9.750	5.097	2.650	RIB
9.813	5.129	3.748	RIB
9.875	4.161	4.104	2.157
9.938	3.413	4.142	2.667
10.000	2.531	3.775	3.022
10.063	RIB	3.286	2.863
10.125	RIB	2.824	2.793
10.188	RIB	RIB	2.801
10.250	2.910	RIB	2.469
10.313	4.997	RIB	RIB
10.375	5.048	2.709	RIB
10.438	4.484	3.755	RIB
10.500	3.971	3.966	2.117
10.563	3.005	3.978	2.508
10.625	1.926	3.780	2.931
10.688	RIB	3.257	3.009
10.750	RIB	2.709	2.863
10.813	RIB	RIB	2.750
10.875	2.489	RIB	2.401
10.938	4.247	RIB	RIB
11.000	5.207	2.652	RIB
11.063	4.964	3.377	RIB
11.125	3.985	3.840	1.950
11.188	2.970	3.890	2.452
11.250	1.824	3.611	2.757
11.313	RIB	2.738	2.821
11.375	RIB	2.094	2.759
11.438	RIB	RIB	2.653
11.500	3.107	RIB	2.339
11.563	4.743	RIB	RIB
11.625	4.391	2.273	RIB

IN TURN

11.875	1.878	2.965	3.460
12.375	2.352	2.287	1.819
12.875	2.590	1.972	2.059
13.125	2.382	2.070	1.954
13.625	2.014	1.897	1.893
14.125	1.880	1.907	1.803

	AFTER	TURN	
14.375	1.736	1.527	RIB
14.438	1.342	RIB	RIB
14.500	1.788	RIB	1.597
14.563	RIB	RIB	1.942
14.625	RIB	2.023	2.306
14.688	RIB	3.191	2.419
14.750	2.121	3.621	2.620
14.813	3.369	3.761	2.905
14.875	3.522	3.724	2.980
14.938	3.725	3.800	RIB
15.000	3.712	3.591	RIB
15.063	3.610	RIB	RIB
15.125	3.456	RIB	2.136
15.188	RIB	RIB	2.695
15.250	RIB	2.178	2.751
15.313	RIB	3.535	2.660
15.375	2.188	3.637	2.595
15.438	3.357	3.669	2.460
15.500	3.619	3.471	2.408
15.563	3.433	3.029	RIB
15.625	3.458	2.797	RIB
15.688	2.950	RIB	RIB
15.750	2.897	RIB	1.913
15.813	RIB	RIB	2.682
15.875	RIB	1.440	2.989
15.938	RIB	2.532	3.045
16.000	1.649	3.116	2.858
16.063	2.652	3.212	2.605
16.125	2.851	2.953	2.320
16.188	2.947	2.972	RIB
16.250	2.803	2.699	RIB
16.313	2.634	RIB	RIB
16.375	2.541	RIB	1.996
16.438	RIB	RIB	2.991
16.500	RIB	1.500	2.996
16.563	RIB	2.619	2.716
16.625	1.750	3.053	2.533
16.688	2.449	2.857	2.233
17.313		3.199	
17.938		2.703	
18.375		2.603	
18.438		3.980	
18.500		4.110	
18.563		4.072	
18.625		3.801	
18.688		3.524	
18.750		2.437	
19.000		2.758	

19.063	4.014
19.125	4.378
19.188	4.030
19.250	3.862
19.313	3.647
19.375	2.773
19.813	3.796
20.438	3.610
21.063	3.575
21.688	3.331
22.313	3.267
22.938	3.288
23.563	3.542
24.188	3.720
24.625	2.739
24.688	4.069
24.750	4.479
24.813	3.951
24.875	3.765
24.938	3.356
25.000	3.232
25.250	3.155
25.313	2.738
25.375	3.212
25.438	3.381
25.500	2.880
25.563	2.486
25.625	2.219

OUTER WALL		AND	INNER WALL	

X/D	I.L.	C.L.	I.L.	C.L.

BEFORE TURN				

	OUTER	WALL	INNER	WALL

0.563		3.765		4.046
1.188		3.222		3.321
1.813		2.800		2.861
2.438		2.551		2.749
3.063		2.314		2.449
3.688		2.162		2.554
4.313		2.092		2.451
4.938		1.860		2.264
5.563		2.013		2.086
6.188		2.122		2.200
6.813		2.289		2.137
7.438		2.303		2.114
8.063		2.402		1.937
8.688		2.463		1.874
9.375	2.297	2.675	2.283	1.649
9.500	2.247	2.339	2.574	1.682
9.625	2.183	2.566	2.477	1.729
9.750	2.127	2.355	2.129	1.652
9.875	2.122	2.194	2.361	1.640
10.000	2.193	2.298	2.760	1.686
10.125	2.201	2.350	3.048	1.661
10.250	2.139	2.352	2.951	1.720
10.375	2.089	2.276	2.579	1.747
10.500	2.096	2.411	2.201	1.856
10.625	2.180	2.347	2.481	1.914
10.750	2.238	2.322	2.984	1.921
10.875	2.182	2.324	2.811	1.845
11.000	2.152	2.306	2.563	1.801
11.125	2.101	2.268	2.625	1.814
11.250	2.127	2.223	3.097	1.845
11.375	2.197	2.236	3.469	1.890
11.500	2.091	2.149	3.354	2.023
11.625	2.238	2.000		

		IN	TURN	

11.875	2.399	2.103		
12.375	2.200	2.449		
12.875	2.933	2.573		
13.125	2.349	2.040		
13.625	2.376	2.405		
14.125	2.617	2.241		

		AFTER	TURN	

14.375	2.694	2.295		
14.500	2.775	2.174	2.995	3.072
14.625	2.604	1.996	3.092	3.080
14.750	2.490	2.014	3.260	3.033
14.875	2.301	1.976	3.202	3.070
15.000	2.105	1.874	3.219	3.042
15.125	1.887	1.835	2.993	3.154
15.250	1.956	1.833	2.881	3.156
15.375	2.057	1.851	2.769	2.911
15.500	2.147	1.915	2.536	2.780
15.625	2.197	1.901	2.500	2.687
15.750	2.286	1.983	2.463	2.631
15.875	2.343	1.962	2.439	2.537
16.000	2.349	2.000	2.358	2.520
16.125	2.284	2.077	2.405	2.497
16.250	2.264	2.076	2.388	2.422
16.375	2.289	2.048	2.493	2.255
16.500	2.346	2.060	2.624	2.476
16.625	2.248	2.091	2.627	2.887
17.313		2.532		2.666
17.938		2.595		2.708
18.563		2.529		2.576
19.188		2.310		2.512
19.813		2.358		2.397
20.438		1.922		2.111
21.063		1.916		2.151
21.688		1.934		2.105
22.313		2.148		2.089
22.938		2.273		2.326
23.563		2.377		2.563
24.188		2.376		2.622
24.813				2.852
25.438				3.390

Rough Channel: $Re=60,000$, $P/e=10$, $e/D=0.063$, $\alpha = 60^\circ$

	----- TOP WALL -----		
X/D	O.L.	C.L.	I.L.
	----- BEFORE TURN -----		
9.313	3.522	3.871	3.413
9.375	2.614	3.512	3.247
9.438	RIB	3.342	3.093
9.500	RIB	3.022	2.889
9.563	RIB	RIB	2.747
9.625	2.813	RIB	2.567
9.688	3.992	RIB	RIB
9.750	4.465	2.190	RIB
9.813	4.276	3.421	RIB
9.875	3.719	3.717	1.948
9.938	3.142	3.574	2.382
10.000	2.095	3.290	2.609
10.063	RIB	3.021	2.609
10.125	RIB	2.692	2.495
10.188	RIB	RIB	2.443
10.250	3.052	RIB	2.382
10.313	4.394	RIB	RIB
10.375	4.447	2.524	RIB
10.438	4.019	2.978	RIB
10.500	3.316	3.672	2.072
10.563	2.595	3.881	2.671
10.625	1.826	3.697	2.880
10.688	RIB	3.270	2.945
10.750	RIB	2.712	2.915
10.813	RIB	RIB	2.771
10.875	2.628	RIB	2.719
10.938	4.089	RIB	RIB
11.000	4.233	2.555	RIB
11.063	3.671	2.915	RIB
11.125	2.834	3.669	1.816
11.188	2.085	3.649	2.471
11.250	1.802	3.210	2.683
11.313	RIB	2.689	2.853
11.375	RIB	2.067	2.835
11.438	RIB	RIB	2.583
11.500	2.874	RIB	2.335
11.563	4.159	RIB	RIB
11.625	3.719	2.625	RIB

	IN TURN		

11.875	1.732	2.643	3.340
12.375	1.631	1.680	1.720
12.875	1.927	1.728	1.987
13.125	1.794	1.785	1.902
13.625	1.669	1.910	2.071
14.125	1.907	2.221	2.265

	AFTER TURN		

14.375	1.702	2.209	RIB
14.438	1.531	RIB	RIB
14.500	2.438	RIB	2.355
14.563	RIB	RIB	2.554
14.625	RIB	2.287	2.599
14.688	RIB	2.928	2.673
14.750	2.352	3.151	2.696
14.813	2.873	3.299	2.646
14.875	3.362	3.299	2.684
14.938	3.506	3.182	RIB
15.000	3.529	3.065	RIB
15.063	3.389	RIB	RIB
15.125	3.199	RIB	2.531
15.188	RIB	RIB	3.009
15.250	RIB	2.675	3.008
15.313	RIB	3.440	2.878
15.375	2.566	3.600	2.753
15.438	3.397	3.498	2.639
15.500	3.394	3.220	2.547
15.563	3.280	3.083	RIB
15.625	3.169	2.789	RIB
15.688	2.985	RIB	RIB
15.750	2.805	RIB	1.967
15.813	RIB	RIB	2.674
15.875	RIB	1.817	2.815
15.938	RIB	2.874	2.761
16.000	2.012	2.969	2.618
16.063	2.637	2.908	2.419
16.125	2.917	2.827	2.245
16.188	2.898	2.631	RIB
16.250	2.844	2.526	RIB
16.313	2.670	RIB	RIB
16.375	2.599	RIB	2.719
16.438	RIB	RIB	3.269
16.500	RIB	2.226	3.215
16.563	RIB	2.958	2.960
16.625	2.179	3.015	2.569
16.688	2.781	3.096	2.503

	OUTER	WALL	AND	INNER	WALL

X/D	I.L.	C.L.		I.L.	C.L.

	BEFORE		TURN		

	OUTER	WALL		INNER	WALL

9.375	2.070	2.983		2.191	1.682
9.500	2.004	2.596		2.575	1.670
9.625	1.926	2.075		2.504	1.634
9.750	1.880	2.159		2.237	1.622
9.875	1.918	2.177		2.208	1.590
10.000	1.932	2.142		2.413	1.643
10.125	1.939	2.137		2.595	1.638
10.250	1.916	2.148		2.566	1.618
10.375	1.881	2.109		2.308	1.721
10.500	1.918	2.108		2.085	1.742
10.625	1.936	2.083		2.128	1.740
10.750	1.905	2.063		2.434	1.716
10.875	1.863	2.013		2.512	1.696
11.000	1.843	2.009		2.328	1.657
11.125	1.835	1.924		2.144	1.671
11.250	1.788	1.885		2.482	1.707
11.375	1.788	1.813		2.849	1.710
11.500	1.761	1.805		2.881	1.743
11.625	1.803	1.779			

		IN	TURN	

11.875	1.987	1.773		
12.375	2.232	2.776		
12.875	2.566	2.228		
13.125	2.426	1.998		
13.625	2.171	2.100		
14.125	2.696	2.158		

		AFTER	TURN	

14.375	2.528	1.975		
14.500	2.653	1.968	2.486	1.830
14.625	2.624	2.040	2.587	2.077
14.750	2.543	2.041	2.685	2.171
14.875	2.485	2.047	2.686	2.356
15.000	2.404	2.094	2.724	2.489
15.125	2.352	2.113	2.751	2.557
15.250	2.365	2.221	2.754	2.518
15.375	2.549	2.234	2.751	2.621
15.500	2.625	2.362	2.718	2.577
15.625	2.650	2.368	2.673	2.523
15.750	2.636	2.400	2.569	2.511
15.875	2.603	2.378	2.518	2.503
16.000	2.490	2.337	2.434	2.457
16.125	2.350	2.301	2.357	2.369
16.250	2.301	2.267	2.376	2.314
16.375	2.302	2.241	2.275	2.305
16.500	2.218	2.196	2.266	2.274
16.625	2.030	2.170	2.176	2.157

Rough Channel: $Re=15,000$, $P/e=10$, $e/D=0.063$, $\alpha = 45^\circ$

	----- TOP WALL -----		
X/D	O.L.	C.L.	I.L.
	----- BEFORE TURN -----		
8.875	2.150	3.253	1.848
8.938	3.974	4.462	RIB
9.000	1.544	4.184	RIB
9.063	RIB	3.619	2.739
9.125	RIB	2.443	2.849
9.188	4.958	2.706	2.448
9.250	6.088	2.233	2.306
9.313	6.454	RIB	2.327
9.375	4.465	RIB	2.231
9.438	3.302	2.124	2.117
9.500	2.705	2.671	1.968
9.563	2.261	4.512	RIB
9.625	1.810	3.960	RIB
9.688	RIB	3.017	2.734
9.750	RIB	2.565	2.541
9.813	5.757	2.443	2.303
9.875	6.855	RIB	2.225
9.938	6.631	RIB	2.219
10.000	5.114	RIB	2.274
10.063	3.547	2.240	1.737
10.125	2.258	3.576	1.643
10.188	2.039	4.460	RIB
10.250	1.751	4.117	RIB
10.313	RIB	3.140	2.842
10.375	RIB	1.953	2.210
10.438	4.899	2.079	2.046
10.500	6.040	1.317	2.267
10.563	5.424	RIB	2.243
10.625	4.345	RIB	1.904
10.688	3.514	2.176	2.117
10.750	2.360	2.939	1.848
10.813	1.882	4.356	RIB
10.875	1.257	4.199	RIB
10.938	RIB	3.459	2.458
11.000	RIB	2.276	2.565
11.063	4.808	1.722	2.341
11.125	5.763	1.698	2.978
11.188	5.718	RIB	3.856
11.250	4.530	RIB	3.354

11.313	3.646	2.548	3.061
11.375	2.868	2.879	2.647
11.438	2.472	4.332	RIB
11.500	2.190	4.126	RIB
11.563	1.959	3.316	1.860
11.625	1.954	2.688	2.173

IN TURN

11.875	2.120	2.195	1.935
12.375	2.179	2.411	2.139
12.875	2.639	2.434	2.180
13.125	2.543	2.415	2.292
13.625	2.651	2.141	2.151
14.125	2.319	2.321	2.117

AFTER TURN

14.375	2.518	2.310	2.230
14.438	2.525	2.307	2.202
14.500	2.453	2.089	RIB
14.563	2.451	2.656	RIB
14.625	2.310	3.598	2.220
14.688	2.022	2.254	3.283
14.750	1.751	RIB	2.770
14.813	1.201	RIB	3.080
14.875	2.544	2.273	3.609
14.938	1.437	1.862	3.956
15.000	RIB	2.225	4.182
15.063	RIB	2.763	4.007
15.125	2.326	3.214	RIB
15.188	2.114	3.736	RIB
15.250	2.697	4.549	2.719
15.313	3.588	4.943	2.184
15.375	4.026	RIB	2.480
15.438	4.455	RIB	2.907
15.500	4.622	3.215	3.432
15.563	4.790	3.012	3.713
15.625	RIB	3.503	3.669
15.688	RIB	3.978	2.857
15.750	2.832	3.968	RIB
15.813	2.839	3.790	RIB
15.875	3.597	3.710	1.463
15.938	4.348	3.267	2.097
16.000	4.446	RIB	2.785
16.063	4.428	RIB	3.209
16.125	3.966	2.535	3.261
16.188	3.593	2.720	2.975
16.250	RIB	3.011	2.938
16.313	RIB	3.276	2.393
16.375	1.565	3.105	RIB

16.438	1.722	3.495	RIB
16.500	2.665	3.351	2.411
16.563	3.486	1.553	2.758
16.625	3.816	RIB	3.078
16.688	3.896	RIB	3.130
16.750	3.590	1.121	2.859
16.813	2.053	1.746	2.723
16.875	RIB	2.731	2.532
16.938	RIB	3.044	2.457
17.000	RIB	3.222	RIB
17.063	1.879	3.175	RIB
17.125	2.534	3.055	2.476

OUTER WALL		AND	INNER WALL	

X/D	I.L.	C.L.	I.L.	C.L.

BEFORE TURN				

	OUTER	WALL	INNER	WALL

8.875	1.903	2.069	2.270	1.950
9.000	1.918	2.129	2.555	2.020
9.125	1.943	2.109	2.497	1.918
9.250	1.922	2.132	2.421	1.879
9.375	2.017	2.165	2.506	1.822
9.500	1.987	2.143	2.627	1.757
9.625	1.949	2.149	2.266	1.826
9.750	1.991	2.155	2.307	1.796
9.875	1.987	2.249	2.658	1.820
10.000	1.922	2.343	2.494	1.844
10.125	1.884	2.391	2.542	1.893
10.250	1.898	2.405	2.838	1.917
10.375	1.975	2.340	3.035	1.940
10.500	2.024	2.204	2.897	2.007
10.625	1.907	2.121	2.769	2.012
10.750	1.947	2.091	3.026	2.017
10.875	1.892	2.123	3.108	2.066
11.000	1.880	2.093	3.068	2.089
11.125	1.825	2.107	3.375	1.990
11.250	1.710	2.035	3.447	1.926
11.375	1.664	1.980	3.155	1.940
11.500	1.627	1.666	3.141	1.859
11.625	1.659	1.543		

		IN	TURN
11.875	1.935	1.640	
12.375	2.435	2.707	
12.875	2.854	2.709	
13.125	2.894	2.209	
13.625	2.495	2.361	
14.125	2.760	3.040	

		AFTER	TURN	
14.375	2.650	3.114		
14.500	2.743	2.957	2.962	2.964
14.625	2.724	2.947	3.075	2.982
14.750	2.670	2.859	3.172	3.087
14.875	2.581	2.736	3.242	3.314
15.000	2.344	2.517	3.305	3.237
15.125	2.167	2.270	3.272	3.160
15.250	1.884	1.987	3.221	3.188
15.375	1.767	1.914	3.109	3.277
15.500	1.675	1.805	2.917	3.086
15.625	1.786	1.846	2.813	3.009
15.750	2.232	1.824	2.681	2.771
15.875	2.600	1.935	2.673	2.736
16.000	2.722	1.994	2.514	2.507
16.125	2.774	2.097	2.541	2.480
16.250	2.808	2.165	2.470	2.605
16.375	2.716	2.242	2.674	2.676
16.500	2.687	2.337	2.656	2.774
16.625	2.560	2.406	3.256	2.846
16.750	2.459	2.546	3.042	2.901
16.875	2.402	2.553	2.917	2.766
17.000	2.488	2.577	2.998	2.856
17.125	2.269	2.547	3.197	2.991

Rough Channel: $Re=30,000$, $P/e=10$, $e/D=0.063$, $\alpha = 45^\circ$

TOP WALL			

X/D	O.L.	C.L.	I.L.

	BEFORE	TURN	

0.625		1.609	
0.688		3.180	
0.750		4.713	
0.813		4.237	
0.875		3.835	
0.938		3.459	
1.000		2.919	
1.063		3.247	
1.250		1.849	
1.313		2.604	
1.375		3.197	
1.438		3.676	
1.500		3.370	
1.563		3.002	
1.625		2.799	
1.688		2.733	
2.125		2.706	
2.750		2.550	
3.375		2.535	
4.000		2.475	
4.625		2.416	
5.250		2.320	
5.875		2.147	
6.250		1.886	
6.313		3.014	
6.375		2.750	
6.438		2.579	
6.500		2.358	
6.563		2.153	
6.625		1.896	
6.688		1.910	
6.875		1.758	
6.938		3.074	
7.000		2.705	
7.063		2.520	
7.125		2.267	
7.188		2.109	
7.250		1.963	
7.313		1.912	

7.750		2.296	
8.375		2.400	
8.875	2.375	2.892	1.786
8.938	1.461	3.882	RIB
9.000	1.308	3.634	RIB
9.063	RIB	3.106	2.473
9.125	RIB	2.319	2.531
9.188	4.483	1.666	2.594
9.250	4.321	1.501	2.634
9.313	5.166	RIB	2.726
9.375	4.289	RIB	2.469
9.438	3.442	1.692	2.189
9.500	2.664	2.207	1.686
9.563	1.758	3.792	RIB
9.625	1.781	3.775	RIB
9.688	RIB	3.387	1.905
9.750	RIB	2.755	2.521
9.813	3.892	2.021	2.282
9.875	3.862	2.112	2.600
9.938	4.751	RIB	2.963
10.000	3.865	RIB	2.860
10.063	3.043	1.859	2.639
10.125	2.306	1.848	2.356
10.188	1.719	3.430	RIB
10.250	1.771	3.520	RIB
10.313	RIB	3.164	2.367
10.375	RIB	2.566	2.368
10.438	4.784	1.924	2.187
10.500	4.832	1.930	2.491
10.563	4.784	RIB	2.828
10.625	3.761	RIB	2.710
10.688	3.064	2.329	2.630
10.750	2.391	2.339	2.143
10.813	2.089	4.096	RIB
10.875	1.703	4.016	RIB
10.938	RIB	3.473	2.607
11.000	RIB	2.820	2.869
11.063	4.035	2.524	2.668
11.125	4.328	2.145	3.330
11.188	4.538	RIB	3.602
11.250	3.659	RIB	3.468
11.313	3.119	2.313	3.367
11.375	2.618	2.873	2.800
11.438	2.474	3.997	RIB
11.500	2.369	3.686	RIB
11.563	2.507	3.204	2.129
11.625	2.496	2.550	2.616

	IN	TURN	

11.875	2.562	2.658	2.379
12.375	2.359	2.477	2.460
12.875	2.718	2.562	2.590
13.125	2.731	2.652	2.707
13.625	2.476	2.459	2.661
14.125	2.860	2.835	2.833

	AFTER	TURN	

14.375	2.965	2.889	2.939
14.438	3.187	2.939	3.831
14.500	3.182	2.868	RIB
14.563	3.166	3.627	RIB
14.625	2.601	5.242	2.719
14.688	2.180	5.279	3.392
14.750	2.057	RIB	3.143
14.813	1.967	RIB	3.410
14.875	2.535	1.740	3.884
14.938	4.609	2.062	4.309
15.000	RIB	2.246	4.535
15.063	RIB	2.983	4.229
15.125	3.228	3.553	RIB
15.188	3.324	3.840	RIB
15.250	3.622	4.479	3.388
15.313	4.448	4.841	3.368
15.375	4.523	RIB	3.206
15.438	4.609	RIB	3.263
15.500	4.764	3.123	3.607
15.563	4.930	3.338	3.660
15.625	RIB	3.570	3.650
15.688	RIB	3.830	2.844
15.750	2.786	3.820	RIB
15.813	2.730	3.781	RIB
15.875	3.929	3.743	2.624
15.938	4.514	3.507	2.959
16.000	4.499	RIB	3.447
16.063	4.251	RIB	3.448
16.125	3.924	2.835	3.471
16.188	3.562	2.977	3.137
16.250	RIB	3.296	3.132
16.313	RIB	3.718	2.825
16.375	2.635	3.724	RIB
16.438	2.732	3.811	RIB
16.500	3.548	3.623	2.580
16.563	4.150	3.505	2.814
16.625	4.123	RIB	3.021
16.688	3.998	RIB	2.918
16.750	3.816	1.972	2.706

16.813	3.622	2.155	2.442
16.875	RIB	2.791	2.327
16.938	RIB	2.975	2.275
17.000	1.675	2.997	RIB
17.063	1.926	2.813	RIB
17.125	2.547	2.796	2.002
17.625		3.092	
18.250		3.295	
18.688		1.894	
18.750		2.368	
18.813		3.378	
18.875		2.663	
18.938		2.376	
19.000		2.247	
19.063		2.085	
19.125		2.026	
19.313		1.744	
19.375		2.572	
19.438		3.430	
19.500		3.020	
19.563		2.649	
19.625		2.443	
19.688		2.212	
19.750		2.031	
20.125		2.835	
20.750		2.725	
21.375		2.568	
22.000		2.552	
22.625		2.491	
23.250		2.400	
23.875		2.511	
24.313		1.908	
24.375		2.667	
24.438		3.480	
24.500		2.979	
24.563		2.704	
24.625		2.318	
24.688		2.058	
24.750		2.017	
24.938		1.816	
25.000		2.041	
25.063		3.219	
25.125		2.577	
25.188		2.076	
25.250		1.925	
25.313		1.910	
25.375		2.279	

OUTER WALL		AND	INNER WALL	

X/D	I.L.	C.L.	I.L.	C.L.

BEFORE TURN				

	OUTER	WALL	INNER	WALL

0.875		2.904		2.717
1.500		2.255		2.195
2.125		2.020		1.959
2.750		1.898		2.011
3.375		1.793		1.964
4.000		1.661		1.967
4.625		1.605		1.889
5.250		1.528		2.004
5.875		1.539		1.982
6.500		1.538		2.002
7.125		1.489		1.811
7.750		1.464		1.829
8.375		1.829		1.700
8.875	1.891	2.135	2.011	1.470
9.000	1.890	2.214	1.980	1.583
9.125	1.951	2.160	1.971	1.501
9.250	1.955	2.169	1.934	1.676
9.375	2.016	2.144	2.125	1.639
9.500	2.060	2.164	2.150	1.573
9.625	1.915	2.139	1.895	1.656
9.750	1.982	2.177	2.092	1.580
9.875	1.991	2.169	2.167	1.582
10.000	1.886	2.155	2.004	1.579
10.125	1.946	2.186	2.029	1.571
10.250	1.921	2.223	2.070	1.590
10.375	1.970	2.029	2.202	1.689
10.500	1.984	2.195	2.096	1.759
10.625	1.954	2.169	2.047	1.756
10.750	2.029	2.116	2.379	1.724
10.875	1.932	2.029	2.548	1.782
11.000	1.952	2.049	2.627	1.779
11.125	1.928	2.063	2.873	1.837
11.250	1.870	2.017	2.951	1.934
11.375	1.990	2.020	2.851	1.953
11.500	2.049	1.929	2.896	2.110
11.625	2.068	1.910	2.260	2.172

		IN	TURN
11.875	2.163	1.916	
12.375	2.281	2.604	
12.875	2.155	2.076	
13.125	1.729	1.891	
13.625	2.220	2.242	
14.125	2.831	2.968	

		AFTER	TURN	
14.375	2.507	2.698	2.733	2.736
14.500	2.229	2.682	2.537	2.529
14.625	2.145	2.459	2.778	2.576
14.750	2.178	2.465	2.982	2.768
14.875	2.054	2.542	2.995	2.915
15.000	1.924	2.374	3.033	2.880
15.125	1.761	2.239	3.109	2.983
15.250	1.680	2.188	3.062	2.981
15.375	1.757	2.238	2.938	2.991
15.500	1.756	2.260	2.907	2.989
15.625	2.013	2.175	2.771	2.875
15.750	2.181	2.213	2.784	2.805
15.875	2.276	2.302	2.640	2.711
16.000	2.304	2.268	2.564	2.607
16.125	2.388	2.233	2.487	2.564
16.250	2.365	2.215	2.427	2.550
16.375	2.301	2.293	2.389	2.398
16.500	2.294	2.377	2.283	2.360
16.625	2.327	2.291	2.291	2.288
16.750	2.274	2.375	2.218	2.147
16.875	2.261	2.391	2.197	2.142
17.000	2.259	2.447	2.197	2.161
17.125	2.240	2.382	2.158	2.110
17.625		2.048		2.345
18.250		1.868		2.008
18.875		1.705		1.891
19.500		1.553		1.806
20.125		1.359		1.680
20.750		1.512		1.635
21.375		1.663		1.571
22.000		1.575		1.530
22.625		1.575		1.597
23.250		1.469		1.588
23.875		1.462		1.611
24.500		1.592		1.726
25.125				2.434

Rough Channel: $Re=60,000$, $P/e=10$, $e/D=0.063$, $\alpha = 45^\circ$

	----- TOP WALL -----		
X/D	O.L.	C.L.	I.L.
	----- BEFORE TURN -----		
8.875	2.650	2.902	1.722
8.938	2.854	3.341	RIB
9.000	2.590	2.842	RIB
9.063	RIB	2.297	2.200
9.125	RIB	1.664	2.211
9.188	4.133	2.459	2.273
9.250	4.253	2.232	2.412
9.313	4.341	RIB	2.341
9.375	2.846	RIB	2.175
9.438	2.105	2.482	1.899
9.500	1.464	3.053	1.620
9.563	1.104	3.216	RIB
9.625	0.9461	2.898	RIB
9.688	RIB	2.251	2.253
9.750	RIB	1.888	2.194
9.813	3.947	1.596	2.276
9.875	3.455	1.445	2.464
9.938	3.317	RIB	2.454
10.000	2.609	RIB	2.334
10.063	2.039	1.903	2.134
10.125	1.536	3.142	1.867
10.188	2.040	3.008	RIB
10.250	1.862	2.524	RIB
10.313	RIB	2.054	2.221
10.375	RIB	1.540	1.928
10.438	4.182	1.769	2.167
10.500	4.250	1.630	2.297
10.563	3.644	RIB	2.175
10.625	2.780	RIB	1.896
10.688	2.110	2.548	1.869
10.750	1.681	2.521	1.538
10.813	2.006	3.110	RIB
10.875	1.683	2.720	RIB
10.938	RIB	2.125	1.451
11.000	RIB	1.583	1.773
11.063	3.610	1.737	1.847
11.125	3.741	1.627	2.265
11.188	3.189	RIB	2.231
11.250	2.360	RIB	2.034

11.313	1.862	1.732	1.983
11.375	1.578	2.464	1.766
11.438	1.521	2.679	RIB
11.500	1.484	2.102	RIB
11.563	1.579	1.605	1.334
11.625	1.542	1.399	1.525

IN TURN

11.875	1.724	1.514	1.452
12.375	1.613	1.824	1.680
12.875	1.860	1.767	1.708
13.125	1.816	1.723	1.814
13.625	1.736	1.663	1.775
14.125	2.067	1.722	1.884

AFTER TURN

14.375	1.891	1.675	2.302
14.438	1.959	1.587	1.903
14.500	1.895	1.516	RIB
14.563	1.794	1.858	RIB
14.625	1.713	3.398	1.816
14.688	1.514	3.045	2.200
14.750	1.384	RIB	1.911
14.813	1.754	RIB	2.025
14.875	2.319	1.529	2.406
14.938	3.456	1.980	3.018
15.000	RIB	2.177	3.571
15.063	RIB	2.500	2.996
15.125	2.066	2.914	RIB
15.188	2.337	3.427	RIB
15.250	2.891	3.783	1.750
15.313	3.733	2.876	2.308
15.375	4.083	RIB	2.566
15.438	4.179	RIB	2.618
15.500	4.243	1.667	2.681
15.563	3.823	2.388	2.709
15.625	RIB	2.601	2.673
15.688	RIB	2.727	2.311
15.750	2.314	2.811	RIB
15.813	2.728	2.930	RIB
15.875	3.586	2.983	2.492
15.938	4.302	3.124	2.826
16.000	4.162	RIB	2.995
16.063	3.972	RIB	2.784
16.125	3.726	1.578	2.649
16.188	3.437	1.962	2.540
16.250	RIB	2.647	2.440
16.313	RIB	2.894	2.277
16.375	1.667	2.894	RIB

16.438	1.981	2.893	RIB
16.500	2.700	2.861	2.802
16.563	3.349	3.028	2.976
16.625	3.559	RIB	2.870
16.688	3.498	RIB	2.571
16.750	3.428	1.826	2.410
16.813	3.677	2.035	2.172
16.875	RIB	2.479	2.010
16.938	RIB	2.692	1.828
17.000	1.958	2.673	RIB
17.063	1.864	2.548	RIB
17.125	2.545	2.461	2.634

	OUTER WALL	AND	INNER WALL	
X/D	I.L.	C.L.	I.L.	C.L.
	BEFORE TURN			
	OUTER	WALL	INNER	WALL
8.875	1.862	2.049	2.484	1.747
9.000	1.850	2.069	2.223	1.740
9.125	1.855	2.035	2.301	1.712
9.250	1.829	2.054	2.325	1.793
9.375	1.859	2.055	2.341	1.772
9.500	1.867	2.042	2.358	1.775
9.625	1.848	2.040	2.162	1.764
9.750	1.843	2.056	2.253	1.697
9.875	1.869	2.100	2.429	1.665
10.000	1.881	2.073	2.290	1.738
10.125	1.833	2.038	2.274	1.671
10.250	1.842	2.018	2.189	1.643
10.375	1.833	1.929	2.255	1.660
10.500	1.831	2.018	2.344	1.681
10.625	1.755	2.022	2.200	1.740
10.750	1.774	1.975	2.327	1.739
10.875	1.787	1.976	2.215	1.697
11.000	1.789	1.999	2.225	1.694
11.125	1.745	1.934	2.331	1.718
11.250	1.737	1.925	2.490	1.732
11.375	1.791	1.924	2.402	1.849
11.500	1.768	1.867	2.471	1.981
11.625	1.712	1.810		

		IN	TURN	

11.875	1.695	1.747		
12.375	1.961	2.141		
12.875	2.080	1.896		
13.125	1.803	1.757		
13.625	2.037	2.003		
14.125	2.257	2.570		

		AFTER	TURN	

14.375	2.140	2.538		
14.500	2.113	2.449	2.888	2.886
14.625	2.044	2.443	2.928	2.880
14.750	2.006	2.396	3.051	3.001
14.875	2.069	2.424	3.123	2.940
15.000	2.070	2.356	3.133	2.880
15.125	2.081	2.336	2.982	2.899
15.250	2.131	2.358	2.802	2.758
15.375	2.177	2.384	2.693	2.754
15.500	2.315	2.515	2.653	2.661
15.625	2.551	2.559	2.592	2.590
15.750	2.595	2.585	2.534	2.651
15.875	2.564	2.551	2.589	2.593
16.000	2.545	2.490	2.602	2.673
16.125	2.568	2.530	2.636	2.725
16.250	2.531	2.497	2.666	2.777
16.375	2.415	2.303	2.696	2.771
16.500	2.367	2.201	2.641	2.844
16.625	2.347	2.376	2.796	2.836
16.750	2.277	2.282	2.905	2.870
16.875	2.189	2.219	2.964	2.816
17.000	2.093	2.144	2.937	2.831
17.125	2.022	2.048	2.864	2.762

Rough Channel: $Re=30,000$, $P/e=20$, $e/D=0.063$, $\alpha = 90^\circ$

TOP WALL			

X/D	O.L.	C.L.	I.L.

	BEFORE	TURN	

6.875	2.713	2.373	2.834
7.000	2.617	2.613	2.715
7.125	2.432	2.468	2.538
7.250	2.167	2.144	2.268
7.375	2.016	2.133	2.110
7.500	1.854	1.923	2.051
7.625	1.715	1.700	1.922
7.750	1.423	1.491	1.597
7.875	1.986	1.737	2.222
8.000	RIB	RIB	RIB
8.125	2.465	2.446	2.413
8.250	2.657	2.733	2.751
8.375	2.457	2.438	2.506
8.500	2.307	2.154	2.371
8.625	1.897	2.030	2.149
8.750	1.919	1.889	2.026
8.875	1.860	1.762	1.920
9.000	1.460	1.546	1.585
9.125	2.248	2.035	2.488
9.250	RIB	RIB	RIB
9.375	2.267	2.385	2.460
9.500	2.618	2.664	2.782
9.625	2.456	2.416	2.523
9.750	2.312	2.186	2.322
9.875	2.004	1.997	2.099
10.000	1.847	1.807	1.892
10.125	1.733	1.686	1.788
10.250	1.409	1.451	1.575
10.375	1.749	1.695	2.204
10.500	RIB	RIB	RIB
10.625	2.404	2.329	2.540
10.750	2.646	2.610	2.740
10.875	2.405	2.454	2.474
11.000	2.207	2.206	2.255
11.125	2.083	1.988	2.005
11.250	2.058	1.812	1.972
11.375	1.840	1.731	1.776
11.500	1.546	1.413	1.583
11.625	2.379	1.821	1.841

	IN	TURN	

11.875	3.168	2.894	2.773
12.375	1.673	1.689	2.027
12.875	2.097	1.916	2.043
13.125	2.001	2.020	2.121
13.625	2.335	2.115	1.974
14.125	1.476	1.534	1.989

	AFTER	TURN	

14.375	3.120	1.724	1.557
14.500	4.606	2.712	2.042
14.625	3.545	3.102	2.253
14.750	2.792	3.182	2.317
14.875	2.781	3.037	2.420
15.000	2.477	2.744	2.482
15.125	2.306	2.556	2.434
15.250	2.120	2.286	2.417
15.375	1.803	2.185	2.203
15.500	RIB	RIB	RIB
15.625	2.548	2.436	3.120
15.750	4.012	3.286	3.357
15.875	3.744	3.147	2.974
16.000	3.161	2.922	2.499
16.125	2.689	2.675	2.294
16.250	2.354	2.448	2.141
16.375	2.216	2.213	2.052
16.500	2.033	1.916	1.784
16.625	1.879	1.743	1.510
16.750	RIB	RIB	RIB
16.875	1.873	1.755	2.105
17.000	3.181	3.013	3.154
17.125	3.336	3.019	2.763
17.250	3.039	2.815	2.479
17.375	2.766	2.592	2.253
17.500	2.506	2.340	2.032
17.625	2.249	2.097	1.872
17.750	1.944	1.755	1.690
17.875	1.692	1.488	1.362
18.000	RIB	RIB	RIB
18.125	1.503	1.475	1.621
18.250	2.804	2.855	2.955
18.375	3.029	2.879	2.840
18.500	2.811	2.573	2.577
18.625	2.647	2.310	2.152
18.750	2.435	2.167	2.020
18.875	2.199	2.005	1.810
19.000	1.963	1.739	1.592
19.125	1.634	1.480	1.347

----- OUTER WALL AND INNER WALL -----				
X/D	I.L.	C.L.	I.L.	C.L.

BEFORE TURN -----				
	OUTER	WALL	INNER	WALL

6.875	1.591	1.416	1.758	1.757
7.125	1.443	1.397	1.602	1.594
7.375	1.329	1.342	1.754	1.783
7.625	1.508	1.312	1.722	1.732
7.875	1.730	1.560	1.694	1.704
8.125	1.672	1.626	1.639	1.525
8.375	1.613	1.578	1.557	1.447
8.625	1.666	1.660	1.570	1.413
8.875	1.635	1.619	1.552	1.559
9.125	1.676	1.545	1.636	1.535
9.375	1.601	1.394	1.593	1.556
9.625	1.421	1.262	1.465	1.472
9.875	1.456	1.365	1.553	1.545
10.125	1.525	1.413	1.638	1.584
10.375	1.625	1.471	1.712	1.648
10.625	1.596	1.464	1.637	1.650
10.875	1.503	1.449	1.609	1.651
11.125	1.610	1.465	1.824	1.771
11.375	1.713	1.652	1.855	1.708
11.625	1.686	1.440	1.858	1.676

		IN	TURN
11.875	1.852	1.213	
12.375	1.841	1.734	
12.875	2.130	2.278	
13.125	1.921	2.121	
13.625	1.525	1.606	
14.125	1.825	1.809	

		AFTER	TURN	
14.375	2.261	2.183	2.784	2.652
14.625	1.974	1.912	2.329	2.252
14.875	1.800	1.731	2.428	2.396
15.125	1.832	1.760	2.422	2.411
15.375	1.981	1.922	2.655	2.379
15.625	1.959	1.900	2.735	2.356
15.875	1.939	1.898	2.710	2.251
16.125	1.834	1.796	2.556	2.202
16.375	1.852	1.803	2.424	2.176
16.625	1.977	1.961	2.150	2.078
16.875	1.936	1.880	1.920	1.776
17.125	1.962	1.909	1.861	1.666
17.375	2.108	2.026	1.903	1.656
17.625	2.119	2.026	1.923	1.635
17.875	2.105	1.953	1.909	1.672
18.125	1.935	1.856	1.803	1.645
18.375	1.690	1.721	1.789	1.807
18.625	1.645	1.570	1.934	2.004
18.875	1.559	1.546	2.094	1.998
19.125	1.484	1.481	2.191	1.910

Rough Channel: $Re=30,000$, $P/e=10$, $e/D=0.094$, $\alpha = 90^\circ$

	----- TOP WALL -----		
X/D	O.L.	C.L.	I.L.
	----- BEFORE TURN -----		
9.063	1.77	1.47	1.41
9.125	2.27	1.79	2.08
9.188	3.05	2.42	2.79
9.250	3.44	2.90	3.05
9.313	3.57	3.18	3.10
9.375	3.50	3.15	3.05
9.438	3.41	3.03	2.88
9.500	3.28	3.00	2.80
9.563	3.12	2.93	2.63
9.625	2.99	2.78	2.55
9.688	2.72	2.66	2.57
9.750	3.04	2.78	2.74
9.875	RIB	RIB	RIB
10.000	1.61	1.45	1.40
10.063	3.01	2.88	2.97
10.125	3.33	3.26	3.16
10.188	3.46	3.35	3.12
10.250	3.44	3.38	2.96
10.313	3.29	3.28	2.88
10.375	3.20	3.19	2.82
10.438	3.09	3.06	2.67
10.500	2.90	2.86	2.56
10.563	2.64	2.64	2.55
10.625	2.69	2.68	2.74
10.688	3.15	2.83	2.84
10.813	RIB	RIB	RIB
10.938	1.97	2.12	2.07
11.000	2.81	2.96	2.87
11.063	3.25	3.33	3.12
11.125	3.41	3.37	3.18
11.188	3.46	3.32	3.08
11.250	3.35	3.19	2.91
11.313	3.24	3.08	2.79
11.375	3.04	3.01	2.65
11.438	2.95	2.77	2.53
11.500	2.64	2.54	2.42
11.563	2.85	2.57	2.42
11.625	3.28	2.98	2.70

	IN	TURN	

11.875	4.10	3.82	3.41
12.375	2.38	2.51	2.81
12.875	2.95	2.61	2.93
13.125	2.74	2.74	2.76
13.625	3.08	2.54	2.30
14.125	1.88	2.04	2.61

	AFTER	TURN	

14.375	2.77	2.32	2.68
14.438	3.44	2.75	3.20
14.500	4.31	3.22	3.33
14.563	4.64	3.50	3.52
14.625	4.76	3.65	3.60
14.688	4.63	3.73	3.57
14.750	4.50	3.81	3.57
14.813	4.28	3.72	3.61
14.875	3.99	3.73	3.52
14.938	3.77	3.53	3.53
15.000	3.43	3.34	3.45
15.063	4.18	3.55	3.37
15.188	RIB	RIB	RIB
15.313	2.42	2.41	2.85
15.375	3.41	3.27	3.82
15.438	4.07	3.84	4.12
15.500	4.49	4.11	4.19
15.563	4.55	4.00	4.01
15.625	4.43	3.91	3.53
15.688	4.21	3.71	3.36
15.750	3.92	3.51	3.13
15.813	3.65	3.31	2.89
15.875	3.41	3.12	2.64
15.938	3.07	2.83	2.51
16.000	4.04	3.47	3.17
16.125	RIB	RIB	RIB
16.250	2.65	2.59	2.99
16.313	3.51	3.32	3.57
16.375	3.86	3.57	3.76
16.438	4.05	3.66	3.65
16.500	4.04	3.54	3.46
16.563	3.84	3.38	3.24
16.625	3.75	3.27	3.07
16.688	3.49	3.17	2.79
16.750	3.21	2.90	2.63
16.813	2.90	2.71	2.41
16.875	3.32	2.89	2.60
16.938	3.77	3.19	3.08

----- OUTER WALL AND INNER WALL -----				
X/D	I.L.	C.L.	I.L.	C.L.

BEFORE TURN -----				
	OUTER	WALL	INNER	WALL

9.063	2.37	1.87	2.16	2.10
9.125	2.55	2.10	2.29	2.18
9.250	2.42	2.02	2.29	2.18
9.375	2.43	2.02	2.29	2.13
9.500	2.38	1.99	2.30	2.17
9.625	2.54	2.04	2.23	2.11
9.750	2.46	2.07	2.17	2.03
10.000	2.46	1.80	2.17	2.10
10.063	2.57	2.12	2.19	2.12
10.188	2.23	1.90	2.27	2.04
10.313	2.34	1.93	2.29	2.14
10.438	2.40	2.03	2.30	2.13
10.563	2.51	1.86	2.29	2.24
10.688	2.49	1.93	2.33	2.25
10.938	2.47	1.97	2.40	2.16
11.000	2.32	2.15	2.41	2.14
11.125	2.32	1.89	2.40	2.03
11.250	2.24	1.90	2.29	1.86
11.375	2.40	1.93	2.29	1.96
11.500	2.39	1.93	2.31	2.10
11.625	2.45	1.90	2.35	2.22

		IN	TURN
11.875	2.63	2.05	
12.375	2.42	2.42	
12.875	3.29	3.26	
13.125	2.78	2.90	
13.625	3.04	3.08	
14.125	3.01	3.26	

		AFTER	TURN	
14.375	2.93	2.88	3.29	2.83
14.500	2.89	2.94	3.20	2.92
14.625	2.90	2.82	3.28	3.00
14.750	2.73	2.80	3.32	3.02
14.875	2.90	2.83	3.26	3.05
15.000	2.89	2.84	3.34	3.09
15.063	2.91	2.89	3.31	3.13
15.313	2.92	2.82	3.31	3.16
15.438	2.88	2.75	3.40	3.19
15.563	2.94	2.76	3.33	3.15
15.688	2.91	2.87	3.33	3.12
15.813	2.93	2.83	3.25	3.14
15.938	2.97	2.81	3.24	3.17
16.000	3.02	2.65	3.31	3.21
16.250	2.86	2.66	3.34	3.18
16.375	2.69	2.56	3.17	3.13
16.500	2.68	2.64	3.24	3.11
16.625	2.66	2.45	3.26	3.17
16.750	2.82	2.47	3.24	3.16
16.875	2.86	2.54	3.18	3.16
16.938	2.88	2.60	3.27	3.11

APPENDIX C

PRESSURE DROP DATA

LIST OF PRESSURE DROP TEST RUNS

CHANNEL	Re	P/e	e/D	α
SMOOTH	10,000	—	—	—
	20,000	—	—	—
	30,000	—	—	—
	40,000	—	—	—
	50,000	—	—	—
	60,000	—	—	—
ROUGH	10,000	10	0.063	90°
	20,000	10	0.063	90°
	30,000	10	0.063	90°
	40,000	10	0.063	90°
	50,000	10	0.063	90°
	60,000	10	0.063	90°
ROUGH	10,000	10	0.063	60°
	20,000	10	0.063	60°
	30,000	10	0.063	60°
	40,000	10	0.063	60°
	50,000	10	0.063	60°
	60,000	10	0.063	60°
ROUGH	10,000	10	0.063	45°
	20,000	10	0.063	45°
	30,000	10	0.063	45°
	40,000	10	0.063	45°
	50,000	10	0.063	45°
	60,000	10	0.063	45°
ROUGH	10,000	20	0.063	90°
	20,000	20	0.063	90°
	30,000	20	0.063	90°
	40,000	20	0.063	90°
	50,000	20	0.063	90°
	60,000	20	0.063	90°
ROUGH	10,000	10	0.094	90°
	20,000	10	0.094	90°
	30,000	10	0.094	90°
	40,000	10	0.094	90°
	50,000	10	0.094	90°
	60,000	10	0.094	90°

Re : REYNOLDS NUMBER

P/e : PITCH-TO-RIB HEIGHT RATIO

e/D : RIB HEIGHT-TO-HYDRAULIC DIAMETER RATIO

α : RIB ANGLE-OF-ATTACK

Smooth Channel

$$2(P - P_{atm})/\rho V^2$$

TAP	X/D	RE=10000	RE=20000	RE=30000	RE=40000	RE=50000	RE=60000
1	0.3125	-1.9935	-1.9470	-1.9049	-1.8840	-1.8534	-1.7971
2	2.1875	-1.2931	-1.1763	-1.1142	-1.0900	-1.0776	-1.0633
3	4.6875	-1.3200	-1.2061	-1.1387	-1.0934	-1.0905	-1.0992
4	7.1875	-1.4009	-1.2710	-1.1980	-1.1640	-1.1638	-1.1382
5	9.6875	-1.4655	-1.3250	-1.2579	-1.2111	-1.1853	-1.1681
6	10.3125	-1.5086	-1.3440	-1.2639	-1.2313	-1.2069	-1.1981
7	10.9375	-1.5086	-1.3656	-1.2819	-1.2280	-1.2177	-1.2205
8	11.5625	-1.2392	-1.1493	-1.0603	-1.0429	-1.0345	-1.0034
9	13.0000	-2.1552	-1.9470	-1.9049	-1.8840	-1.8534	-1.8271
10	14.4375	-2.9095	-2.7582	-2.6956	-2.6578	-2.5862	-2.5459
11	15.0625	-4.2026	-3.8061	-3.6540	-3.5830	-3.5345	-3.3696
12	15.6875	-3.6638	-3.3532	-3.2587	-3.2297	-3.1034	-2.9802
13	16.3125	-3.2328	-3.0557	-2.9232	-2.8596	-2.8448	-2.6957
14	18.8125	-3.1789	-3.0287	-2.8813	-2.8260	-2.8017	-2.6657
15	21.3125	-3.3405	-3.1301	-2.9831	-2.9135	-2.8621	-2.7705
16	23.8125	-3.5022	-3.2856	-3.1149	-3.0279	-2.9957	-2.8604

Rough Channel: $P/e = 10$, $e/D = 0.063$, $\alpha = 90^\circ$
 $2(P - P_{atm})/\rho V^2$

TAP	X/D	RE=10000	RE=20000	RE=30000	RE=40000	RE=50000	RE=60000
1	0.3125	-2.1013	-2.0552	-2.0247	-2.0186	-1.9828	-1.8570
2	2.1875	-1.6918	-1.6766	-1.6473	-1.6149	-1.5948	-1.4976
3	4.6875	-1.7996	-1.7847	-1.7042	-1.6990	-1.6810	-1.5725
4	7.1875	-2.1121	-2.0957	-2.0367	-1.9849	-1.9612	-1.8870
5	9.6875	-2.4246	-2.4067	-2.3002	-2.2877	-2.2629	-2.1565
6	10.3125	-2.5108	-2.4986	-2.3961	-2.3550	-2.3362	-2.2614
7	10.9375	-2.5970	-2.5622	-2.4560	-2.4559	-2.4310	-2.3153
8	11.5625	-2.3707	-2.2985	-2.1265	-2.1868	-2.0690	-2.0367
9	13.0000	-3.3190	-3.2856	-3.1748	-3.1288	-3.0603	-2.9353
10	14.4375	-4.0409	-4.0427	-3.8936	-3.8689	-3.7931	-3.6541
11	15.0625	-4.8006	-4.7052	-4.5525	-4.4577	-4.3319	-4.1932
12	15.6875	-4.7953	-4.7323	-4.5525	-4.4745	-4.3103	-4.1633
13	16.3125	-4.8491	-4.7593	-4.5525	-4.5081	-4.3534	-4.2532
14	18.8125	-5.1724	-5.1109	-4.9119	-4.8782	-4.7414	-4.5826
15	21.3125	-5.5496	-5.4759	-5.2234	-5.1810	-5.0431	-4.9121
16	23.8125	-5.9267	-5.8140	-5.5709	-5.5174	-5.3879	-5.2715

Rough Channel: $P/e = 10$, $e/D = 0.063$, $\alpha = 60^\circ$

$$2(P - P_{atm})/\rho V^2$$

TAP	X/D	RE=10000	RE=20000	RE=30000	RE=40000	RE=50000	RE=60000
1	0.3125	-2.2629	-2.2309	-2.2224	-2.2137	-2.1983	-2.1865
2	2.1875	-1.9397	-1.8253	-1.7611	-1.6821	-1.6379	-1.6174
3	4.6875	-2.1821	-2.1498	-2.0726	-1.9513	-1.9181	-1.8540
4	7.1875	-2.5862	-2.5690	-2.4560	-2.3886	-2.3491	-2.2913
5	9.6875	-3.0172	-2.9746	-2.9352	-2.8596	-2.8017	-2.7556
6	10.3125	-3.1358	-3.1098	-3.0550	-3.0009	-2.9095	-2.8754
7	10.9375	-3.2597	-3.2518	-3.1628	-3.0649	-3.0172	-2.9547
8	11.5625	-2.8556	-2.8123	-2.7555	-2.6914	-2.6293	-2.5908
9	13.0000	-3.3405	-3.3396	-3.2946	-3.2297	-3.0388	-2.9053
10	14.4375	-4.3103	-4.2726	-4.1931	-4.1044	-3.8793	-3.7140
11	15.0625	-5.2802	-5.2190	-5.1516	-5.0801	-4.9138	-4.7024
12	15.6875	-5.2802	-5.1379	-4.9718	-4.8446	-4.6983	-4.4928
13	16.3125	-5.0647	-4.8675	-4.7322	-4.6494	-4.4828	-4.3730
14	18.8125	-5.2263	-5.1109	-4.9718	-4.8446	-4.6983	-4.4928
15	21.3125	-5.6573	-5.5435	-5.3912	-5.2483	-5.0754	-4.8522
16	23.8125	-6.0884	-5.9762	-5.8105	-5.6520	-5.4741	-5.2715

Rough Channel: $P/e = 10$, $e/D = 0.063$, $\alpha = 45^\circ$

$$2(P - P_{atm})/\rho V^2$$

TAP	X/D	RE=10000	RE=20000	RE=30000	RE=40000	RE=50000	RE=60000
1	0.3125	-2.2091	-2.2174	-2.1565	-2.1531	-2.0690	-2.0517
2	2.1875	-1.7241	-1.6495	-1.5874	-1.5812	-1.5086	-1.4676
3	4.6875	-1.9935	-1.9511	-1.8719	-1.8739	-1.7672	-1.6923
4	7.1875	-2.3168	-2.2715	-2.1565	-2.1195	-2.0043	-1.9169
5	9.6875	-2.6401	-2.5960	-2.4560	-2.4223	-2.2845	-2.2015
6	10.3125	-2.6940	-2.6501	-2.5159	-2.4896	-2.3621	-2.2763
7	10.9375	-2.7478	-2.7244	-2.6177	-2.5703	-2.4375	-2.3362
8	11.5625	-2.3707	-2.3526	-2.2763	-2.2204	-2.0474	-2.0068
9	13.0000	-3.1250	-3.0287	-2.9951	-2.8596	-2.6724	-2.5759
10	14.4375	-3.9871	-3.9481	-3.7738	-3.5998	-3.2974	-3.1899
11	15.0625	-5.6573	-5.5638	-5.3612	-5.1474	-4.8168	-4.7174
12	15.6875	-5.1724	-5.0568	-4.8520	-4.6764	-4.3534	-4.2831
13	16.3125	-4.7414	-4.6241	-4.4926	-4.3736	-4.0948	-4.0135
14	18.8125	-4.8491	-4.7323	-4.6124	-4.5081	-4.2241	-4.1333
15	21.3125	-5.1185	-5.0027	-4.8520	-4.7436	-4.4181	-4.3430
16	23.8125	-5.3879	-5.2731	-5.1156	-5.0464	-4.6767	-4.5976

Rough Channel: $P/e = 20$, $e/D = 0.063$, $\alpha = 90^\circ$

$$2(P - P_{atm})/\rho V^2$$

TAP	X/D	RE=10000	RE=20000	RE=30000	RE=40000	RE=50000	RE=60000
1	0.3125	-2.1552	-2.0552	-2.0247	-2.0186	-2.0259	-1.9768
2	2.1875	-1.6164	-1.5955	-1.5215	-1.4803	-1.4655	-1.3778
3	4.6875	-1.7241	-1.7442	-1.6114	-1.5812	-1.5970	-1.4976
4	7.1875	-1.9935	-2.0011	-1.8330	-1.8167	-1.8534	-1.7372
5	9.6875	-2.2629	-2.2309	-2.0966	-2.0724	-2.0690	-1.9469
6	10.3125	-2.3168	-2.2985	-2.1565	-2.1195	-2.1336	-1.9768
7	10.9375	-2.3707	-2.3526	-2.2164	-2.2204	-2.2198	-2.0442
8	11.5625	-2.1013	-2.0822	-1.9528	-1.9176	-1.8534	-1.7372
9	13.0000	-3.1250	-3.1098	-2.9352	-2.8933	-2.8448	-2.7855
10	14.4375	-3.9332	-3.8940	-3.8337	-3.7344	-3.5991	-3.4445
11	15.0625	-4.3103	-4.2658	-4.1332	-4.0371	-3.9009	-3.7290
12	15.6875	-4.5259	-4.4889	-4.3129	-4.2390	-4.1379	-3.9536
13	16.3125	-4.3642	-4.2726	-4.1452	-4.0371	-3.9655	-3.7589
14	18.8125	-4.6121	-4.5700	-4.3728	-4.2726	-4.1595	-3.9836
15	21.3125	-4.9030	-4.8675	-4.6124	-4.5418	-4.4397	-4.2831
16	23.8125	-5.2263	-5.1109	-4.8520	-4.8109	-4.6983	-4.5527

Rough Channel: $P/e = 10$, $e/D = 0.094$, $\alpha = 90^\circ$
 $2(P - P_{atm})/\rho V^2$

TAP	X/D	RE=10000	RE=20000	RE=30000	RE=40000	RE=50000	RE=60000
1	0.3125	-2.1552	-2.1633	-2.1205	-2.0522	-2.0043	-1.9469
2	2.1875	-1.9073	-1.8929	-1.8510	-1.8167	-1.7241	-1.6174
3	4.6875	-2.3437	-2.2715	-2.2164	-2.1700	-2.0690	-1.9768
4	7.1875	-2.8556	-2.7582	-2.6956	-2.6578	-2.5431	-2.4860
5	9.6875	-3.3405	-3.2450	-3.1748	-3.1086	-3.0259	-2.9053
6	10.3125	-3.4698	-3.3667	-3.3305	-3.2297	-3.1466	-3.0251
7	10.9375	-3.6261	-3.4884	-3.4144	-3.3878	-3.2759	-3.1599
8	11.5625	-3.3405	-3.1909	-3.1149	-3.0951	-2.9310	-2.8754
9	13.0000	-4.6336	-4.5971	-4.6124	-4.4745	-4.3103	-4.3131
10	14.4375	-5.4418	-5.3813	-5.2714	-5.1474	-5.0000	-4.9420
11	15.0625	-5.9806	-5.8140	-5.6907	-5.5847	-5.3448	-5.2116
12	15.6875	-6.1961	-6.0844	-5.9303	-5.7866	-5.5603	-5.3913
13	16.3125	-6.3039	-6.2196	-5.9902	-5.9211	-5.7328	-5.5710
14	18.8125	-6.6272	-6.5441	-6.3496	-6.2576	-6.0345	-5.8106
15	21.3125	-7.1390	-7.0308	-6.8288	-6.7286	-6.5517	-6.2899
16	23.8125	-7.7047	-7.5446	-7.3679	-7.2669	-7.0590	-6.8290



National Aeronautics and
Space Administration

Report Documentation Page

1. Report No. NASA CR-179635 AVSCOM TR-87-C-14		2. Government Accession No.		3. Recipient's Catalog No.	
4. Title and Subtitle Local Heat/Mass Transfer and Pressure Drop in a Two-Pass Rib-Roughened Channel for Turbine Airfoil Cooling				5. Report Date September 1987	
				6. Performing Organization Code	
7. Author(s) J.C. Han and P.R. Chandra				8. Performing Organization Report No. None	
				10. Work Unit No. 1L162209AH76 505-31-4K	
9. Performing Organization Name and Address Texas A&M University Turbomachinery Laboratories College Station, Texas 77843-3123				11. Contract or Grant No. NAS3-24227	
				13. Type of Report and Period Covered Contractor Report Final	
12. Sponsoring Agency Name and Address U.S. Army Aviation Research and Technology Activity - AVSCOM, Propulsion Directorate, Lewis Research Center, Cleveland, Ohio 44135 and NASA Lewis Research Center, Cleveland, Ohio 44135				14. Sponsoring Agency Code	
15. Supplementary Notes Project Manager, Robert J. Boyle, Internal Fluid Mechanics Division, NASA Lewis Research Center.					
16. Abstract <p>The heat transfer characteristics of turbulent air flow in a multipass channel were studied via the naphthalene sublimation technique. The naphthalene-coated test section, which consisted of two straight, square channels joined by a sharp 180° turn, resembled the internal cooling passages of gas turbine airfoils. The top and bottom surfaces of the test channel were roughened by rib turbulators. The rib height-to-hydraulic diameter ratio (e/D) were 0.063 and 0.094, and the rib pitch-to-height ratio (P/e) were 10 and 20. The local heat/mass transfer coefficients on the roughened top wall and on the smooth divider and side walls of the test channel were determined for three Reynolds numbers of 15,000, 30,000, and 60,000, and for three angles-of-attack (α) of 90°, 60°, and 45°. The results showed that the local Sherwood numbers on the ribbed walls were 1.5 to 6.5 times those for a fully developed flow in a smooth square duct. The average ribbed-wall Sherwood numbers were 2.5 to 3.5 times higher than the fully developed values, depending on the rib angle-of-attack and the Reynolds number. The results also indicated that, before the turn, the heat/mass transfer coefficients in the cases of $\alpha = 60^\circ$ and 45° were higher than those in the case of $\alpha = 90^\circ$. However, after the turn, the heat/mass transfer coefficients in the oblique-rib cases were lower than those in the traverse-rib case. Correlations for the average Sherwood number ratios for individual channel surfaces and for the overall Sherwood number ratios are reported. Correlations for the fully developed friction factors and for the loss coefficients are also provided.</p>					
17. Key Words (Suggested by Author(s)) Heat transfer Augmentation Ducts Turbine cooling			18. Distribution Statement Unclassified - Unlimited Subject Category 34		
19. Security Classif. (of this report) Unclassified		20. Security Classif. (of this page) Unclassified		21. No of pages 170	
				22. Price* A	